Growth and Characterization of ZnO Nanowires

Dissertation

zur Erlangung des akademischen Grades

doctor rerum naturalium (Dr. rer. nat.)

vorgelegt der

Mathematisch-Naturwissenschaftlich-Technischen Fakultät
(mathematisch-naturwissenschaftlicher Bereich)
der Martin-Luther-Universität Halle-Wittenberg

von Dong Sik Kim

geboren am 8. August 1977

Gutachter /in

1. Prof. Ulrich Gösele
2. Prof. Wolf Widdra
3. Prof. Carsten Ronning

Halle (Saale), den January 5, 2009

Verteidigungsdatum: May 25, 2009

This **cumulative thesis** is based on the follwing papers.

I. D.S. Kim, R. Scholz, U. Gösele, M. Zacharias, Gold at the root or at the tip of ZnO nanowires: A model. *Small*, **4**, 1615 (2008).

II. D.S. Kim, U. Gösele, M. Zacharias, Surface diffusion induced growth of ZnO nanowires. *Journal of Crystal Growth*, **311**, 3216 (2009).

III. D.S. Kim, R. Ji, H. J. Fan, F. Bertram, R. Scholz, R. Dadgar, K. Nielsch, A. Krost, J. Christen, U. Gösele, and M. Zacharias, Laser-interference lithography tailored for highly symmetrically arranged ZnO nanowire arrays. *Small*, **3**, 76 (2007).

IV. D.S. Kim, J. Fallert, A. Lotnyk, R. Scholz, E. Pippel, S. Senz, H. Kalt, U. Gösele, M. Zacharias, Growth and optical properties of phosphorus-doped ZnO nanowires. *Solid State Commun.*, **143**, 570 (2007).

V. Y. Yang, D.S. Kim, M. Knez, R. Scholz, A. Berger, E. Pippel, U. Gösele, M. Zacharias, Kirkendall effect induced evolution of coaxial ZnO/Al_2O_3 one-dimensional heterostructures: from core-shell nanowires to spinel nanotubes and mesoporous nanowires. *J. Phys. Chem. C*, **112**, 4068-4074 (2008).

VI. H.J. Fan, A. Lotnyk, R. Scholz, Y. Yang, D.S. Kim, E. Pippel, D. Hesse, M. Zacharias, Surface reaction of ZnO nanowires with electron-beam generated alumina vapor. *J. Phys. Chem. C*, **112**, 6770-6774 (2008).

VII. D.S. Kim, S.-M. Lee, R. Scholz, M. Knez, U. Gösele, J. Fallert, H. Kalt, M. Zacharias, Synthesis and optical properties of ZnO and carbon nanotube based coaxial heterostructures. *Appl. Phys. Lett.*, **93**, 103108/1-3 (2008).

Contents

Introduction and Survey

Studying naturally occurring or artificial structures with dimensions in the range of a few or tens of nanometers is categorized as nanoscience. At this scale, materials show fundamentally different electrical, optical, and mechanical characteristics compared to their bulk or atomic or molecular form. Understanding these novel properties promises to be able to tune the functionality of materials and manipulate ultimately new nanostructures into complex functional structures and nanodevices controlling the flow of electrons, spins, and photons.

Nanomaterials include thin film, nanowires, nanotubes, and nanoparticles. In particular, interest first in carbon nanotubes and later on in nanowires has continued to grow due to their potential use in advanced electronic and optoelectronic device applications. For most potential applications nanowires with well defined size, structure, and composition have to be synthesized for reliable performance of such devices.

In order to gets a general picture concerning nanowires science and technology the essential literature will be briefly surveyed in the following part. Firstly, principles of nanowire growth mechanisms are described based on a few examples. Understanding growth habits of nanowires is indispensable for tuning functionalities of nanowires. Secondly, controlled growth of nanowires is outlined in terms of position, size, and compositions of nanowires, which provide essential steps for realization of nanowires-based devices. Subsequently, the challenging task of tuning electrical properties by impurity doping will be reviewed. Finally, unique physical properties of semiconductor nanowires, which are mostly originated from their geometrical character, are summarized. In addition, material properties of ZnO will be presented, since the present cumulative thesis will concentrate on ZnO nanostructures either in the form of nanowires or nanoshells or nanotubes.

Nanowire Growth Mechanisms

The most generally accepted method for nanowire growth is the vapor-liquid-solid (VLS) process. This vapor-liquid-solid mechanism was first proposed by Wagner and Ellis [Wag64]. The essential feature of the concept is forming a liquid phase metallic droplet at the growth interface with a substrate and/or vapor phase constituents. The liquid metallic catalyst acts as a preferential adsorption site for the incoming vapor species due to its high sticking coefficient. Once the vapor phase constituent has been reached beyond the equilibrium concentration in the liquid droplet the species start to condensate at the liquid-substrate interface. Subsequently, a one-dimensional nanowire is growing on the substrate capped with the liquid catalytic droplet. Usually the liquid droplet solidifies upon cooling down the samples from the processing to room temperature. There are three principle steps in VLS growth i.e., (i) catalytic reactions on the liquid droplet, (ii) diffusion in the liquid phase, and (iii) incorporation of the material into the crystalline nanowire [Giv87].

As an example, the process for silicon nanowire growth with gold as a catalyst is illustrated in Fig. 1.1. If gold is deposited on a silicon substrate, and the substrate is heated to a temperature above 363 °C, a gold-silicon liquid alloy is formed (see Fig. 1.1c). When a silicon containing vapor such as $SiCl_4$ and SiH_4 is introduced into the growth chamber the vapor phase species of Si is stuck on the liquid droplet of Si-Au alloy due to their relatively large sticking coefficient and is catalytically decomposed. The silicon is then incorporated into the gold/Si alloy droplet. For sufficiently high vapor pressure the droplet becomes supersaturated with Si and the excess Si is crystallizing out at the solid-liquid interface as long as the supply of silicon-containing vapor is maintained. Silicon nanowires with a liquid gold/Si alloys cap are forming on the substrate. After cooling down the Au/Si droplets solidify leading solid gold cap with negligible silicon on top of the silicon nanowires [Giv87].

Typically, nanowire growth takes place only if a catalyst is supplied. The nanowire diameter is normally determined by the droplet size. However, due to Oswald ripening process, the surface migration of Au atoms may limit the growth of nanowires with uniform diameter [Han06]. Furthermore, impurities from the catalyst droplets may be dissolved in the nanowires while the VLS growth proceeds and lead to high density of these impurities in

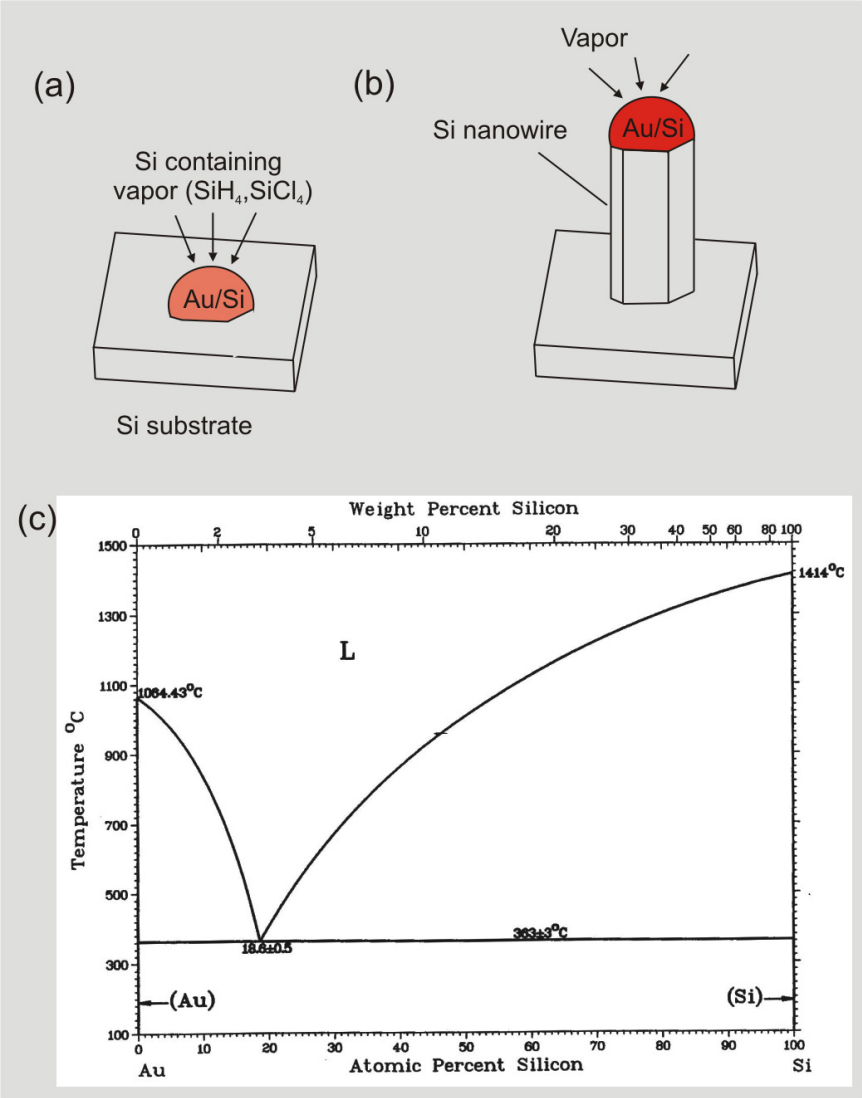

Figure 1.1: Schematic illustration of wire growth: (a) the liquid alloy formation, (b) wire growth. (c) Au-Si phase diagram [Mas90].

the semiconductor nanowires. For instance, the density of Au atoms, which is known to reduce the carrier lifetime, was estimated to be in the range of 10^{20} atoms/cm^3 close to the nanowire surfaces [Oh08].

VLS growth has been used for the nanowire growth of elemental semiconductors [Wu00], III-V semiconductors [Wan01], and II-VI semiconductors [Dua00]. VLS growth can be accomplished by either physical or chemical methods. Typical physical methods include laser ablation and vapor transport deposition. Also molecular beam epitaxy may be used, even though the growth species is mostly supplied to the catalyst by surface diffusion

[Sch04, Dub05]. Chemical methods such as chemical vapor deposition (CVD), metal organic chemical vapor deposition (MOCVD), and chemical beam epitaxy (CBE) have been used for the growth of nanowires [Sch05, Day07, Jen04]. These systems offer the advantage of scalability as well as integration to standard industrial device fabrication processes. Semiconductor nanowire growth takes place also below the bulk eutectic temperature. In this case the catalyst remains solid during growth and the growth mechanism is known as vapor-solid-solid (VSS) growth. This concept has been demonstrated for Si nanowire growth with Al and Ti [Wan06, Kam01] as well as for Ge and GaAs nanowire growth with a solid Au catalyst [Boo71, Hir95]. Though the basic processes of the VSS growth are similar to those of the VLS method, the involved growth kinetics and thermodynamics may differ. In particular, the diffusion of the growth species through or around the solid catalyst particle is typically slower for the VSS mechanism. In controlled growth experiments carried out via *in situ* transmission electron microscopy, it was disclosed for the case of Ge nanowires growth catalyzed by Au that VSS growth is 10 to 100 times slower than VLS growth at the same source pressure and temperature [Kod07]. Also the state of the catalyst could influence growth kinetics and direction, and morphology of nanowire. For instance, a solid catalyst should lead to sharper interface within heterostructure nanowires compared to the case of liquid catalysts, which is important for functional nanowire based applications. The reason for this behavior is the generally much lower solubility of the growth species (e.g. Si) in a solid catalytic particles (e.g. Au) than in a liquid catalytic droplet.

Furthermore, certain types of nanowires may also grow without any catalytic particles, which is then known as vapor-solid (VS) growth if the growth species is supplied from the vapor phase. Very early nanowire growth by the VS process was already observed in the condensation experiments of mercury vapor [Sea53]. Under supersaturation of mercury vapor, mercury nanowires formed on the glass surface without assistance of any catalysts. In order to explain nanowire growth, a diffusion-dislocation model was suggested. According to this model, an axial screw dislocation acts as a preferential adsorption site and nanowires are continuing to grow with supplying the species through a surface diffusion. But this mechanism has turned out not to be of importance in most cases of nanowire growth except the specific case of PbS nanowire growth [Bie08].

In the dislocation-mediated growth model, many important aspects of nanowire growth are also not clear, such as the increase of the nucleation rate with catalytic impurities, the growth of lateral faces and morphological instabilities [Giv87]. Thus, the dislocation-mediated growth model should be considered only as a model applicable to a few exceptional systems.

Typically, ZnO nanowires have been grown via the vapor-solid mechanism involving neither liquid nor solid catalysts at the tip of the growing nanowires. Physical vapor deposition (vapor transport and deposition method) as well as metal organic vapor-phase epitaxy (MOPVE) were used to realize ZnO nanowires based on this growth mode [Par02].

In VS growth, ordered nanowire arrays can be achieved by mask patterning instead of positioning of catalysts for controlled growth, which is typically used in the VLS process. The possibility to fabricate GaAs nanowires of defined length, diameter, shape, and positions were nicely demonstrated based on MOVPE [Nob05]. Furthermore, nanowire growth occurring by the VS mode is expected to avoid any impurity incorporation from catalyst particles.

Controlled Nanowire Growth

An important requirement for many device applications involving photonics, electronics, or optoelectonics is the precise control of the location and the size of nanowires. For example, an ordered nanowire array in a microfluidic system may work as a molecule filter. Further, regularly arranged nanowires may provide a model system for studying entangled optical properties of nanowires such as interference of light emitted from nanowires.

Typically, the diameter and the location of the nanowires can be controlled by the size and the location of the metal particles if nanowires are grown by the VLS or the VSS process. The application of lithographic methods for regularly arranged nanowires, thus, is desired. Many efforts have been put into fabricating ordered arrays of catalyst particles. For instance, diblock-copolymer lithography and nanoimprint lithography allowed to fabricate patterns in a flexible way and/or with small feature sizes (the resolution of such patterns might reach about 10 nm or even lower values) [Fan06].

Not only the position but also the size of wires is necessary to be controlled because the

electrical and optical properties of nanowires are strongly size-dependent. In particular, in order to examine the effects of wire assembles in an array, nanowires with well-defined and monodisperse diameters are required.

Growth of epitaxial nanowires with diameters below about 20 nm is challenging. Such nanowires would attract considerable attention due to their potential use in vertical wrap-around-gate transistors [Sch06]. Especially the better control of the channel compared to a normal planer field effect transistor (FET) associated with an enhanced transconductance and reduced the off-current is the most interesting aspect of such devices.

Performance of devices based on nanowires as an active channel is closely related to functional interfaces or heterostructures. Precise control over the composition and interfaces of heterostructures is important for the reliable operation of new nanowire-based devices.

There are three basic heterostructures considered: axial heterostructure, radial heterostructures, and branched heterostructures. See figure 1.2.

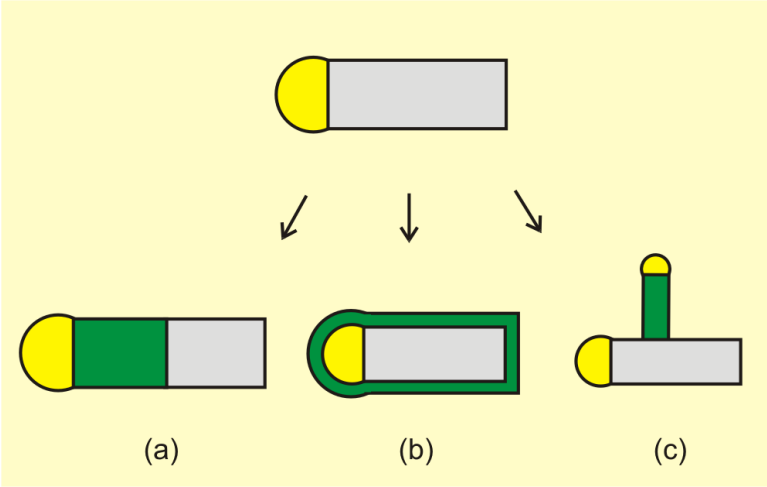

Figure 1.2: Nanowire heterostructure synthesis: (a) Axial heterostructure growth, (b) radial heterostructure growth by incorporation of the species uniformly on the nanowire surface. Multi-step metal catalyzed VLS process leads to branched nanowires (c).

VLS grown axial heterojunctions of nanowire can be produced by providing different precursor material sequentially during wire growth. For instance, single-crystalline Si/SiGe superlattices have been obtained by a hybrid pulsed laser ablation and chemical vapor deposition process [Wu02]. Material and catalyst have to be carefully chosen to create compatible and well-defined interfaces.

It is important to passivate nanowire surfaces to avoid deleterious effects created by electrical charges and/or traps at the surfaces. From this point of view, core-shell structured nanowires, which are synthesized coaxially on a wire core might benefit the device performance efficiently. Radial shell growth can be achieved by controlling the reaction parameters such as temperature, gas composition, and pressure. Growth of a radial heterostructure of Si/Ge core-shell were successfully demonstrated by Lau *et al.* [Lau02].
Conceptually, branched nanowires may provide an alternative approach for enhancing structural complexity and functionality. Control over the density and the size of secondary branches would be required for the design of devices units. Branched Si nanowires are synthesized via a multi-step metal catalyzed VLS process [Wan04].

Doping in Nanowires

For an optimum performance of electronic devices based on semiconductor nanowires such as field-effect transistors (FETs) and light-emitting diodes, quantitative control of doping levels is necessary. Both p-type and n-type doping of nanowires including Si, GaAs, and InP wires has been demonstrated [Cui01, Hir95, Min07].
However, heavy doping may cause large doping fluctuations in the nanowires as well as a tapering [Ase03, Lin05]. The dopant incorporated partly into the nanowire through the nanowire surface might not result in uniform doping along and within the nanowire [Tut06]. Furthermore, due to confinement effects, the impurity ionization energy increases as the diameter of nanowire decrease [Lee84]. Another issue in doping is interaction between dopant atoms and the catalyst particle as well as a detailed understanding on the incorporation mechanism of such impurity atoms into the semiconductor nanowire during the VLS growth process [Li07].
Finally, many semiconductors are rather difficult to dope even in the case of bulk or thin film samples due to material specific doping limits. For example, reliable and stable p-type doping of ZnO has not been demonstrated experimentally. Such doping limits in various bulk semiconductors may attribute to the amphoteric nature of compensating native defects. In the amphoteric defect model (ADM) [Wal89] the formation energy of native defects decreases linearly as the position of the Fermi level with respect to the Fermi stabilization

energy moves away. Thus it is difficult to achieve p-type conductivity by external doping due to easy compensation of the dopants by native defects.

Physical Properties of Nanowires

Understanding optical properties of semiconductor nanowires is important for nanowire-based devices. Typically the optical properties of nanowires are determined by those of the well known bulk material unless the size of the wire is in the quantum confinement regime. However, the influence of the surface region considerably increases with decreasing wire diameter since the weight of the surface-to-volume ratio increases relativly. Therefore, nanowires are an ideal structure for studying the effect of the wire surface on optical properties. For example, it was reported that surface exciton emission heavily contribute to near band-edge emission in the PL spectra of ZnO nanowires [Wis06]. Another distinct feature in the PL spectra of the nanowires is the broader and stronger deep level emission compared to bulk ZnO. This implies that the deep level emission might be originated from surface states [Bek07]. In addition, by taking advantage of the one dimensional nature of the nanowires, a nanoscale stimulated emission from single nanowires has been demonstrated [Hau06]. The nanowire body does not only act as the gain medium, but also as laser resonator. The emission wavelength defined by the guided modes inside the nanowire cavity can be tuned with the length of the nanowire.

Concerning the electrical properties of nanowires, nanowire offer a unique structure for carrier transport due to its confined geometry. The size and shape of the nanowires could affect the overall current flow, which in many cases differs from what is expected based on the bulk properties. Integration of semiconducting nanowires in electronic devices would require understanding of relevant electrical properties of nanowires such as the effects of the surface, defects, and dopants. In addition, both the carrier concentration and carrier mobility should be optimized for the improved performance of nanowire devices [The06]. If the size of a nanowire reaches the quantum scale which means the diameter is comparable to the Fermi wavelength the quantum confinement effects occur. Synthesis of such thin wires and contacting them is challenging. Nevertheless, Coulomb blockade behavior in InP nanowires at 0.35 K was demonstrated [Fra03]. A resonant tunneling diode [Bjo02] and a

single electron transistor [The03] using a heterostructured nanowire were also realized.

Zinc Oxide

In the present cumulative thesis ZnO is the material used to fabricate various types of nanostructures such as nanowires, or nanotubes. Therefore some relevant basic properties of ZnO are given here. ZnO is a wide-band gap (3.437 eV at low temperatures), normally n-type semiconductor [Ozg05]. In particular, the high exciton binding energy of about 60 meV and the small excitonic Bohr radius of 1.8 nm makes ZnO as considerable material for optoelectronic applications. For example, excitonic lasing at room temperature with low thresholds can be realized based on ZnO. The observed high free charge carrier density might be attributed to the nonstoichiometric nature of ZnO. ZnO is an ionic dielectric with a wurtzite structure. Both Zn^{2+} and O^{2-} ions tetrahedrally coordinate to each other. Such spatial arrangement results in two complementary, Zn and O rich surfaces normal to the *c* axis. Polar surfaces are characterized by unique chemical and physical properties. In addition, ZnO shows piezoelectric properties due to the partial ionic bonding character and a lack of a central inversion.

Overview of Results

The aim of this dissertation is understanding the growth and characteristic of the ZnO in the form of one-dimensional nanostructures. In particular, nanowire growth studies and controlled nanowire growth as well as various physical properties are presented. In addition, ZnO-alumina core-shell nanowires were prepared to apply a chemical reaction. This approach allowed examining reactivity and stability of the ZnO nanowires. Instead of physical vapor deposition an alternative chemical method of atomic layer deposition is also addressed for growth of ZnO nanostructures.

Basically, this cumulative thesis is composed of seven papers. The contribution of other co-authors is mentioned on a page in front of each paper in this thesis.

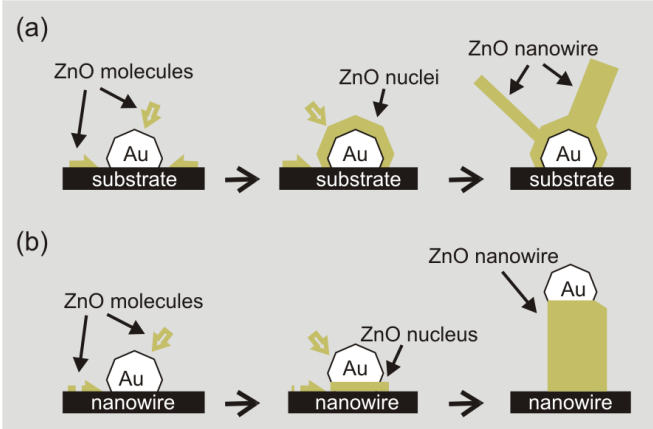

Figure 2.1: Schematic view of selection mechanism: a) nanowire growth with Au particles at the root, b) Au particle capped nanowire growth. Adapted from [Kim08].

Unique growth aspects of ZnO nanowires have remained a wide open area with limited progress. In paper I, the question is addressed that in Au-assisted ZnO nanowire growth, Au nanoparticles were sometimes observed at the root of wires after growth and in other cases at the tip of the wires. The later case is rather typical for Au catalyzed semiconductor

nanowire growth. A selection mechanism is proposed defining whether the Au particle remains on the substrate at the root of the nanowire serving as an initial template for wire nucleation or is lifted up from the substrate, catalyzing wire growth at the tip (see Fig. 2.1). In the later case, the diameter of the nanowires does not match that of the Au particles, in contrast to the well-accepted cases of the vapor-liquid-solid and vapor-solid-solid process for Si and III-V compound nanowires.

In paper II, it is demonstrated that the surface migration of Au atoms on lattice matched substrates limits the position-controlled growth of ZnO nanowires. Surface diffusion of ZnO admolecules leads to anisotropic ZnO nanowire growth with a diameter-dependent growth rate. Narrower nanowires grow faster than thicker ones (see Fig. 2.2). This is just opposite to what is expected and observed for the typical VLS growth in which supplied via the vapor phase [Giv87]. The observed diameters dependence of the growth rate of ZnO nanowires is in agreement with the that of Si nanowires and GaAs by MBE, in which also surface diffusion supplies the growth species to the catalyst [Sch04, Dub05].

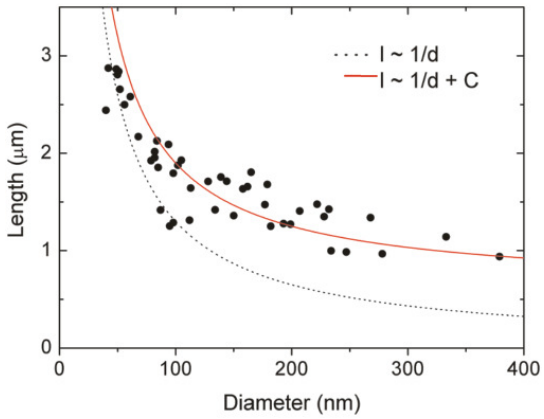

Figure 2.2: Length *vs* diameter of ZnO nanowires [paper II].

In paper III, based on the understanding of such nanowire growth behavior growth of epitaxial ZnO nanowire arrays is demonstrated which is important in an application point of view. By the use of laser interference lithography for patterning of Au nanodots, well arranged ZnO nanowires over larger area were fabricated (see Fig. 2.3). A growth mechanism is proposed for the one-to-one growth of ZnO nanowires. In addition, optical properties are discussed based on the results of scanning cathodoluminescence and photoluminescence experiments.

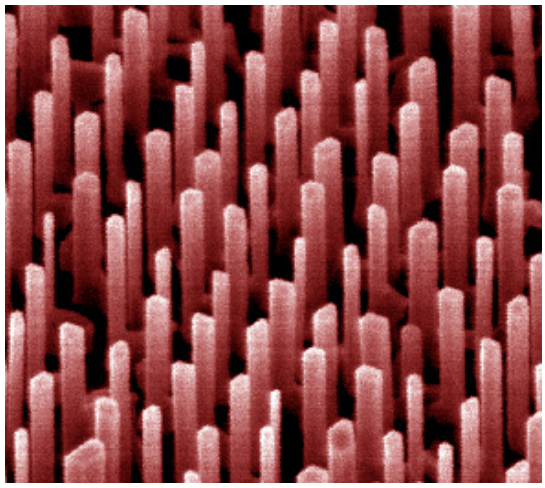

Figure 2.3: Regularly arranged ZnO nanowires [paper III].

Device applications based on ZnO nanowires require reliable p-type ZnO material, which has been a quite hot and controversial topic in ZnO community. Thus, in paper IV an attempt to grow phosphorus-doped nanowires by the VLS process and to characterize their optical properties was made. Based on a single source precursor, Zn_2P_3, single-crystalline phosphorus-doped ZnO nanowires were produced in a reproducible way. Low temperature PL spectra showed that the presence of phosphorus strongly enhances a peak at 3.316 eV (see Fig. 2.4). However, the amphoteric nature of compensating native defects makes it difficult to realize stable and reliable p-type doping in ZnO nanowires.

In paper V and VI, reactivity of ZnO nanowires with solid or vapor phase reactants are examined. In particular, the chemical reaction between ZnO and Al_2O_3, and Al-O vapor shell are investigated, respectively. By varying the reaction temperature and the thickness of the alumina shell around the ZnO nanowire it is revealed that the nanoscale Kirkendall effect plays an important role for the formation of $ZnAl_2O_4$ nanotubes. The Kirkendall effect refers to the different diffusion fluxes of atom/molecules moving in opposite direction. The difference in flux is taken up by vacancies which may then condense into "Kirkendall voids" [Yan08]. An example is shown in Fig. 2.5a. Both cation and anion species of ZnO were effectively mobile towards the alumina shell. In case of an alumina vapor-ZnO nanowire reaction, highly symmetric structures consisting of nanocrystals of $ZnAl_2O_4$ were produced instead of hollow structures. The resulting morphology is understood by taking into account surface diffusion of ZnO and thermal instability of the wire

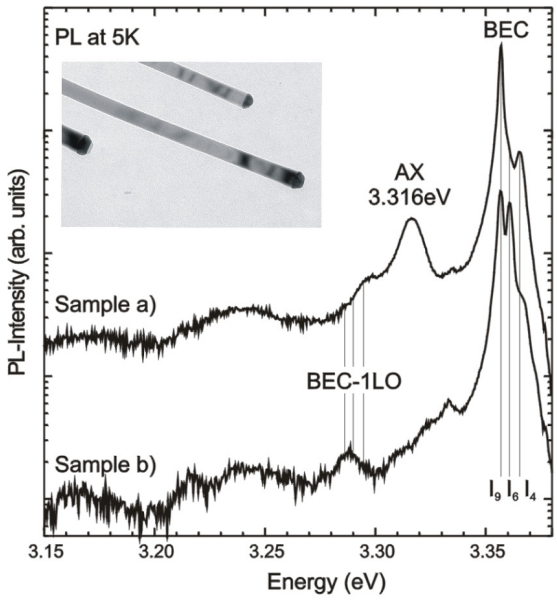

Figure 2.4: PL of phosphorus-doped (inset, a TEM image) and undoped ZnO nanowires [paper IV].

body at high temperatures. See Fig. 2.5b.

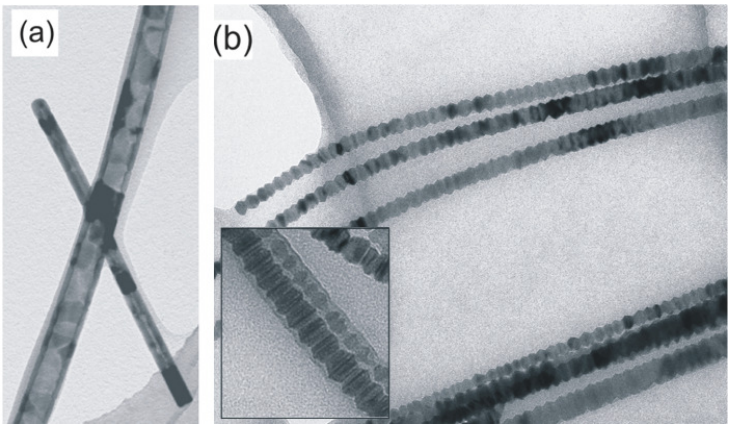

Figure 2.5: a) TEM image of $ZnAl_2O_4$ nanotubes, b) highly symmetric ZnO nanowires after reaction with Al-O vapors [paper V and VI].

In paper VII, by atomic layer deposition ZnO layers were grown on either chemically inert or hydrophilic template surfaces. While smooth and continuous ZnO layers were deposited on alumina coated carbon nanotubes (Fig. 2.6a), irregular forms of ZnO layers were synthesized on bare carbon nanotubes (see Fig. 2.6b). Furthermore, PL of ZnO deposited directly on carbon nanotubes show an unusual emission shifted to the orange spectral range.

In contrast, ZnO on alumina/carbon nanotubes show the typical PL behavior of ZnO, i.e., a broad green emission with an UV band, which indicates that high quality ZnO was successfully deposited on alumina coated carbon nanotubes whereas direct deposition of ZnO on carbon nanotubes did not lead to a high quality ZnO coating.

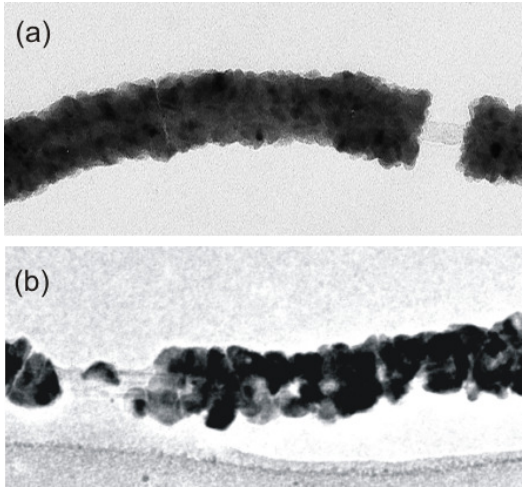

Figure 2.6: TEM image of ZnO-alumina/carbon nanotube (a) and ZnO-carbon nanotube (b) [paper VII].

Without any intentional doping ZnO shows n-type conductivity due to intrinsic native point defects. In the last part, the influence of the relative content of residual oxygen during wire growth on the physical properties of the nanowire is studied by means of electrical transport as well as by photoluminescence. This part of the work was performed in cooperation with R.T. Weitz, H. Klauk, and M. Burghard (Max Planck Institute for Solid State Research, Stuttgart) and J.-P. Richters and T. Voss (the Institute of Solid-State Physics, University of Bremen) [Kim09].

ZnO nanowires that had been grown under either comparably oxygen poor (OP) or oxygen rich (OR) conditions both showed a gate-source voltage dependence of the current flowing through the channel when investigated in a FET-configuration. The FETs based on ZnO nanowires grown under comparably oxygen poor conditions showed, however, a higher on-state current in the transfer characteristics. The origin of this higher on-state current will be discussed by taking into account the relatively high amount of n-type defect density in the ZnO nanowires grown under comparably oxygen poor conditions, which is attributed to the low formation energy of oxygen vacancies. Furthermore the relative free carrier

densities are roughly estimated based on the intensity ratio between the surface exciton (SX) emission and the bound exciton emission.

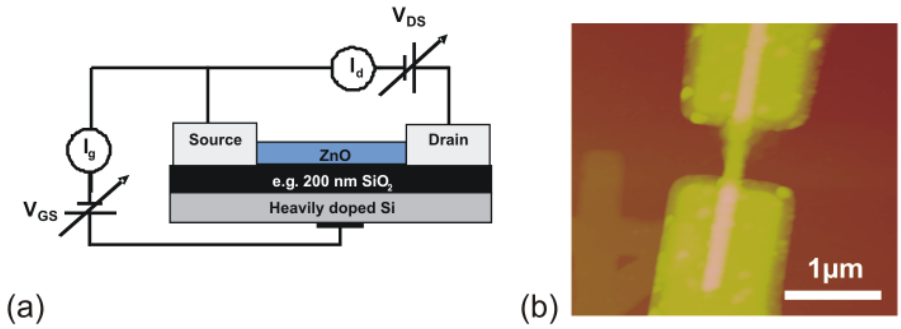

Figure 2.7: (a) Schematic depiction of the FET device and (b) AFM image of the ZnO nanowire-FET with a channel length of L $\approx$ 0.8 μm and diameter of 86 nm. Al was used as source and drain electrode. Contacting was performed at MPI Solid State Research, Stuttgart.

In order to evaluate the conductivity of the respective wires, The FETs of both wires of type-OP and -OR were fabricated. The nanowires were deposited onto silicon dioxide-coated highly doped silicon substrates and contacted with aluminum electrodes. A schematic of the device geometry is shown in Figure 2.7a, an atomic force microscopy (AFM) image of a ZnO nanowire FET is shown in Figure 2.7b.

A detailed description of the wire growth method can be found in paper I. The relative content of oxygen was controlled by adjusting the Ar flow rate instead of the oxygen flow rate since wire growth events were completely stopped even with the low oxygen flow rate of about 2sccm along with an Ar flow rate of 30 sccm. This is partly due to the oxidation of the graphite powder prior to catalyzing the ZnO power. The ZnO nanowires grown under Ar flow of 30 sccm are denoted as wires-OP whereas the nanowires grown with a 20 sccm flow rate are denoted as wires-OR. It is worth noting the flow rate of Ar is a critical factor for the growth of ZnO nanowires. Growth of ZnO nanowires was strongly suppressed when an Ar flow rate of 50 sccm was maintained during wire growth.

PL investigations were carried out in a liquid helium bath cryostat at 5 K. A HeCd laser excited the sample with a wavelength of 325 nm and an excitation density of 100 mW/cm^2. Figure 2.8 shows the electrical characteristics of the FETs fabricated from the wires grown under comparably oxygen poor (Figure 2.8a) and comparably oxygen rich (Figure 2.8b)

conditions. From the transfer characteristics (Figure 2.8a (left)) of the wire-OP and wire-OR (Figure 2.8b) it can be deserved that both types of wires can be utilized for the fabrication of FETs, as they both show a dependence of the drain current on the gate-source voltage. While the modulation ratio of the drain current (ON/OFF ratio) for the FET based on the wire-OP is 10^7, it is only 10^4 in the FET based on the wire-OR. The FET based on the wire-OP has a transconductance of 0.7 μS and a subthreshold swing of 200 mV/dec. It is noticeable, that while the maximum current of FET-OP at a drain-source voltage of 2 V (taken from the output curve shown in Figure 2.8a (right)) is about 0.6 μA, it is only about 0.02 μA at the same V_{DS} in wire-OR (Figure 2.8b).

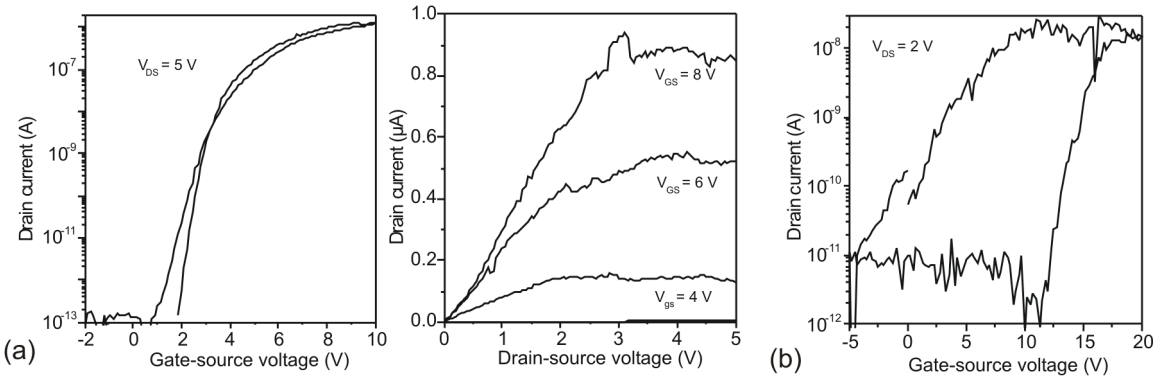

Figure 2.8: Transfer (left) and output (right) characteristics of wire-OP. (b) Transfer characteristics of wire-OR. Both wires were contacted with 80 nm of aluminum and measured under ambient conditions.

The observed higher on-state current in the wire grown under relatively oxygen poor conditions can have multiple origins. It is well-known that the on-current of a FET is related to the carrier concentration in the semiconductor [Sze81]. One possible explanation for the higher on-current in the wires grown under comparably oxygen poor conditions with respect to the wires grown under oxygen rich conditions could be a higher density of electrons in the wires OP. Since it is not possible to reliably determine the doping density in the wires from a two-terminal measurement, alternative approaches must be found. One possibility to gain insight into the charge carrier concentration of a material is photoluminescence.

Recently, an enhanced surface excitonic emission (SX) in PL spectra of ZnO nanowires

coated with a polymer and Al_2O_3 layers was reported [Ric08a, Ric08b]. The coated layers act as an effective dielectric medium and screen the surface states of the ZnO nanowires. This leads to a lowered effective band bending. A reduced band bending results in a high probability of forming excitons near the surface and increases the relative intensity of the SX emission with respect to the donor-bound exciton (D^0X) emission. The higher carrier concentration in ZnO nanowires may also lead to a similar trend (i.e., enhanced intensity of SX compared to that of D^0X) in the PL spectra. Due to the decreased extension of the depletion space charge layer, the overlap probability of electron and hole wave functions in the vicinity of the surface should be enhanced.

Figure 2.9 shows the normalized near band-edge spectra of wires grown under comparably oxygen poor or oxygen rich conditions at 5 K. The spectra of wires-OR and OP are dominated not only by sharp D^0X emission lines at 3.356 eV but also show a surface exciton (SX) band at about 3.365 eV [Wis06]. At the lower energy side of the spectrum, one additional small feature is observed, the broad peak at about 3.31 eV. This peak also appeared in phosphorus doped ZnO nanowires [Kim07] and undoped ZnO powder samples [Fal07]. Recently it was assigned to electron-acceptor transitions (e,A^0) where stacking faults were involved in the recombination based on low temperature cathodoluminescence study [Sch08]. Apparently, the relative intensity of the SX emission is stronger in wires-OP compared to that of the wires-OR. Thus, one can argue that the relative carrier density in wires-OP is higher than that in wires-OR although quantitative values for both wires are unknown.

In ZnO, a large O-deficient nonstoichiometry is present regardless of the growth conditions. Such deficiency has been attributed to either the O vacancy or the Zn interstitial. Based on a first-principles calculation it was, however, predicted that these intrinsic defects lead only to moderate carrier concentration due to the deep level nature of the O vacancy and an insufficient density of the Zn interstitials [Lan07]. Thus, free carrier densities of the 10^{17} - 10^{19} cm^{-3}, which are typically observed in ZnO, can not attributed to intrinsic defects [Hal05]. Alternatively, persistent photoconductivity caused by the O vacancy through the optical $V_0 \rightarrow V_0^+ + e$ and $V_0^+ \rightarrow V_0^{2+} + e$ excitation was suggested to account for the high carrier concentration in ZnO [Lan07]. Since O vacancies can be present in a concentration of about 10^{20} cm^{-3} under equilibrium conditions the above proposed model is likely to

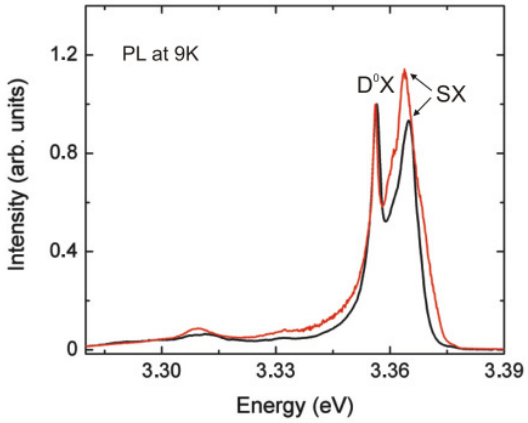

Figure 2.9: Photoluminescence of ZnO nanowires grown under comparably oxygen poor (red) and oxygen rich (black) conditions. The spectra are normalized to their respective D^0X peak intensity at 3.356 eV.

account for the observed free carrier concentration in ZnO.

The density of O vacancies can be varied depending on growth conditions. For instance, the calculated defect formation energy of O vacancies was lower in oxygen poor condition [Lan07]. Thus, it is expected that the density of O vacancies is higher in wires-OP. In other words, the free carrier concentration in wires-OP is supposed to be higher than that in wires-OR. It was also experimentally shown that the oxygen partial pressure during growth is able to modulate the free carrier density in ZnO film by more than three order magnitudes [Xio02].

These results demonstrate that the point defect density can be tuned during nanowire growth and such effects have to be considered for ZnO nanowires based electronic and optoelectronic applications.

In the present cumulative thesis various forms of ZnO related nanowires or nanotubes were grown or fabricated by various reactions. The growth and reaction mechanisms were investigated and clarified and physical properties of these one-dimensional nanostructures were determined. The results presented contribute to a deeper understanding of the growth mechanisms and electronic and optical properties of ZnO-related nanostructures.

References

[Ase03] A. Asenov, A. R. Brown, J. H. Davies, S. Kaya, and G. Slavcheva, Simulation of intrinsic parameter fluctuations in decananometer and nanometer-scale MOSFETs. *IEEE Trans. Electron Devices*, **50**, 1837 (2003).

[Bek07] C. Bekeny, T. Voss, B. Hilker, J. Gutowski, R. Hauschild, H. Kalt, B. Postels, A. Bakin, A. Waag, Influence of ZnO seed crystals and annealing on the optical quality of low-temperature grown ZnO nanorods. *J. Appl. Phys.*, **102**, 044908 (2007).

[Bie08] M. J. Bierman, Y. K. Albert Lau, A. V. Kvit, A. L. Schmitt, S. Jin, Dislocation-driven nanowire growth and eshelby twist. *Science*, **320**, 1060-1063 (2008).

[Bjo02] M.T. Björk, B.J. Ohlsson, C. Thelander, A.I. Persson, K. Deppert, L. R. Wallenberg, L. Samuelson, Nanowire resonant tunneling diodes. *Appl. Phys. Lett.*, **81**, 4458-4460 (2002).

[Boo71] G. A. Bootsma, H. J. Gassen, A quantitative study on the growth of silicon whiskers from silane and germanium whiskers from germane. *J. Cryst. Growth*, **10**, 223-234 (1971).

[Cui01] Y. Cui, C. M. Lieber, Functional nanoscale electronicdevices assembled using silicon nanowire building blocks. *Science*, **291**, 851-853 (2001).

[Day07] S. A. Dayeh, E. T. Yu, D. Wang, III-V nanowire growth mechanism: V/III ratio andtemperature effects. *Nano Lett.*, **7**, 2486-2490 (2007).

[Dua00] X. Duan and C. M. Lieber, General synthesis ofcompound semiconductor nanowires. *Adv. Mater.*, **12**, 298-302 (2000).

[Dub05] V. G. Dubrovskii, G. E. Cirlin, I. P. Soshnikov, A. A. Tonkikh, N. V. Sibirev, Yu. B. Samsonenko, V. M. Ustinov, Diffusion-induced growth of GaAs nanowhiskers during molecular beam epitaxy: theory and experiment. *Phys. Rev. B*, **71**, 205325 (2005).

[Fan06] H. J. Fan, P. Werner, M. Zacharias, Semiconductor nanowires: from self-organization to patterned growth. *Small*, **2**, 700-717 (2006).

[Fal07] J. Fallert, R. Hauschild, F. Stelzl, A. Urban, M. Wissinger, H. Zhou, C. Klingshirn, H. Kalt, Surface-state related luminescence in ZnO nanocrystals. *J. Appl. Phys.*, **101**, 73506 (2007).

[Fra03] S. De Franceschi, J.A. van Dam, E.P.A.M. Bakkers, L.F. Feiner, L. Gurevich, L.P. Kouwenhoven, Single-electron tunneling in InP nanowires. *Appl. Phys. Lett.*, **83**, 344-346 (2003).

[Giv87] E. I. Givargizov, *Highly anisotropic crystals* Dordrecht, Reidel, (1987).

[Han06] J. B. Hannon, S. Kodambaka, F. M. Ross, R. M. Tromp, The influence of the surface migration of gold on the growth of silicon nanowires. *Nature*, **440**, 69-71 (2006).

[Hal05] L. E. Halliburton, N. C. Giles, N. Y. Garces, M. Luo, C. Xu, L. Baic, L. A. Boatner, Production of native donors in ZnO by annealing at high temperature in Zn vapor. *Appl. Phys. Lett.*, **87**, 172108 (2005).

[Hau06] R. Hauschild, H. Kalt, Guided modes in ZnO nanorods. *Appl. Phys. Lett.*, **89**, 123107 (2006).

[Hir95] K. Hiruma et al., Growth and optical properties of nanometer-scale GaAs and InAs whiskers. *J. Appl. Phys.*, **77**, 447 (1995).

[Jen04] L. E. Jensen, M. T. Bjork, S. Jeppesen, A. I. Persson, B. J. Ohlsson, L. Samuelson, Role of surface diffusion in chemical beam epitaxy of InAs nanowires. *Nano Lett.*, **4**, 1961-1964 (2004).

[Kam01] T. I. Kamins, R. S. Williams, D. P. Basile, T. Hesjedal, J. S. Harris, Ti-catalyzed Si nanowires by chemical vapor deposition: Microscopy and growth mechanisms. *J. Appl. Phys.*, **89**, 1008 (2001).

[Kim07] D.S. Kim, J. Fallert, A. Lotnyk, R. Scholz, E. Pippel, S. Senz, H. Kalt, U. Gsele, M. Zacharias, Growth and optical properties of phosphorus-doped ZnO nanowires. *Solid State Commun.*, **143**, 570 (2007).

[Kim08] D.S. Kim, R. Scholz, U. Gösele, M. Zacharias, Gold at the root or at the tip of ZnO nanowires: A model. *Small*, **4**, 1615 (2008).

[Kim09] D.S. Kim, R.T. Weitz, J. Richters, H. Klauk, M. Burghard, T. Voss, R. Scholz, K. Kern, M. Zacharias, U. Gösele, Defect engineering of ZnO nanowires for field effect transistors. *In preparation*.

[Kod07] S. Kodambaka, J. Tersoff, M. C. Reuter, F. M. Ross, Germanium nanowire growth below the eutectic temperature. *Science*, **316**, 729-732 (2007).

[Lan07] S. Lany, A. Zunger, Dopability, Intrinsic conductivity, and nonstoichiometry of transparent conducting oxides. *Phys. Rev. Lett.* **98**, 045501 (2007).

[Lau02] L. J. Lauhon, M. S. Gudiksen, D. Wang, C. M. Lieber, Epitaxial coreshell and coremultishell nanowire heterostructures. *Nature*, **420**, 57-61 (2002).

[Lee84] J. Lee, H. N. Spector, Hydrogenic impurity states in a quantum well wire. *J. Vac. Sci. Technol. B*, **2**, 16-20 (1984).

[Li05] H. Li, A. H. Chin, M. K. Sunkara, Direction-dependent homoepitaxial growth of GaN nanowires. *Adv. Mater.*, **18**, 216-220 (2005).

[Li07] H.-Y. Li, O. Wunnicke, M. T. Borgström, W. G. G. Immink, M. H. M. van Weert, M. A. Verheijen, E. P. A. M. Bakkers, Remote p-doping of InAs nanowires. *Nano Lett.*, **7**, 11441148 (2007).

[Lin05] P. Ling, K. K. Lew, J. M. Redwing, and E. Dickey, Effect of diborane on the microstructure of boron-doped silicon nanowires. *J. Cryst. Growth*, **277**, 428 (2005).

[Mas90] T. B. Massalski, H. Okamoto, P.R. Subramanian, L. Kacprzak, *Binary Alloy Phase Diagrams*, Volume 1. ASM International, Materials Park, Ohio, 2nd edition, 1990.

[Min07] E. D. Minot, F. Kelkensberg, M. van Kouwen, J. A. van Dam, L. P. Kouwenhoven, V. Zwiller, M. T. Borgström, O. Wunnicke, M. A. Verheijen, E. P. A. M. Bakkers, Single quantum dot nanowire LEDs. *Nano Lett.*, **7**, 367-371, (2007).

[Nob05] J. Noborisaka, J. Motohisa, T. Fukui, Catalyst-free growth of GaAs nanowires by selective-area metalorganic vapor-phase epitaxy. *Appl. Phys. Lett.*, **86**, 213102 (2005).

[Oh08] S. H. Oh, K. v. Benthem, S. I. Molina, A. Y. Borisevich, W. Luo, P. Werner, N. D. Zakharov, D. Kumar, S. T. Pantelides, S. J. Pennycook, Point defect configurations of supersaturated Au atoms inside Si nanowires. *Nano Lett.*, **8**, 10161019 (2008).

[Ozg05] U. Özgür, Y.I. Alivov, C. Liu, A. Teke, M.A. Reshchikov, S. Dogan, V. Avrutin, S.-J. Cho, H. Morkoc, A comprehensive review of ZnO materials and devices. *J. Appl. Phys.*, **98**, 041301 (2005).

[Par02] W. I. Park, D. H. Kim, S.-W. Jung, G.-C. Yi, Metalorganic vapor-phase epitaxial growth of vertically well-aligned ZnO nanorods. *Appl. Phys. Lett.*, **80**, 4232 (2002).

[Ric08a] J.-P. Richters, T.Voss, L.Wischmeier, I. Rckmann, J. Gutowski, Influence of polymer coating on the low-temperature photoluminescence properties of ZnO nanowires. *Appl. Phys. Lett.*, **92**, 011103 (2008).

[Ric08b] J.-P. Richters, T. Voss, D. S. Kim, R. Scholz, M. Zacharias, Enhanced surface-excitonic emission in ZnO/$Al_2 2O_3$ coreshell nanowires. *Nanotechnology*, **19**, 305202 (2008).

[Sea53] G. W. Sears, Mercury whiskers. *Acta Metal*, **1**, 457-459 (1953).

[Sch05] V. Schmidt, S. Senz, U. Gösele, Diameter-dependent growth direction of epitaxial silicon nanowires. *Nano Letters*, **5**, 931-935 (2005).

[Sch06] V. Schmidt, H. Riel , S. Senz , S. Karg , W. Riess , U. Gösele, Realization of a silicon nanowire vertical surround-gate field-effect transistor. *Small*, **2**, 85-88 (2006)

[Sch04] L. Schubert, P. Werner, N. D. Zakharov, G. Gerth, F. M. Kolb, L. Long, U. Gösele, Silicon nanowhiskers grown on (111) Si substrates by molecular beam epitaxy. *Appl. Phys. Lett.*, **84**, 4968-4970 (2004)

[Sch08] M. Schirra, R. Schneider, A. Reiser, G. M. Prinz, M. Feneberg, J. Biskupek, U. Kaiser, C. E. Krill, K. Thonke, R. Sauer, Stacking fault related 3.31 eV luminescence at 130 meV acceptors in zinc oxide. *Phys. Rev. B*, **77**, 125215 (2008)

[Sze81] S. M. Sze, *Physics of Semiconductor Devices, 2nd ed.* (Wiley, New York, 1981)

[The03] C. Thelander, T. Martensson, M.T. Bjöork , B.J. Ohlsson, M.W. Larsson, L. R. Wallenberg, L. Samuelson, Single-electron transistors in heterostructure nanowires. *Appl. Phys. Lett.*, **83**, 2052-2054, (2003).

[The06] C. Thelander, P. Agarwal, S. Brongersma, J. Eymery, L.F. Feiner, A. Forchel, M. Scheffler, W. Riess, B.J. Ohlsson, U. Gösele, L. Samuelson, Nanowire-based one-dimensional electronics . *Mater. Today*, **9**, 28-35, (2006).

[Tut06] E. Tutuc, J. Appenzeller, M. C. Reuter, S. Guha, Realization of a linear germanium nanowire p-n junction. *Nano Lett.*, **6**, 2070 (2006).

[Wag64] R. S. Wagner, W. C. Ellis, Vapor-liquid-solid mechanism of single crystal growth. *Appl. Phys. Lett.*, **4**, 89-90 (1964).

[Wal89] W. Walukiewicz, Amphoteric native defects in semiconductors. *Appl. Phys. Lett.*, **54**, 2094 (1989).

[Wan01] J. Wang, M. S. Gudiksen, X. Duan, Y. Cui, C. M. Lieber, Highly polarized photoluminescence and photodetection from single indium phosphide nanowires. *Science*, **293**, 1455-1457 (2001).

[Wan04] D. Wang, F. Qian, C. Yang, Z. Zhong, C. M. Lieber, Rational growth of branched and hyperbranched nanowire structures. *Nano Lett.*, **4**, 871 -874 (2004).

[Wan06] Y. Wang, V. Schmidt, S. Senz, U. Gösele, Epitaxial growth of silicon nanowires using an aluminium catalyst. *Nat. Nanotechnol.*, **1**, 186-189 (2006).

[Wis06] L. Wischmeier, T. Voss, I. Rückmann, J. Gutowski, A. C. Mofor, A. Bakin, A. Waag, Dynamics of surface-excitonic emission in ZnO nanowires. *Phys. Rev. B*, **74**, 195333 (2006).

[Wu00] Y. Wu, P. Yang, Germanium nanowire growth via simple vapor transport. *Chem. Mater.*, **12**, 605-607 (2000).

[Wu02] Y. Wu, R. Fan, P. Yang, Block-by-block growth of single-crystalline Si/SiGe superlattice nanowires. *Nano Lett.*, **2**, 83-86 (2002).

[Xio02] G. Xiong, J. Wilkinson, B. Mischuck, S. Tuzemen, K. B. User, and R. T. Williams, Control of p- and n-type conductivity in sputter deposition of undoped ZnO. *Appl. Phys. Lett.*, **80**, 1195 (2002).

[Yan08] Y. Yang, D.S. Kim, M. Knez, R. Scholz, A. Berger, E. Pippel, U. Gösele, M. Zacharias, Kirkendall effect induced evolution of coaxial ZnO/$Al_2 2O_2$ one-dimensional heterostructures: from core-shell nanowires to spinel nanotubes and mesoporous nanowires. *J. Phys. Chem. C*, **112**, 4068-4074 (2008).

Acknowledgments

First of all I would like to thank my supervisor, Prof. U. Gösele, for his support, for his critical comments and suggestions, and kind advice. Prof. M. Zacharias has aided me in numerous ways, such as in providing encouraging and collaborative environment.

The papers involved in this cumulative thesis resulted from several collaborations. The detailed contributions can be found in front of each of the appended papers. I would like to sincerely thank each of my collaborators. Above all, I thank Dr. Y. Yang (MPI-Halle) and Dr. H.J. Fan (MPI-Halle and later Cambridge University and Nanyang Technological University) for the work and discussions on spinel nanowires and nanotubes. I am indebted to J. Fallert (Universität Karlsruhe), J. Richters (University of Bremen), and Dr. T. Voss (University of Bremen) for optical characterizations and productive discussions on P-doped and undoped ZnO nanowires. I would also like to thank the group at the MPI of Solid State Research in Stuttgart. T. Weitz aided me to demonstrate FET devices and to measure numerous samples. Dr. W. Erfurth and H. Hofmeister of MPI-Halle have been instrumental in running of SEM and TEM, respectively. Dr. R. Scholz also performed numerous TEM investigations, and I thank them sincerely. Of course, I thank many others who helped in one way or the other, but are not mentioned here by name.

Finally, I would like to thank my wife, a source of constant support and encouragement, and my daughter Sabin.

Eidesstattliche Erklärung

Hiermit erkläre ich, dass ich meine Dissertation selbständig und ohne fremde Hilfe verfasst und keine anderen als die von mir angegebenen Quellen und Hilfsmittel zur Erstellung meiner Dissertation verwendet habe. Den benutzten Werken wörtlich oder inhaltlich entnommene Stellen sind als solche gekennzeichnet.

Dong Sik Kim,

Halle (Saale), January 5, 2009

Curriculum Vitae

First Name:	Dong Sik
Last Name:	Kim
Date of Birth:	8 August 1977
Nationality:	Korean
Sex:	Male
Marital Status:	Married

Education

03/96-02/03	Kyungpook National University, Daegu, Korea B.S. in Physics
03/03-02/05	Gwangju Institute of Science and Technology, Gwangju, Korea M.S. in Materials Science and Engineering Thesis: "Carbon nanotubes: preparation of individual single-walled carbon nanotubes and their modification for electronic structure control" Advisor: Prof. Kurt E. Geckeler
since 10/05	Martin Luther University Halle-Wittenberg, Halle, Germany Doctorate student at the Institute of Physics
since 10/05	Doctorate study at Max Plank Institute of Microstructure Physics Thesis: "Growth and characterization of ZnO nanowires" Advisor: Prof. U. Gösele

List of Publications

1) D. Nepal, D.S. Kim, K. E. Geckeler, A facile and rapid purification method for single-walled carbon nanotubes. *Carbon*, **43**, 660 (2005).

2) D.S. Kim, D. Nepal, K. E. Geckeler, Individualization of single-walled carbon nanotubes: is the solvent important? *Small*, **1**, 1117 (2005).

3) D.S. Kim, T. Lee, K. E. Geckeler, Hole-doped single-walled carbon nanotubes: ornamenting with gold nanoparticles in water. *Angew. Chem. Int. Ed.*, **45**, 104 (2006).

4) T. Premkumar, D.S. Kim, K. Lee, K. E. Geckeler, Polysorbate 80 as a tool: synthesis of gold nanoparticles. *Macromol. Rapid Commun.*, **27**, 1346 (2006).

5) T. Premkumar, D.S. Kim, K. Lee, K. E. Geckeler, A facile and efficient "One-Step" synthesis of gold nanoparticles with tunable size. *Gold Bull.*, **40**, 321-327 (2007).

6) D.S. Kim, R. Ji, H. J. Fan, F. Bertram, R. Scholz, R. Dadgar, K. Nielsch, A. Krost, J. Christen, U. Gösele, and M. Zacharias, Laser-interference lithography tailored for highly symmetrically arranged ZnO nanowire arrays. *Small*, **3**, 76 (2007).

7) D.S. Kim, R. Scholz, U. Gösele, M. Zacharias, Gold at the root versus at the tip of ZnO nanowires: A model. *Small*, **4**, 1615-1619 (2008).

8) D.S. Kim, J. Fallert, A. Lotnyk, R. Scholz, E. Pippel, S. Senz, H. Kalt, U. Gösele, M. Zacharias, Growth and optical properties of phosphorus-doped ZnO nanowires. *Solid State Commun.*, **143**, 570 (2007).

9) Y. Yang, D.S. Kim, M. Knez, R. Scholz, A. Berger, E. Pippel, U. Gösele, M. Zacharias, Kirkendall effect induced evolution of coaxial ZnO/$Al_2 2O_2$ one-dimensional heterostructures: from core-shell nanowires to spinel nanotubes and mesoporous nanowires. *J. Phys. Chem. C*, **112**, 4068-4074 (2008).

10) Y. Yang, D.S. Kim, R. Scholz, M. Knez, S.-M. Lee, U. Gösele, M. Zacharias, Hierarchical three-dimensional ZnO and their shape-preserving transformation into hollow $ZnAl_2O_4$ nanostructures. *Chem. Mater.*, **20**, 3487-3494 (2008).

11) H.J. Fan, A. Lotnyk, R. Scholz, Y. Yang, D.S. Kim, E. Pippel, D. Hesse, M. Zacharias, Surface reaction of ZnO nanowires with electron-beam generated alumina vapor. *J. Phys. Chem. C*, **112**, 6770-6774 (2008).

12) D.S. Kim, S.-M. Lee, R. Scholz, M. Knez, U. Gösele, J. Fallert, H. Kalt, M. Zacharias, Synthesis and optical properties of ZnO and carbon nanotube based coaxial heterostructures. *Appl. Phys. Lett.*, **93**, 103108/1-3 (2008).

13) J.-P. Richters, T. Voss, D.S. Kim, R. Scholz, M. Zacharias, Enhanced surface-excitonic emission in ZnO/$_2O_3$ core-shell nanowires. *Nanotechnology*, **19**, 305202 (2008).

14) K. Subannajui, D.S. Kim, M. Zacharias, Electrical analysis of individual ZnO nanowires. *J. Appl. Phys.*, **104**, 014308/1-6 (2008).

15) D.S. Kim, U. Gösele, M. Zacharias, Surface diffusion induced growth of ZnO nanowires. *Journal of Crystal Growth*, **311**, 3216 (2009).

16) Y. Yang, R. Scholz, A. Berger, D.S. Kim, M. Knez, D. Hesse, U. Gösele, M. Zacharias, TEM in-situ fabrication of ZnO/Al_2O_3 composite nanotubes by electron-beam irradiation induced local etching of ZnO/Al_2O_3 core-shell nanowires. *Small*, **4**, 2112-2117 (2008).

17) A. Pan, L. Yao, Y. Qin, Y. Yang, D. S. Kim, R. Yu, B. Zou, P. Werner, M. Zacharias, U. Gösele, Si-CdSSe core/shell nanowires with continuously tunable light emission. *Nano Letters*, **8**, 3414-3417 (2008).

18) J. Fallert, F. Stelzl, H. Zhou, M. Wissinger, M. Hauser, C. Klingshirn, H. Kalt, D. S. Kim, M. Zacharias, A. Reiser, K. Thonke, R. Sauer, Dynamics of stimulated emission in single ZnO nanorod resonators. *J. Korean Phys. Soc.*, **53**, 2840-2843 (2008)

Papers

Paper I

Gold at the root or at the tip of ZnO nanowires: A model

D. S. Kim, R. Scholz, U. Gösele, M. Zacharias, *Small* **4**, 1615 (2008)

Growth habits of ZnO nanowires nucleated from predefined Au particles on planar substrates or on nanowire backbones are presented. Depending on ZnO supply conditions, Au particles were observed either at the root for planar substrates or the tip for wires nucleated from nanowire backbones. A model is presented explaining the seemingly contradicting observations.

The author of this thesis (D.S.Kim) performed all growth experiments and wrote the paper. The TEM investigations were done by R. Scholz.

ZnO nanowires

DOI: 10.1002/smll.200800060

Gold at the root or at the Tip of ZnO Nanowires: A Model**

Dong Sik Kim, Roland Scholz, Ulrich Gösele, and Margit Zacharias*

Semiconducting nanowires have many unique features that are required for potential applications in future electronics and optoelectronics. Nanowires with reliable functionality can be incorporated into advanced electronic devices. Much effort has been devoted to engineering nanowire properties, for example, to achieve segmented doping along a nanowire and precise controlling over interfaces within a heterostructure nanowire.[1,2] A quantitative understanding of nanowire growth is of particular importance for better control of nanowire properties. Several investigations have shown some unexpected aspects of growth behavior. For instance, the dynamic reshaping of catalyst particles during nanowire growth determines the length and shape of Si nanowires.[3,4] A self-oscillation process results in the irregular morphology of nanowires.[5] Most nanowires are grown by the vapor–liquid–solid (VLS) process, however, in some cases a solid catalytic metal particle is also assisting the condensation of material into the one-dimensional form.[6,7,8]

Compared to element[9] and III-V semiconductor nanowires[10] the growth behavior of oxide semiconductor nanowires, in particular ZnO — an important functional oxide material with a direct band gap around 3.4 eV and a high exciton binding energy of 60 meV — are not well understood. For Au catalyzed ZnO nanowire growth, Au nanoparticles were not only observed at the tip[11] of the wires, which is typical for Au catalyzed semiconductor nanowire growth, but sometimes also at the root[12] of wires after growth. Such complex and diverse nucleation and growth processes were also found in carbon nanotube formation: growth can occur either at the tip[13] or at the root[14] of the tube, and with a tube diameter that does not necessarily match that of the catalyst particle.[15]

[*] D. S. Kim, Dr. R. Scholz, Prof. U. Gösele
Max Planck Institute of Microstructure Physics
Weinberg 2, 06120 Halle (Germany)
Fax: (+49) 345-551-1223
E-mail: dskim@mpi-halle.de
Prof. M. Zacharias
Faculty of Applied Science (IMTEK), Albert-Ludwigs University Freiburg Georges-Köhler-Allee, 79110 Freiburg (Germany)

[**] This work was supported by the International Max Planck Research School for Science and Technology of Nanostructures (Nano-IMPRS) in Halle. We thank A. Dadgar and A. Krost for supplying GaN/Si substrates and N. Zakharov for useful discussions.

Supporting Information is available on the WWW under http://www.small-journal.com or from the author.

Here we compare the growth behavior of ZnO nanowires nucleated from predefined Au particles on planar substrates or on nanowire backbones in order to get a better quantitative picture of the growth mechanisms. In addition, we study the influence of the surface migration of Au atoms for the epitaxial growth of ZnO nanowires at lattice-matched substrate.

Typical morphologies of ZnO nanowires grown at the SiO_2/Si substrate and the ZnO nanowire backbones are shown in Figure 1a and b, respectively. Here we denote ZnO nanowires grown at the SiO_2/Si substrate as wires A, and ZnO nanowires grown at the ZnO nanowire backbones as wires B. All wires A were grown from the positions of Au colloid particles. In many cases, a number of wires A originated from a single position. Transmission electron microscopy (TEM) investigations reveal that the wires A with a length of several tens of micrometers are terminated by a flat plane (Figure 1c). In all cases, the nucleating Au particles remained at the root of the wires A (see for instance Figure S3 in the Supporting Information). In contrast, for wires B, all nanowire branches end with Au nanoparticles at their tips. There are two kinds of branches: the first kind lifts off from the nanowire backbone (straight branch) and the other kind grows along the surface of the wires (crawling branch) as shown in Figure 1b. Compare also the corresponding TEM images Figure 1d and e. In Figure 1f we show a TEM image of a junction at the nanowire backbone and branch. Figure Figure 1g is the magnified view of the solid line box in Figure 1f. Both, the nanowire backbone and the branch have a preferential growth direction of [0001]. A selected-area diffraction pattern from the junction is shown in Figure 1h confirming the above-mentioned growth direction of the nanowires.

The difference between wires A and B is the position of Au particles in the nanowires: the Au particles are located at the root of wires A but at the tip of wires B. Also the size distribution of the wires A is broader than that of wires B, wires A vary from 20 to 500 nm but wires B only from 50 to 100 nm. (See size-distribution plots of Figure S4 in the Supporting Information.)

In order to explain the differences in modes of growth in the experimental studies, we first concentrate on the nucleation process and then on the subsequent wire growth. We assume that single adsorbed ZnO molecules are the only species that are effectively mobile on the surface. The interactions between the adsorbed ZnO molecules and Au are schematically illustrated in Figure 2. When the nucleation process proceeds in the beginning of the growth stage, the population of adsorbed ZnO molecules changes as a result of the competition between the *arrival* of particles from the incoming flux of ZnO vapor and *loss* by evaporation and deposition on the substrate, and by diffusion capture or direct impingement on the Au particle. Because nucleation events do not take place without the presence of Au on the substrate, the only considerable *loss* is diffusive capture by the Au particles and evaporation. Note that Au atoms have a strong binding affinity to ZnO that results from the polarity of ZnO: the binding energy for Au on the polar surface of ZnO was estimated to be 0.94 eV.[16] In spite of the relatively large misfit of 11%, Au films grow epitaxially on ZnO substrates even at low temperature.[17]

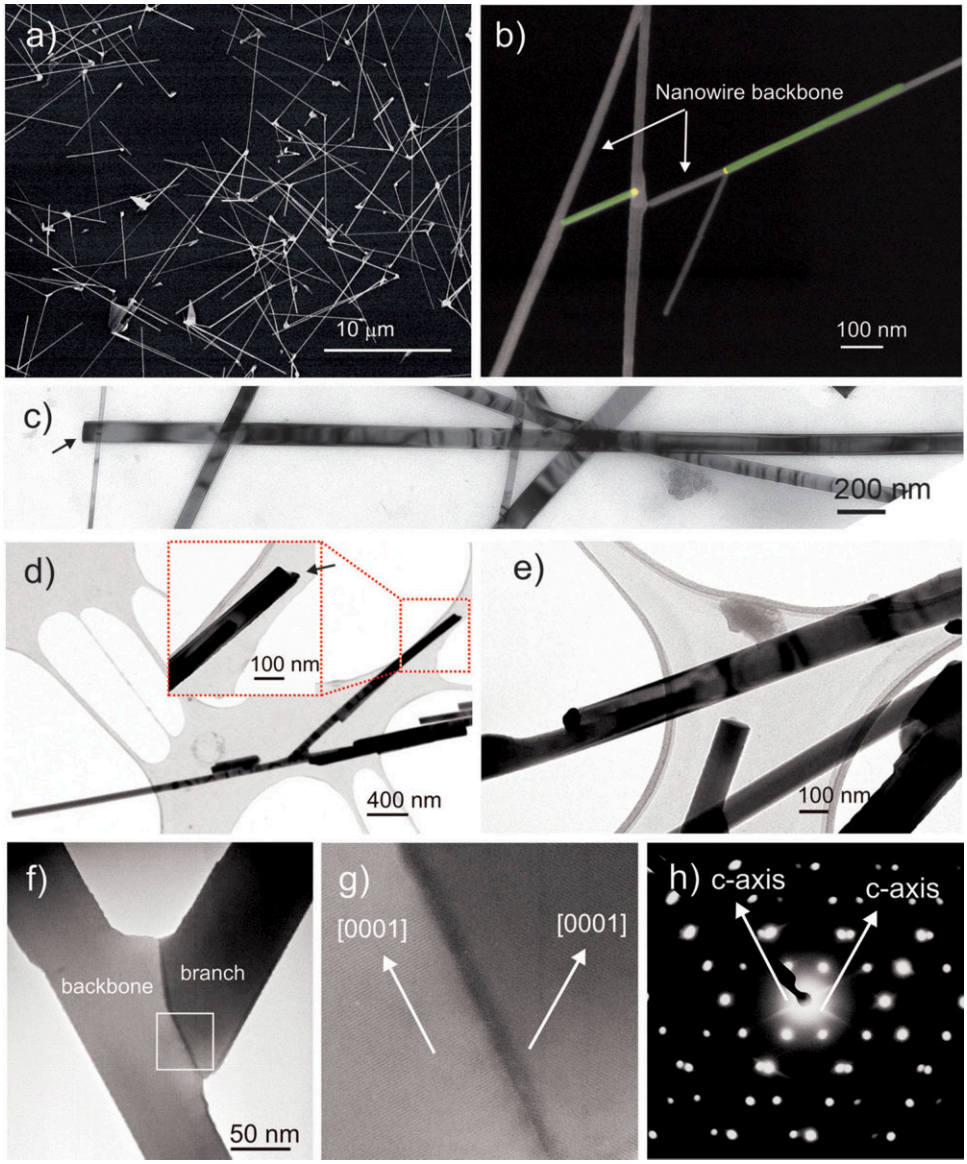

Figure 1. Scanning electron microscopy (SEM) and TEM images of ZnO nanowires grown at SiO_2/Si substrate and nanowire backbones. a) SEM image of wires A. b) SEM image of wires B. Nanowires branches and Au particles in the image are colored in light green and light yellow, respectively. For an original image see Figure S2 in the Supporting Information. c) TEM image of wire A. An arrow indicates the tip of the nanowire. d) TEM image of straight branch. Inset shows a high-magnification image from the tip of wire (dotted line box). An arrow indicates an Au particle. e) TEM image of a crawling branch. f) TEM image at the junction of wire B. g) High-magnification image of junction (solid line box) in Figure 1f. The lattice of a ZnO nanowire backbone and branch is visible and show their growth direction of [0001]. h) Selected-area electron-diffraction pattern recorded from the junction.

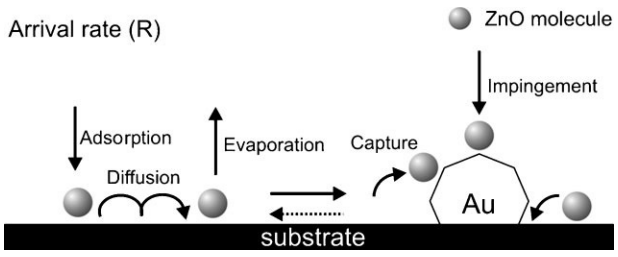

Figure 2. Schematic illustration of nucleation process with the presence of Au particle: ZnO adsorption, evaporation, diffusion, and capture by Au. The arrival rate (*R*) is the experimental variable. The dotted line indicates the process that is less important in this growth mode.

In the regime of the diffusion-induced nanowire growth, the surface of Au particles at the SiO_2/Si substrate become saturated with ZnO during the nucleation process as result of supersaturation, diffusion of adsorbed ZnO molecules, and their affinity to Au. Once Au particles are saturated by ZnO then molecules from the ZnO vapor contribute to the formation of ZnO nuclei since ZnO has unique self-assembly characteristics. ZnO has a tetrahedral fundamental unit cell in which the Zn ions are surrounded tetrahedrally by O ions and vice versa that results from the sp^3 hybridized orbital. Because the normal direction to each plane of the tetrahedron is parallel to the c-axis, ZnO has a preferential orientation toward the c-axis. Accordingly, we found that both 20 and 80 nm Au particles resulted in a similar size distribution

because the size of wires were not dependent on that of the Au particles but is determined by the size of the ZnO nuclei.

Let us now discuss the case of nucleation at Au particles deposited on already existing ZnO nanowires. In this case the only valid pathways for the ZnO molecules are the direct impingement upon the Au particles and the surface diffusion along the pre-existing ZnO nanowire towards the Au particles. Because of the limited supply, the active area of Au particles does not become saturated by ZnO but acts as a preferential adsorption site and promotes the delivery of ZnO molecules to the Au–ZnO nanowire interface. The reduced flux of molecules drives the energetically more favorable epitaxial growth of ZnO layers at the Au–substrate interface with a higher rate (e.g., nucleation rate) than the saturation rate at the surface of the Au particles. Thus wires B grow while keeping the Au particles at the growth front. In Figure 3 the basic steps of the growth modes of wires A and B are shown schematically. In addition, the fluxes of ZnO molecules contributing to the growth of wires A and B are roughly estimated to be about 1.8×10^7 and 2.4×10^6 molecules $\mu m^{-2} \cdot min^{-1}$, respectively, based on the wire volume per unit area. We assume that all incoming vapor was incorporated into the wires either by diffusion or direct impingement without any loss by evaporation.

It is not clear whether Zn or ZnO vapor dominantly contributes to the anisotropic crystal growth in the presence of Au particles.[18] If Zn atoms are considered to be the main species, then Au particles should alloy with Zn and ZnO nanowires should grow with the assistance of liquid catalytic particles, so that the nanowire diameter is determined by the size of the Au particles. The mechanism involved in this catalytic growth is generally referred to as the vapor–liquid–solid (VLS) process.[19] However, the observed growth behavior of ZnO nanowires does not fit the VLS mechanism. The diameter of the nanowires is larger than that of the Au particles as shown in Figure 4. Furthermore, X-ray diffraction (XRD) analyses reveal that the Au particles are solid during ZnO nanowire growth.[20]

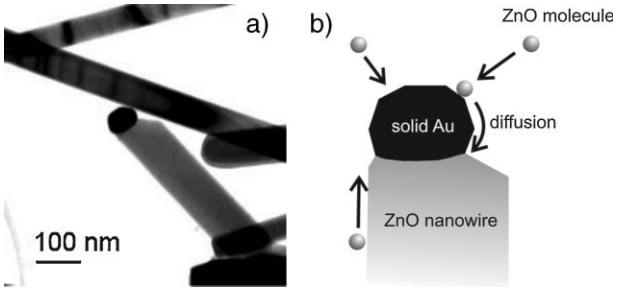

Figure 4. a) TEM image of wire B near tip. b) Schematic illustration of a possible growth mechanism. ZnO vapor sticks to solid Au particle followed by diffusion along the surface and builds up ZnO lattice. Alternatively adatoms of ZnO diffuse along the wire surface and incorporate into growth front.

If ZnO molecules are taken as major vapor-phase constituents, the growth picture of wires B with the assistance of Au particles becomes apparent. It was demonstrated that the metallic Au phase is clearly isolated from the ZnO matrix when the annealing temperature is increased.[21] Also the size of Au particles used in the growth experiments was 50 nm, which excludes a possible liquid phase of Au particles from a size effect.[22] Based on the experimental observations we suggest the growth process illustrated in Figure 4b. ZnO/C source material produces Zn vapor after a carbothermal reduction reaction. During the transportation to the Au particles, the Zn vapor is oxidized by reaction with carbon monoxide and arrives in the form of ZnO molecules.[23] ZnO molecules are incorporated into the growth front by diffusion along the nanowire surface or direct impingement on a Au particle. Therefore, the growth mechanism is slightly different from a typical vapor–solid–solid (VSS) process. From this point of view, the growth mode of ZnO nanowires has different characteristics compared to elemental or III–V semiconductors. With respect to the Au particles that assisted wire growth, initially spherical Au particles become approximately hemispherical and their volume decreases during wire growth. For instance, an Au particle with the volume of 7.4×10^4 nm^3 was reduced to 5.6×10^4 nm^3 after growth. Some Au atoms might have evaporated or migrated along the wires into the substrate.[27]

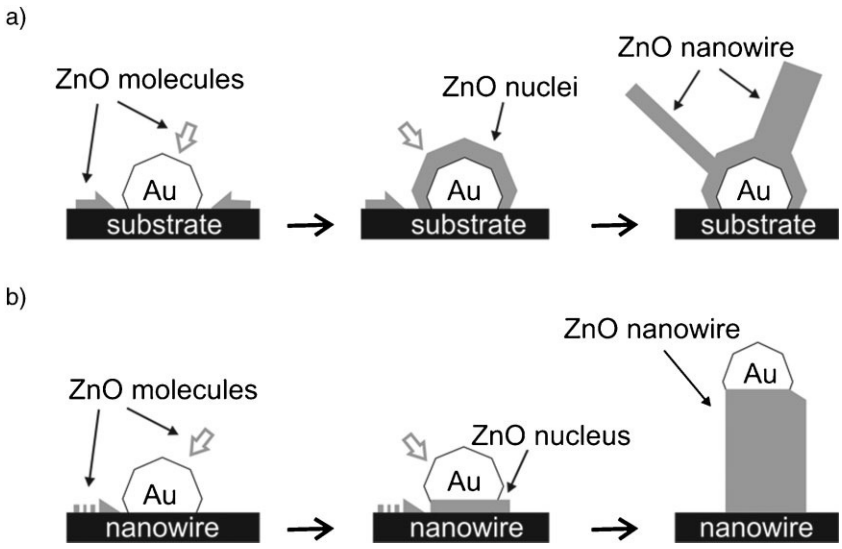

Figure 3. Schematic representation of the basic steps of the growth modes of wires A and B. a) High diffusion flux of adsorbed ZnO molecules (solid arrow) lead to the saturation of ZnO on the Au particle and subsequent formation of ZnO nuclei. Finally ZnO nanowires grow from nuclei. b) Lower flux of adsorbed ZnO molecules (dotted arrow) drives the energetically more favorable ZnO nucleus at the Au–ZnO nanowire interface. Open arrow: direct impingement. The nanowire grows in a layer-by-layer fashion through the reiterative building of successive ZnO layers with assistance of Au particle.

Epitaxial nanowire growth is required for optical studies and device applications such as vertical-surround-gate field-effect transistors. Similar growth condition to

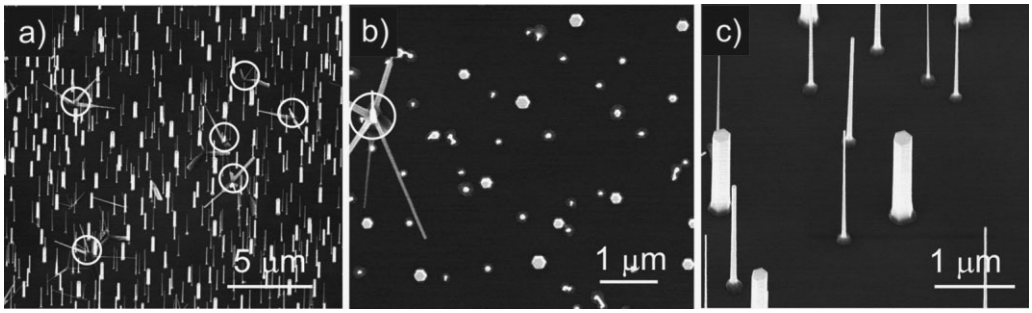

Figure 5. SEM images of epitaxially grown ZnO nanowires on a GaN/Si substrate. a) Low-magnification SEM image. The position of Au particles is marked by a circle. b) Top view of ZnO nanowire grown on a GaN/Si substrate. Hexagonal facets are clearly visible. c) Close view of vertically aligned ZnO nanowires. Nanowires show the developed base shape.

those used for the nonepitaxial growth of wires A on SiO_2/Si substrates was used for epitaxial growth of ZnO nanowires on GaN/Si substrates. As shown in Figure 5, ZnO nanowires are grown not only at the original position of Au particles but also in the surrounding of these positions. Note that this phenomenon was not observed for wires A grown on SiO_2/Si substrates. The phase-mode atomic force microscopy (AFM) image of GaN/Si substrate after deposition of Au particles, followed by annealing at 500 °C with pressure of 1 mbar for 30 min, shows small Au clusters with a height of a few nm near the original Au particles (see Figure S5 in the Supporting Information). The formation of a ZnO nucleus and subsequent nanowire growth at Au site might take place in a similar way as described previously for wires A. However, ZnO nanowires, which were formed by the assistance of small Au clusters, grew epitaxially as shown in Figure 5. The surface migration of Au atoms might initiate nanowires growth near the original Au particles and limit the position control of ZnO nanowires. In addition, one can see clearly the development of the base widening as result of the surface diffusion of vapor species.[24] The cross-section TEM images of vertically aligned nanowires shows a sharp ZnO/GaN interface without Au clusters (Figure S6 in the Supporting Information). Au clusters after supporting the formation of ZnO nuclei may leave the location owing to the high diffusion rate of Au atoms at high growth temperatures. Most probably small Au clusters react with the GaN layer chemically during wire growth.[25] Therefore, in this case the Au particle catalyzing the ZnO nanowire growth remains neither at the root nor the tip after extended nanowire growth periods.

In summary, we have investigated Au-assisted growth of ZnO nanowires and nanowire branches. We first put special emphasis on the interaction between Au and adsorbed ZnO molecules. A simple growth model suggests that competition between the saturation rate and nucleation rate of ZnO on the Au particle results in two different growth modes, leading either to the presence of the catalytic Au particle at the root or at the tip of the ZnO nanowires. For Au-catalyzed wire growth, the diameter of the nanowires did not match that of the Au particles. Finally, it was demonstrated that the surface migration of Au atoms on GaN/Si substrates limits position-controlled growth of ZnO nanowires.

Experimental Section

Commercially available Au colloids (BBI International) were used as catalyst. For growth of typical wires A and B, Au colloids with mean diameter of 52 nm and a concentration of about 4.5×10^9 particles mL^{-1} were used. To disperse Au nanoparticles at the SiO_2/Si (the thickness of SiO_2 is 100 nm) and GaN/Si substrates, a diluted Au colloid solution was dropped on the substrates and subsequently dried by blowing Ar gas for a few seconds. This method resulted in a random distribution of Au particles over the substrate. A typical scanning electron microscopy (SEM) image of dispersed 50 nm Au particles with an approximate density of 0.2 particles μm^{-2} on the substrate is given in the Supporting Information (Figure S1a). The Au colloid solution was diluted with ethanol. If water was used, no Au particles were deposited on the substrate. It was possible for the Au particles to attach to the substrate by van der Waals forces. Then, the sample was cleaned with O_2 plasma at a power of 150 W for 2 min, and then annealed at 500 °C for 30 min. O_2 plasma treatment was carried out with a pressure of 0.7 Torr (the base pressure was 0.2 Torr) and O_2 flow rate of 70 sccm at room temperature. This final step is important for the growth of nanowires because residual organic materials disturb the growth of nanowires. Note that the thin gold oxide shell formed on the nanoparticles after O_2 plasma will be thermally decomposed during the annealing process at 500 °C or at even higher growth temperatures.[26]

The growth experiments were carried out in a tube furnace integrated with Ar gas flowing and pumping systems.[12] ZnO and graphite powder with a ratio of 1:1 in wt % were used as source material. The tube pressure was maintained at 200 mbar under a constant Ar flow of 30 sccm for wire growth. Owing to the temperature gradient in the growth tube, the temperature at the source and the substrates where the nanowires were collected were 920 °C and 850 °C, respectively. The substrates were placed in 12 cm away from the source boat, which was located at the center of the heating zone.

ZnO nanowire branches were grown in a similar way. A diluted 50 nm Au colloid solution (4.5×10^9 particles mL) was dropped on the nanowires grown substrates and subsequently dried by blowing Ar gas. A typical SEM image of Au nanoparticles dispersed on the ZnO naonwires is shown in the Supporting Information

(Figure S1b). The sample was annealed at 500 °C for 30 min prior to the growth run, in which the same growth parameters were used as for the growth of wires A.

Keywords:
chemical vapor transport · crystal growth · nanowires · oxides · semiconductors

[1] C. Yang, Z. Zhong, C. M. Lieber, *Science* **2005**, *310*, 1304.
[2] M. T. Björk, B. J. Ohlsson, T. Sass, A. I. Persson, C. Thelander, M. H. Magnusson, K. Deppert, L. R. Wallenberg, L. Samuelson, *Appl. Phys. Lett.* **2002**, *80*, 1058.
[3] J. B. Hannon, S. Kodambaka, F. M. Ross, R. M. Tromp, *Nature* **2006**, *440*, 69.
[4] F. M. Ross, J. Tersoff, M. C. Reuter, *Phys. Rev. Lett.* **2005**, *95*, 146104.
[5] F. M. Kolb, H. Hofmeister, R. Scholz, M. Zacharias, U. Gösele, D. D. Ma, S. T. Lee, *J. Electrochem. Soc.* **2004**, *151*, G472.
[6] A. I. Persson, M. W. Larsson, S. Stenström, B. J. Ohlsson, L. Samuelson, L. R. Wallenberg, *Nat. Mater.* **2004**, *3*, 677.
[7] Y. Wang, V. Schmidt, S. Senz, U. Gösele, *Nat. Nanotechnol.* **2006**, *1*, 186.
[8] S. Kodambaka, J. Tersoff, M. C. Reuter, *Science* **2007**, *316*, 729.
[9] L. Schubert, P. Werner, N. D. Zakharov, G. Gerth, F. M. Kolb, L. Long, U. Gösele, *Appl. Phys. Lett.* **2004**, *84*, 4968.
[10] S. A. Dayeh, E. T. Yu, D. Wang, *Nano Lett.* **2007**, *7*, 2486.
[11] I. Levin, A. Davydov, B. Nikoobakht, N. Sanford, P. Mogilevsky, *Appl. Phys. Lett.* **2005**, *87*, 103110.
[12] D. S. Kim, R. Ji, H. J. Fan, F. Bertram, R. Scholz, R. Dadgar, K. Nielsch, A. Krost, J. Christen, U. Gösele, M. Zacharias, *Small* **2007**, *3*, 76.
[13] S. Helveg, C. López-Cartes, J. Sehested, P. L. Hansen, B. S. Clausen, J. R. Rostrup-Nielsen, F. Abild-Pedersen, J. K. Nørskov, *Nature* **2004**, *427*, 426.
[14] Y. Li, W. Kim, Y. Zhang, M. Rolandi, D. Wang, H. Dai, *J. Phys. Chem. B* **2001**, *105*, 11424.
[15] J. Gavillet, A. Loiseau, C. Journet, F. Willaime, F. Ducastelle, J.-C. Charlier, *Phys. Rev. Lett.* **2001**, *87*, 275504.
[16] K. Polacer, E. F. Wassermann, *Thin Solid Films* **1976**, *37*, 65.
[17] E. F. Wassermann, K. Polacek, *Appl. Phys. Lett.* **1970**, *16*, 259.
[18] M. H. Huang, Y. Wu, H. Feick, N. Tran, E. Weber, P. Yang, *Adv. Mater.* **2001**, *13*, 113.
[19] R. S. Wagner, W. C. Ellis, *Appl. Phys. Lett.* **1964**, *4*, 89.
[20] M. Kirkham, X. Wang, Z. L. Wang, R. L. Snyder, *Nanotechnology* **2007**, *18*, 365304.
[21] U. Pal, J. García-Serrano, G. Casarrubias-Segura, N. Koshizaki, T. Sasaki, S. Terahuchi, *Sol. Energy Mater. Sol. Cells* **2004**, *81*, 339.
[22] P. Buffat, J.-P. Borel, *Phys. Rev. A* **1976**, *13*, 2287.
[23] L. A. Lewis, A. M. Cameron, *Metal. Mater. Trans. B* **1995**, *26*, 911.
[24] Y. Kim, H. J. Joyce, Q. Gao, H. H. Tan, C. Jagadish, M. Paladugu, J. Zou, A. A. Suvorova, *Nano Lett.* **2006**, *6*, 599.
[25] A. Barinov, L. Casalis, L. Gregoratti, M. Kiskinova, *J. Phys. D: Appl. Phys.* **2001**, *34*, 279.
[26] L. K. Ono, B. Roldan Cuenya, *J. Phys. Chem. C.* **2008**, *112*, 4676.
[27] L. Cao, B. Garipcan, J. S. Atchison, C. Ni, B. Nabet, J. E. Spanier, *Nano Lett.* **2006**, *6*, 1852.

Received: January 4, 2008
Revised: April 7, 2008
Published online: September 3, 2008

Paper II

Surface diffusion induced growth of ZnO nanowires

D.S. Kim, U. Gösele, M. Zacharias, *Journal of Crystal Growth*, **311**, 3216 (2009).

The role of surface migration of Au atoms on a lattice matched substrate is studied. Surface migration prevents the controlled growth of ZnO nanowires at predefined positions. In the regime of surface-diffusion controlled growth, an inverse proportional relation of diameter and length of nanowires is observed i.e., nanowires with smaller diameters grow faster than those with larger ones, in contrast to what is expected from standard models of vapor-liquid-solid (VLS) or vapor-solid-solid (VSS) growth.

The author of this thesis (D.S.Kim) performed all growth experiments and wrote the manuscript.

Journal of Crystal Growth 311 (2009) 3216–3219

Contents lists available at ScienceDirect

Journal of Crystal Growth

journal homepage: www.elsevier.com/locate/jcrysgro

Surface-diffusion induced growth of ZnO nanowires

D.S. Kim [a,*], U. Gösele [a], M. Zacharias [b]

[a] Max Planck Institute of Microstructure Physics, Weinberg 2, 06120 Halle, Germany
[b] IMTEK, Faculty of Applied Science, Albert-Ludwigs-University Freiburg, Georges-Köhler-Allee 103, 79110 Freiburg, Germany

ARTICLE INFO

Article history:
Received 17 February 2009
Accepted 19 March 2009
Communicated by B.A. Korgel
Available online 28 March 2009

PACS:
81.05.Dz
81.15.Aa
81.15.Kk
62.23.Hj

Keywords:
A1. Nanowires
A3. Vapor phase epitaxy
B1. Zinc oxide
B2. Semiconducting II–VI materials

ABSTRACT

The growth rate of ZnO nanowires grown epitaxially on GaN/sapphire substrates is studied. An inverse proportional relation between diameter and length of the nanowires is observed, i.e., nanowires with smaller diameters grow faster than larger ones. This unexpected result is attributed to surface diffusion of ZnO admolecules along the sidewalls of the nanowires. In addition, the unique *c*-axis growth of ZnO nanowires, which does not require a catalytic particle at the tip of the growing nanowires is discussed by taking into account polarity, surface free energy, and ionicity. Activation energies of the nanowire growth are determined as well.

1. Introduction

Semiconductor nanowires have been extensively investigated including their basic growth mechanism [1,2] as well as potential applications in solar cells [3], thermoelectrics[4], and memory devices [5]. A vapor–liquid–solid (VLS) process is typically assumed for nanowire growth, where the vapor species are incorporated into the liquid catalyst and condensed at the liquid–solid interface under supersaturation conditions. However, the growth of semiconductor nanowires can also occur below the bulk eutectic temperature, i.e., vapor–solid–solid (VSS) growth [6] or even without catalytic particles i.e., vapor–solid (VS) growth [7]. Furthermore, some materials do not establish a eutectic alloy with chosen catalysts.

In VLS growth if the Gibbs–Thomson effect is taken into account, then thicker nanowires typically grow faster than thinner ones [8]. In contrast, it was already reported that the growth rate of MBE-grown Si nanowires shows an opposite behavior, i.e., the length of nanowires is inversely proportional to the diameter [9]. Similar effects were observed for the VLS growth of some III–V nanowires [18]. This inverse relationship between the growth rate and the diameter of nanowires is generally interpreted as being caused by the transport of the vapor species by surface diffusion [9,10]. *In situ* measurement of VLS-grown individual Si nanowires showed diameter-independent growth rate under specific growth condition such as low vapor pressure and high temperature [11].

Typically, ZnO nanowire growth on a lattice matched substrate using a thermal evaporation route requires the use of catalysts such as gold. But neither liquid nor solid catalysts seem to be involved in the growth process at the tip of growing wires [12]. Due to surface migration of Au atoms on a GaN substrate ZnO nanowires grew not only at the original Au particles sites but also close to them [13]. Additional efforts may require getting position-controlled growth of ZnO nanowires on GaN substrates. As ZnO nanowires have attracted a broad interest for a wide range of applications such as ultraviolet/blue emission device [14], solar cells [15], and chemical sensors [16] the peculiar aspects of wire growth have to be well clarified.

In this work, surface-diffusion induced epitaxial growth of ZnO nanowires on GaN substrates is presented. The diameter-dependent growth rate of wires will be discussed based on species supply conditions as well as intrinsic material properties such as polarity, surface free energy, and ionicity. In addition, the activation energy of wires with different sizes is estimated.

2. Experimental procedure

For well-separated ZnO nanowire growth small Au clusters were used as nuclei instead of Au nanoparticles. Since several

*Corresponding author. Tel.: +49 345 5582 641; fax: +49 345 5511 223.
E-mail address: dskim@mpi-halle.de (D.S. Kim).

0022-0248/$ - see front matter © 2009 Elsevier B.V. All rights reserved.
doi:10.1016/j.jcrysgro.2009.03.026

inclined wires were formed on a single Au nanoparticle site reliable growth statistics may be deduced only if individually grown wires were used for analysis. To prepare dispersed Au clusters a small amount of Au colloid solution was dropped on the substrates and dried by Ar blowing. For the detailed preparation methods see ref. [13]. Subsequently, the samples were treated with O_2 plasma at a power of 150 W for 1–2 min, followed by a thermal anneal of the sample at 500 °C for 30 min.

The growth experiments were carried out in a tube furnace integrated with Ar gas flowing and pumping systems. ZnO and graphite powder with 1:1 wt % were used as source material. The source boat and the substrate were placed in a small quartz tube (17 mm in diameter, 250 mm in length) separately. This small quartz tube was then put into the growth tube (55 mm in diameter, 650 mm in length) where the source boat was positioned at the center of the heating zone. This tube-in-tube geometry has been selected because we expect that it leads to a high supersaturation of ZnO vapor for wire growth. The growth pressure was maintained at 200 mbar under a constant Ar flow of 10 sccm. The source temperature was 900 °C, whereas the temperature of the nanowire collecting substrates was varied from 720 to 680 °C due to the temperature gradient inside the growth tube.

3. Results and discussion

Fig. 1 shows a typical SEM image of ZnO nanowires epitaxially grown on the GaN/sapphire substrates with the assistance of Au clusters. It is noticeable that thin wires are longer than thick one. ZnO nanowires grew in [0 0 0 1] direction with hexagonal cross-section. The wire sidewalls were faceted into $\{1\,0\,\bar{1}\,0\}$ planes. The density of nanowires varied from about 0.8 to 1.4 wire/μm^2 over a large area of the substrates.

To display the morphology of small Au clusters acting as nucleation sites, AFM analysis was carried out on the sample (see Fig. 2(a)). Typically Au clusters with a height of a few nm were dispersed (one of them indicated by dotted circle). The representative AFM images of an Au nanoparticle and cluster are shown in Fig. 2(b) and (c), respectively.

In Fig. 3 the measured dependence of the nanowire length (L) on the nanowire diameter (d) is plotted. Apparently, as the wire diameter decreases the length of the wires increased.

In general, the atoms or molecules contributing to the growth of the nanowires can either directly attach to the tip of the nanowire (which might or might not be capped with a liquid or solid catalyst) or the atoms or molecules reach the tip of the nanowires via a diffusion process along the sidewalls of the nanowires [17]. In the case of direct attachment at the tip from the vapor phase, which happens in most cases for VLS growth, the growth rate is lower for smaller diameter nanowires due to the Gibbs–Thomson effect, as observed experimentally in many cases [17].

If, however, the supply of material occurs via surface diffusion along the sidewalls of the nanowires just the opposite diameter

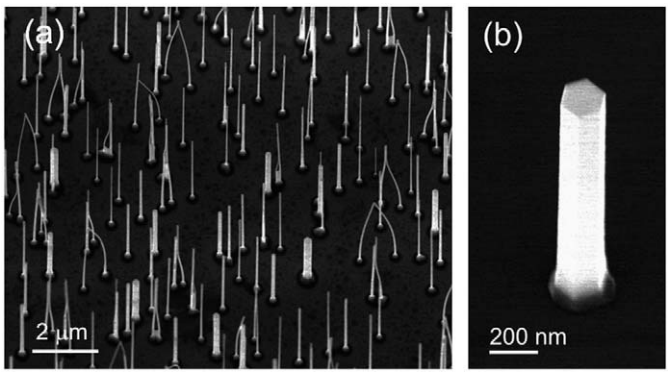

Fig. 1. (a) SEM image of ZnO nanowires grown on a GaN/sapphire substrate. Images were taken with a tilting angle of 30°. (b) High-magnification SEM image of single ZnO nanowire. Hexagonal facet without gold catalyst is apparently visible. Note that some thin wires in Fig. 1(a) were bent due to secondary effects such as e-beam irradiations.

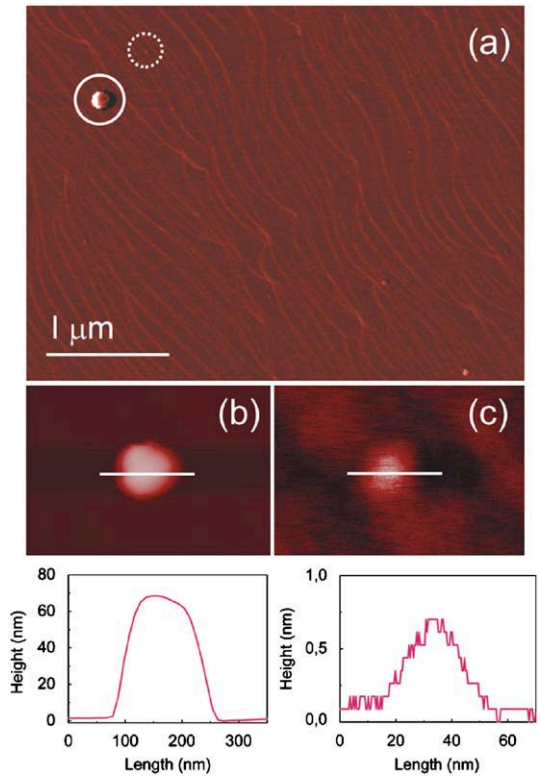

Fig. 2. (a) A phase mode AFM image of Au clusters (dotted circle) on a GaN/sapphire substrate after thermal annealing with Au nanoparticles (solid circle) at 500 °C with a pressure of 1 mbar for 30 min. (b) High magnification of the AFM image of an Au nanoparticle in Fig. 2(a). (c) The AFM image of a representative Au cluster in Fig. 2(a). The profile steps shown below the AFM images correspond to the height of the Au nanoparticle and cluster which are marked by a white bar in Fig. 2(b) and (c), respectively.

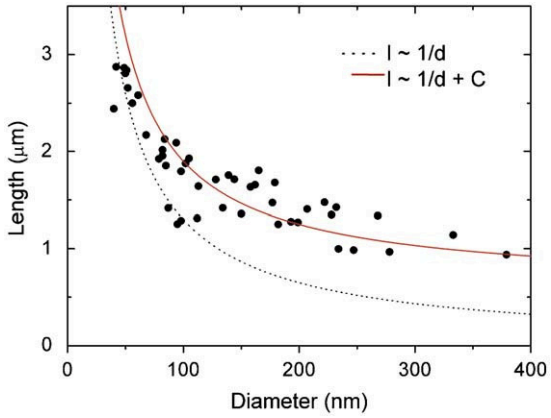

Fig. 3. Correlation between the length and the diameter of ZnO nanowires grown at a temperature around 690 °C for 40 min.

dependence occurs. Thicker nanowires have a reduced growth rate, i.e., the length of the wire is inversely proportional to the diameter,

$$L \propto \frac{1}{d} \tag{1}$$

For instance, the length of MBE grown Si and GaAs nanowires were reported to be inversely proportional to the diameter of the wires [9,18,27].

In case of ZnO nanowire growth, Eq. (1) roughly fits the resulting size-dependent growth rate as shown in Fig. 3. However, the data is fitted better if a direct impingement term is taken into account. Since the impingement of vapors is proportional to the area of the growing tip, the growth rate is given by

$$L \approx \frac{1}{d} + C \tag{2}$$

here, C is a constant.

Although the diffusion length of ZnO admolecules on a GaN surface is not known, a size-dependent growth rate was observed for a wire density up to 1.4 wire/μm^2. For a sufficiently high wire density direct impingement may finally dominate the growth rate.

Supplementary, one can clearly see the development of the base widening as result of the surface diffusion of ZnO admolecules. See Fig. 1(b).

Although the inverse proportional relationship between length and diameter of VLS-grown nanowires was clarified within specific growth conditions [9,18] such growth peculiarity in ZnO nanowires has to be distinguished from those cases in which a catalytic particle is present at the tip of the growing nanowires, since for the ZnO nanowires a flat plane exists at the tip of the nanowire. The catalytic Au cluster assisted only in the nucleation process [13]. Also the nanowires were formed without any significant tapering, i.e., lateral growth on the non polar surface of wires was almost negligible. Hence we suggest that the selective condensation of ZnO vapors supplied via surface diffusion on the growing tip is governed by intrinsic material properties such as polarity, surface free energy, and iconicity.

Recently, controlled experiments of homoepitaxial GaN nanowire growth were carried out and revealed the importance of a polarity effect on the vapor–solid growth process [19]. The hexagonal prism-like island consisting of $\{10\bar{1}0\}$ and $\{10\bar{1}1\}$ facets formed on nanowires grown in the c-direction whereas GaN belts grew on wires grown in the a-direction. Direction-dependent growth habits suggest that surface diffusion of adatoms along preexisting polar or non-polar surface of nanowires play an important role for the formation of anisotropic crystals. In contrast to the limited surface diffusion of adatoms on polar surfaces, the adatoms diffusion length along a non-polar surface of nanowires was longer than several tens of micrometers.

This argument can also be applied for the growth of ZnO nanowires. ZnO molecules diffusing along the nanowires are likely to be incorporated at the tip of the growing wires due to their high sticking coefficient at the (0 0 0 1) surface rather than the sidewall of the non-polar surface. Within the growth conditions used in our experiments, nanowires with a length of about 10 μm and a diameter of 40 nm were obtained. Thus the diffusion length on a non-polar surface might exceed more than 10 μm but the diffusion length on polar surface would be less than 40 nm. Most probably the incorporation of polar ZnO molecules on the positively charged (0 0 0 1) surface is caused by chemisorption [20].

Note that the polarity effect was already involved in the growth of helical ZnO nanostructures [21]. Also it was reported that such polarity effects present in ZnO films grown along the nonpolar $[11\bar{2}0]$ direction resulted in rhombohedral pyramids exposing polar $\{10\bar{1}1\}$ facets [22].

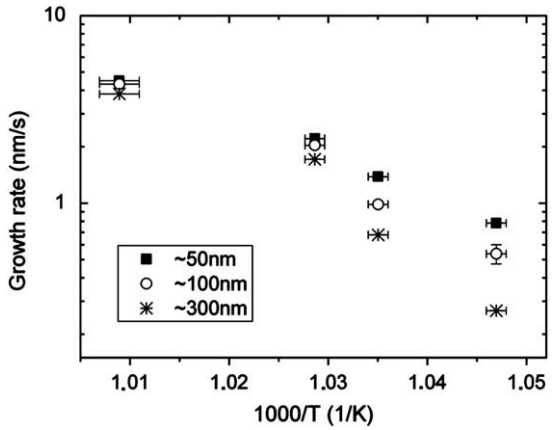

Fig. 4. Size-dependent growth rate of ZnO nanowires as function of growth temperature. The different diameters are given as a parameter.

It is well known that the interface energy at the liquid/solid tip interface of the wire and the surface energy of the wire are the most important factors influencing the growth directions, i.e., nanowires grow to minimize the surface free energy. For example the growth of Si or ZnSe nanowires showed diameter-dependent growth directions [23,24]. In hexagonal ZnO nanowires with wurtzite structure the side faces are the $\{10\bar{1}0\}$ planes. The calculated cleavage energy of $(10\bar{1}0)$ plane was 2.32 J/m^2, which is the lowest energy among all the major planes [25]. Thus the absence of a size-dependent growth direction but the presence of just one preferred orientation in ZnO nanowires might be attributed to the very low surface energy of the sidewalls. Also ZnO with a high ionicity of 0.62 may prefer to form a hexagonal structure with the principle c-axis growth direction [26].

Fig. 4 shows the measured growth rate, v_g, at different growth temperatures, T. As expected, the growth is a thermally activated process and is size dependent. Depending on the growth temperatures, the growth rate varied from 0.78 to 4.5 nm/s for the nanowires with a diameter of around 50 nm. Assuming an Arrhenius behavior of wire growth, the activation energy was roughly estimated to be 167, 201, and 253 kJ/mol for wire diameters of around 50, 100, and 300 nm, respectively. The estimated activation energy for the growth of thick wires is larger than that of thin wires. The apparent decrease of the activation energy for thinner nanowires would indicate that the incorporation of admolecules at the tip is easier for thinner nanowires. However, due to the large scatter of the data points we refrain from a detailed discussion of this feature.

4. Conclusions

In summary, a high supersaturation of the gaseous vapor species results in major contributions of the surface diffusion of the ZnO admolecules to the anisotropic ZnO nanowire growth and in a diameter dependence of the growth rate. Thin wires grow faster than thick ones. The observed growth behavior was explained by taking into account the surface diffusion of admolecules, polarity, surface free energy, and ionicity.

Acknowledgements

This work was supported by the International Max Planck Research School for Science and Technology of Nanostructures

(Nano-IMPRS) in Halle. We thank A. Dadgar and A. Krost for supplying GaN/sapphire substrates.

References

[1] J.B. Hannon, S. Kodambaka, F.M. Ross, R.M. Tromp, Nature 440 (2006) 69.
[2] M.T. Borgström, G. Immink, B. Ketelaars, R. Algra, E.P.A.M. Bakkers, Nat. Nanotechnol. 2 (2007) 541.
[3] B. Tian, X. Zheng, T.J. Kempa, Y. Fang, N. Yu, G. Yu, J. Huang, C.M. Lieber, Nature 449 (2007) 885.
[4] A.I. Hochbaum, R. Chen, R.D. Delgado, W. Liang, E.C. Garnett, M. Najarian, A. Majumdar, P. Yang, Nature 451 (2008) 163.
[5] D. Yu, J. Wu, Q. Gu, H.J. Park, J. Am. Chem. Soc. 128 (2006) 8148.
[6] Y. Wang, V. Schmidt, S. Senz, U. Gösele, Nat. Nanotechnol. 1 (2006) 186.
[7] G.W. Sears, Acta Metall. 1 (1953) 457.
[8] E.I. Givargizov, J. Crystal Growth 31 (1975) 20.
[9] L. Schubert, P. Werner, N.D. Zakharov, G. Gerth, F.M. Kolb, L. Long, U. Gösele, Appl. Phys. Lett. 84 (2004) 4968.
[10] J. Johansson, C.P.T. Svensson, T. Martensson, L. Samuelson, W. Seifert, J. Phys. Chem. B 109 (2005) 13567.
[11] S. Kodambaka, J. Tersoff, M.C. Reuter, F.M. Ross, Phys. Rev. Lett. 96 (2006) 096105.
[12] D.S. Kim, R. Ji, H.J. Fan, F. Bertram, R. Scholz, R. Dadgar, K. Nielsch, A. Krost, J. Christen, U. Gösele, M. Zacharias, Small 3 (2007) 76.
[13] D.S. Kim, R. Scholz, U. Gösele, M. Zacharias, Small 4 (2008) 1615.
[14] J. Bao, M.A. Zimmler, F. Capasso, Nano Lett. 6 (2006) 1719.
[15] M. Law, L.E. Greene, J.C. Johnson, R. Saykally, P. Yang, Nat. Mater. 4 (2005) 455.
[16] Z. Fan, J.G. Lu, Appl. Phys. Lett. 86 (2005) 123510.
[17] E.I. Givargizov, Highly Anisotropic Crystals, Reidel, Dordrecht, 1987.
[18] V.G. Dubrovskii, G.E. Cirlin, I.P. Soshnikov, A.A. Tonkikh, N.V. Sibirev, Yu.B. Samsonenko, V.M. Ustinov, Phys. Rev. B 71 (2005) 205325.
[19] H. Li, A.H. Chin, M.K. Sunkara, Adv. Mater. 18 (2005) 216.
[20] V. Staemmler, K. Fink, B. Meyer, D. Marx, M. Kunat, S. Gil Girol, U. Burghaus, Ch. Wöll, Phys. Rev. Lett. 90 (2003) 106102.
[21] P.X. Gao, Z.L. Wang, Small 1 (2005) 945.
[22] J. Zúñiga-Pérez, V. Muñoz-Sanjosé, E. Palacios-Lidón, J. Colchero, Phys. Rev. Lett. 95 (2005) 226105.
[23] Y. Cai, S.K. Chan, I.K. Sou, Y.F. Chan, D.S. Su, N. Wang, Adv. Mater. 18 (2006) 109.
[24] V. Schmidt, S. Senz, U. Gösele, Nano Lett. 5 (2005) 931.
[25] A. Wander, F. Schedin, P. Steadman, A. Norris, R. McGrath, T.S. Turner, G. Thornton, N.M. Harrison, Phys. Rev. Lett. 86 (2001) 3811.
[26] R. Triboulet, J.O. Ndap, A. Tromson-Carli, P. Lemasson, C. Morhain, G. Neu, J. Crystal Growth 159 (1996) 156.
[27] M.C. Plante, R.R. LaPierre, J. Crystal Growth 286 (2006) 394.

Paper III

Laser-interference lithography tailored for highly symmetrically arranged ZnO nanowire arrays

D. S. Kim, R. Ji, H. J. Fan, F. Bertram, R. Scholz, R. Dadgar, K. Nielsch, A. Krost, J. Christen, U. Gösele, and M. Zacharias, *Small* **3**, 76 (2007).

The growth of well defined regular arrays of ZnO nanowires with a narrow diameter distribution and a uniform spacing is demonstrated based on laser interference lithography and a physical vapor deposition. The resulting morphology and physical properties of these ZnO nanowire arrays are discussed.

The work described in this chapter was done in collaboration with F. Bertram in the group of J. Christen at the Institute of Experimental Physics of the Otto-von-Guericke-University. The author of this thesis (D.S.Kim) performed all growth experiments and wrote the paper. R. Scholz did the TEM investigations. F. Bertram and R. Ji carried out CL measurements and the patterning of the photoresist by laser interference lithography, respectively.

Nanowire arrays

DOI: 10.1002/smll.200600307

Laser-Interference Lithography Tailored for Highly Symmetrically Arranged ZnO Nanowire Arrays**

Dong Sik Kim, Ran Ji, Hong Jin Fan, Frank Bertram, Roland Scholz, Armin Dadgar, Kornelius Nielsch, Alois Krost, Jürgen Christen, Ulrich Gösele, and Margit Zacharias*

The controlled growth of one-dimensional semiconductor nanostructures has been the focus of much attention for the last few years, not only in terms of understanding the fundamental growth mechanism[1] but also due to their possible applications in nanoscale electronics[2] and optoelectronics.[3] In particular, nanostructured zinc oxide (ZnO), an important functional oxide semiconductor, has been discussed in terms of a wide variety of applications including lasers, light-emitting devices,[4] sensors,[5] and solar cells.[6] For the realization of such device applications it is necessary to control both the pattern (e.g., diameter, location, and spacing) and the orientation of the ZnO nanostructures. So far, only relatively little attention has been paid to the reproducibility of the process and the quality of the patterned growth of ZnO nanowires (NWs), even though this is an important issue in producing reliable nanoscale devices and systems. A better understanding of the growth processes and the optimization of the growth conditions are thus necessary.

In general, the diameter and location of the NWs can be determined by controlling the size and position of the catalytic metal particles. Therefore, an area of ordered metal particles is required for controlled NW growth. Previously, ordered arrays of ZnO NWs were demonstrated successfully by various patterning methods, including conventional electron-beam lithography,[2] scanning probe lithography,[7] nanotemplates,[8] and phase-shifting photolithography,[9] followed by different growth techniques. More detailed descriptions of these fabrication techniques and a discussion of their capabilities and limitations can be found in a recent review article.[10]

In this work, we use laser-interference lithography (LIL) to fabricate regularly arranged Au nanodots (NDs) covering areas up to the wafer scale. LIL is a reliable, inexpensive, and fast lithographic tool for the fabrication of large-area dot arrays with tunable lattice constants. Based on this template, we obtain large-area arrays with a long-range order of vertically aligned ZnO NWs by applying a chemical vapor transport and condensation (CVTC) process. Individual ZnO NWs are grown on each Au ND (i.e., one-to-one synthesis). A vapor–solid (VS) mechanism is adapted to describe the growth process instead of the vapor–liquid–solid (VLS) mechanism that is usually considered as the main growth mechanism of ZnO NWs in the presence of Au. Spectrally and spatially resolved cathodoluminescence (CL) measurements are used to study the microscopic spectral emission characteristics of ZnO NW arrays.

The fabrication method of ordered NW arrays is illustrated schematically in Figure 1. After obtaining the Au

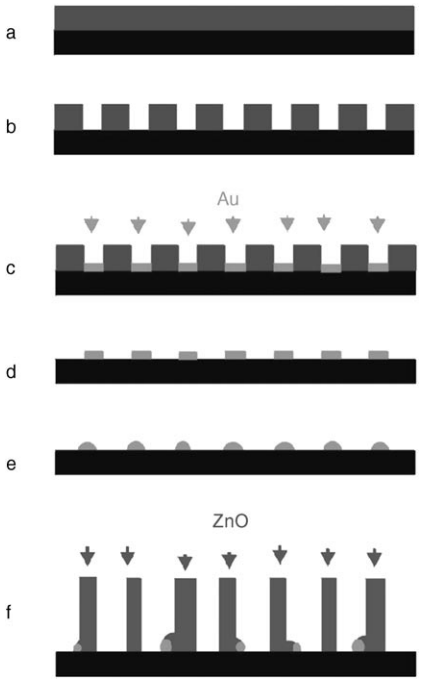

Figure 1. Fabrication process of ZnO NW arrays. a) Deposition of a photoresist/antireflection-coating (PR/ARC) layer on a GaN/Si substrate. b) Double exposure using laser-interference lithography, and developing. c) Deposition of Au by thermal evaporation. d) Removal of the PR/ARC layer. e) Thermal annealing. f) Growth of ZnO NWs by CVTC.

NDs (Figure 1d), an additional annealing step was applied to reduce their lateral dimension and to enhance the surface smoothness of the NDs, as shown in Figure 2a and b. Before the thermal annealing step, the Au NDs show a high roughness (with a mean height of 20 nm) with a diameter of 120 nm. Figure 2c shows typical Au NDs deposited on a GaN/Si substrate after annealing at 500 °C for 1 h. The di-

[*] D. S. Kim, R. Ji, Dr. H. J. Fan, Dr. R. Scholz, Dr. K. Nielsch, Prof. U. Gösele, Dr. M. Zacharias
Max Planck Institute of Microstructure Physics
Weinberg 2, 06120 Halle (Germany)
Fax: (+49) 345-551-1223
E-mail: dskim@mpi-halle.de
Dr. M. Zacharias
FZ Rossendorf, Division of Semiconductor Materials
Bautzner Landstraße 128, 01328 Dresden (Germany)
Dr. F. Bertram, Dr. A. Dadgar, Prof. A. Krost, Prof. J. Christen
Institute of Experimental Physics, Otto von Guericke University
39016 Magdeburg (Germany)

[**] This work was supported by the International Max Planck Research School for Science and Technology of Nanostructures (Nano-IMPRS) in Halle (Germany).

Supporting information for this article is available on the WWW under http://www.small-journal.com or from the author.

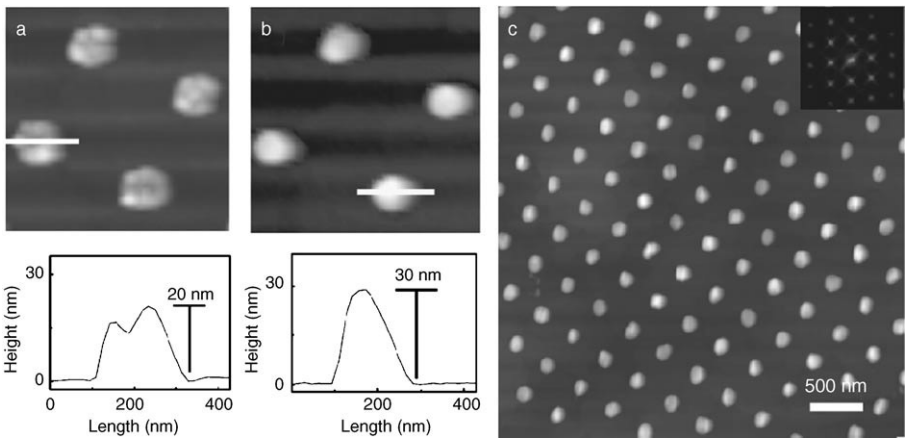

Figure 2. Atomic force microscopy (AFM) images of patterned Au NDs on GaN/Si substrate. a) As deposited; b) after thermal annealing at 500 °C for 1 h. The profile steps shown below correspond to the height of the Au NDs, which are marked by a white bar in Figure 2a and b. c) Typical AFM image of patterned Au NDs with an average diameter of 79 nm (period of 270 nm and height of 30 nm) and its corresponding fast Fourier transform (FFT) diffractogram (inset).

ameter and the height distributions are now regular with a periodic distance of 270 nm. The mean diameter and mean height are about (79.0 ± 7.4) nm and (30.0 ± 5.5) nm, respectively. The resulting arrays of Au NDs are ordered in a monoclinic lattice arrangement with an average density of 9 dots μm^{-2}. Note that a chemical reaction between the Au NDs with the GaN layer might lead to a Au–Ga alloy at an annealing temperature as low as 500 °C.[11]

After the ZnO NW growth, the morphology of the sample was investigated by scanning electron microscopy (SEM) (JEOL JSM-6300F). Figure 3 shows SEM images of regularly ordered ZnO NW arrays, which were epitaxially grown on a GaN/Si substrate. Figure 3a shows a side view of the ZnO NW arrays tilted at 20°. A large area can be observed with a density of 9 nanowires μm^{-2}. Figure 3b clearly shows the highly symmetric alignment of the ZnO NWs. The arrangement of the vertically aligned ZnO NWs (period: 230 nm) can be well distinguished in the magnified view shown in Figure 3c. The ZnO NWs have an average diameter of (109 ± 20) nm. Interestingly, the length of the ZnO NWs is quite uniform and independent of their diameter in domains of at least $10 \times 10\ \mu m^2$. The temperature gradient and the supersaturation of ZnO vapor determine the growth rate of ZnO NWs; this factor led to a variation in the length of the ZnO NWs from 0.5 to 3 μm over the $1 \times 1\ cm^2$ sample region. For a large-scale image of ZnO NW arrays, please see Figure S1 in the Supporting Information. The results shown in Figure 4 reveal that the diameter distribution of ZnO NWs corresponds to that of the Au NDs. The Gaussian fit of the diameter distribution of the Au NDs and ZnO NWs had full width half-maximum (FWHM) values at 5.5 and 13.3 nm, respectively.

Considering the local structure of the ZnO NWs, all NWs are characterized by an atomically flat plane at their top without any tapering. The Au NDs were located around the NW roots, as shown in Figure 5. More detailed SEM and cross-section transmission electron microscopy (TEM) studies reveal that most Au NDs are pushed away after developing a crawling-like nanostructure on the GaN/Si surface. The ZnO NWs are epitaxially grown on a GaN/Si substrate (an additional cross-section TEM image is available in the Supporting Information, Figure S2). We therefore conclude that, under these growth conditions, the ZnO NWs do not grow on the GaN/Si substrate by a VLS growth process even though Au NDs are required for the growth. It is suggested that the main process is a liquid-phase-assisted VS growth mode. In this growth mode, [0001]-oriented ZnO nuclei are formed epitaxially at the interface of the GaN/Si substrate. This happens inherently at the beginning of the growth, with a preferential attachment of the gaseous precursor molecules to the molten-alloy

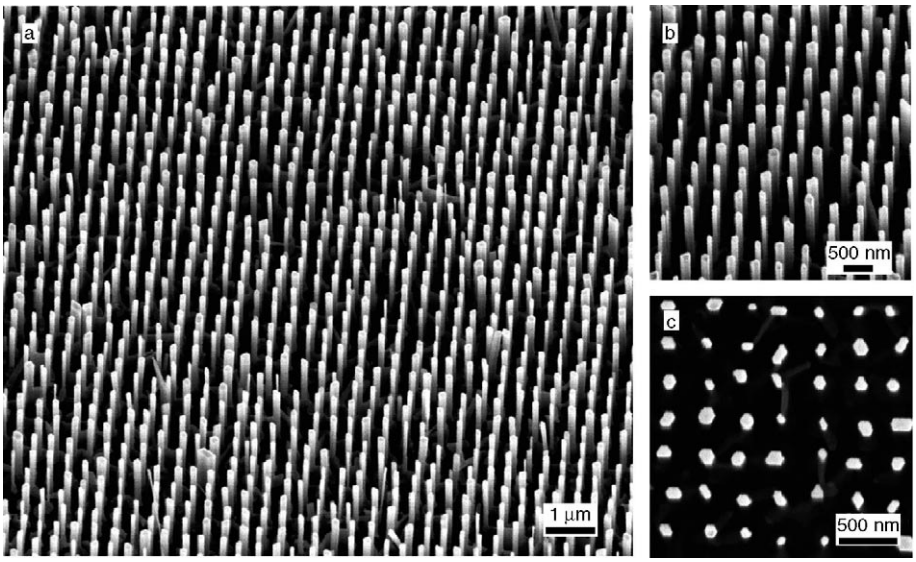

Figure 3. a) Low-magnification 20° tilted view, b) high-magnification 20° tilted view, and c) top-view SEM images of ordered arrays of ZnO NWs grown on a GaN/Si substrate; the average diameter of the NWs is 109 nm with a lattice constant of 230 nm.

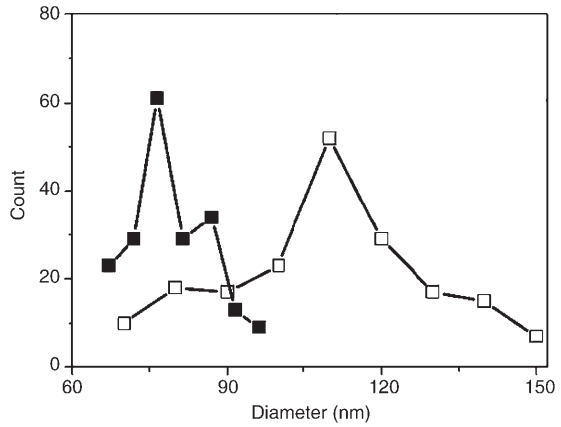

Figure 4. Correlation between the diameter of Au nanodots (solid rectangle) after thermal annealing at 500 °C for 1 h and the diameter of ZnO nanowires (open rectangle).

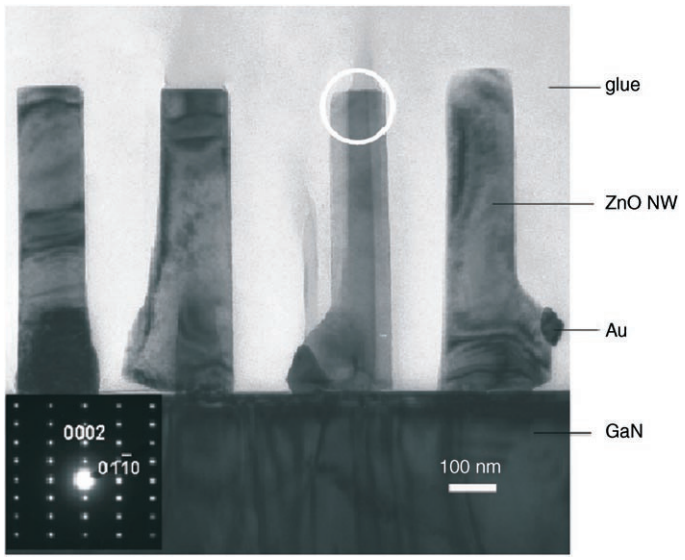

Figure 5. Cross-section TEM image of the ZnO NWs/GaN substrate. The inset is an electron-diffraction pattern of an area (indicated by the circle) of a ZnO NW.

ND. Au NDs thus indirectly affect the size and the shape of ZnO nuclei. It is for this reason that there is a difference in the average diameter of the Au NDs and the resulting ZnO NWs. Such [0001]-oriented ZnO nuclei were also observed at the early growth stages of ZnO pillars in our previous experiments, as well as on the surface of ZnO films prepared by pulsed-laser deposition (PLD).[12,13] After nuclei formation, the ZnO NWs grow continuously with a [0001] preferential growth direction. So far, it is still an open question as to why the highest growth rate occurs along this direction and why the ZnO nuclei are oriented along the *c* axis despite their high surface energy.[14]

It is worth noting that the thickness of the deposited Au NDs before annealing plays an important role in getting such a one-to-one synthesis of ZnO NWs. For instance, the process of patterning Au NDs was repeated but with only a 10-nm Au thickness; the pattered substrate was annealed at 400 °C for 30 min. Under these conditions, we observed that several ZnO NWs grow on each Au ND (see Figure S3 of the Supporting Information). Because of the low thickness, the Au does not reduce in a continuous layer but breaks up into small islands after thermal annealing; each island then provides a nucleation site for a ZnO NW.

The microscopic spectral-emission characteristic of ZnO NW arrays was directly imaged by highly spectrally and spatially resolved low-temperature scanning CL microscopy. Since CL has the advantage of a much higher lateral and depth resolution as compared to photoluminescence, it is a unique tool for the investigation of nanometer-scaled structures. Figure 6a shows the CL spectrum integrated from a sample area of $17 \times 11\ \mu m^2$ in the excitonic energy range. The spectrum is dominated by two clear peaks located at 3.3593 and 3.3556 eV, which are attributed to bound-exciton emissions.[15] The emission line at 3.3593 eV is usually assigned to a neutral-donor bound exciton (D^0X). So far, a distinct assignment of the transition line at 3.3556 eV, either to a neutral donor (D^0X) or to an acceptor (A^0X), has not yet been made since the respective two-electron-satellite (TES) transitions of the bound-exciton lines are not observed.[16] Note that the TES line is a typical characteristic of the D^0X recombination.[17] The FWHM of the peaks at 3.3593 and 3.3556 eV are 2.5 and 1.8 meV, respectively. Figure 6b shows the CL intensity map of the D^0X line at 3.3593 eV (see Figure S4 of the Supporting Information for the corresponding secondary-electron microscopy image of ZnO NW arrays, imaged under a tilt of 45°). Individual NWs are visible and the intensity is distributed homogeneously along the NWs.

In addition, the photoluminescence (PL) spectrum of ZnO NW arrays was measured using a HeCd laser (325 nm) as the excitation source at room temperature (see Figure S5 of the Supporting Information). Only one strong UV emission peak and negligible green-light emission were observed, which indicates a high crystal quality of the grown ZnO NWs.[18]

In summary, we present an effective and reliable approach for the preparation of large-area, long-range ordered ZnO NW arrays by combining laser-interference lithography for templating and a chemical-vapor-transport process for nanowire growth. The resulting ZnO nanowires show a narrow diameter distribution as well as uniform spacing. We demonstrated that a liquid-phase-assisted vapor–solid growth process is responsible for the growth of ZnO NWs

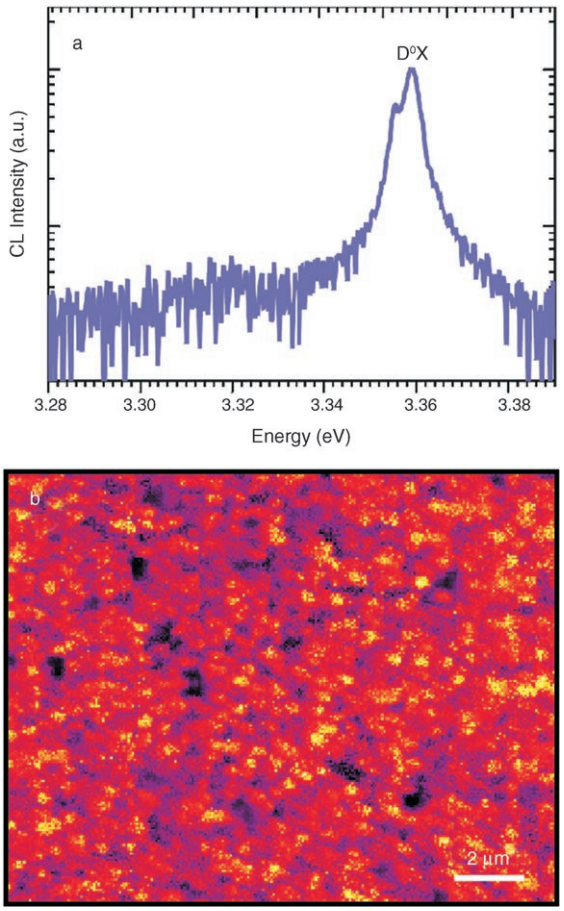

Figure 6. a) CL spectrum of a ZnO NW array, imaged at $T = 5$ K. b) CL intensity map of the D^0X line at 3.3593 eV.

on GaN/Si substrates. The CL spectrum of the ZnO NW arrays is dominated by bound-exciton emissions. Intensity mapping of the neutral-donor bound-exciton line allows visualization of individual nanowires. The patterning and growth approach presented here is suitable for application in electronics, optoelectronics, and biological sensing devices, for which a regular array of well-defined ZnO nanowires is required.

Experimental Section

For laser-interference lithography (LIL), two coherent UV beams were used to produce a periodic interference pattern on a photoresist (PR) film with a spatial period of $P = \lambda/2\sin\theta$, where λ is the wavelength and θ is the half angle between the two beams. A Lloyd's mirror interferometer was used for lithographic exposures and a HeCd laser ($\lambda = 325$ nm) was the light source. The sample was rotated by 90° between two consecutive exposures in order to achieve circular hole patterns. It was also possible to produce an array of hexagonally arranged elliptical holes by changing the rotation angle between the two exposures to 60°. LIL is a multistep process, as illustrated in Figure 1: first an antireflection coating (ARC, WiDE-8B, Brewer Science, America) with a thickness of 70 nm, and a negative-tone photoresist (TSMR-iN027, OHKA, Japan) with a thickness of 180 nm, were spin-coated and baked, respectively, onto a 2-in. GaN/Si substrate. After exposure and developing, the resist pattern obtained by LIL was used as a sputtering mask.

Preparation of Au ND arrays: After the structuring of the PR/ARC on the GaN/Si substrate, gold was thermally evaporated onto the substrate at a deposition rate of 0.1 nm s^{-1}. The background pressure inside the chamber amounted to 2×10^{-6} mbar. After the Au deposition, the PR and ARC layers were removed from the substrate using an RCA-1 cleaning solution for 1 h. Finally, the substrate was thermally annealed at 500 °C for 1 h.

Growth of ZnO NWs: ZnO powder (Alfa Aesar, *99.999*%) and graphite powder (Alfa Aesar, *99.9995*%) were ground together (1:1 wt%) and loaded into an alumina boat. The substrate with the patterned Au ND arrays and the alumina boat were placed into a small quartz tube (diameter 1.7 cm) with a typical distance of 10–11 cm between them. This small quartz tube was then placed inside a furnace quartz tube, with the source boat positioned at the center of the heating zone (length of the heating zone: 20 cm), and the substrate was placed downstream of an argon flow. The temperature of the furnace was set to 925 °C at a heating rate of 40 °C min^{-1} and typically kept at the maximum temperature under a constant flow of argon of 30 standard cubic centimeters per minute for 30 min. After the growth, the furnace was cooled naturally to room temperature.

Keywords:

arrays · chemical vapor transport · lithography · nanowires · semiconductors

[1] L. E. Jensen, M. T. Bjork, S. Jeppesen, A. I. Persson, B. J. Ohlsson, L. Samuelson, *Nano Lett.* **2004**, *4*, 1961–1964.
[2] H. T. Ng, J. Han, T. Yamada, P. Nguyen, Y. P. Chen, M. Meyyappan, *Nano Lett.* **2004**, *4*, 1247–1252.
[3] M. H. Huang, S. Mao, H. Feick, H. Yan, Y. Wu, H. Kind, E. Weber, R. Russo, P. Yang, *Science* **2001**, *292*,1897–1899.
[4] R. Konenkamp, R. C. Word, M. Godinez, *Nano Lett.* **2005**, *5*, 2005–2008.
[5] Q. Wan, Q. H. Li, Y. J. Chen, T. H. Wang , X. L. He, J. P. Li, C. L. Lin, *Appl. Phys. Lett.* **2004**, *84*, 3654–3656.
[6] M. Law, L. E. Greene, J. C. Johnson, R. Saykally, P. Yang, *Nat. Mater.* **2005**, *4*, 455–459.
[7] J. H. He, J. H. Hsu, C. W. Wang, H. N. Lin, L. J. Chen, Z. L. Wang, *J. Phys. Chem. A* **2006**, *110*, 50–53.
[8] a) X. D. Wang, C. J. Summers, Z. L. Wang, *Nano Lett.* **2004**, *4*, 423–426; b) J. Rybczynski, D. Banerjee, A. Kosiorek, M. Giersig, Z. F. Ren, *Nano Lett.* **2004**, *4*, 2037–2040; c) H. Chik, J. Liang, S. G. Cloutier, N. Kouklin, J. M. Xu, *Appl. Phys. Lett.* **2004**, *84*, 3376–3378; d) H. J. Fan, W. Lee, R. Scholz, A. Dadgar, A. Krost, K. Nielsch, M. Zacharias, *Nanotechnology* **2005**, *16*, 913–917.
[9] E. C. Greyson, Y. Babayan, T. W. Odom, *Adv. Mater.* **2004**, *16*, 1348–1352.
[10] H. J. Fan, P. Werner, M. Zacharias, *Small* **2006**, *2*, 700–717.
[11] A. Barinov, L. Casalis, L. Gregoratti, M. Kiskinova, *J. Phys. D* **2001**, *34*, 279–284.
[12] H. J. Fan, W. Lee, R. Hauschild, M. Alexe, G. L. Rhun, R. Scholz, A. Dadgar, K. Nielsch, H. Kalt, A. Krost, M. Zacharias, U. Gösele, *Small* **2006**, *2*, 561–568.
[13] J. Jie, G. Wang, Y. Chen, X. Han, Q. Wang, B. Xu, J. G. Hou, *Appl. Phys. Lett.* **2005**, *86*, 031 909–031 911.

[14] O. Dulub, U. Diebold, G. Kresse, *Phys. Rev. Lett.* **2003**, *90*, 016102.
[15] B. K. Meyer, H. Alves, D. M. Hofmann, W. Kriegseis, D. Forster, F. Bertram, J. Christen, A. Hoffmann, M. Strabetaburg, M. Dworzak, U. Haboeck, A.V. Rodina, *Phys. Status Solidi B* **2004**, *241*, 231 – 260.
[16] Ü. Özgür, Y. I. Alivov, C. Liu, A. Teke, M. A. Reshchikov, S. Dogan, V. Avrutin, S.-J. Cho, H. Morkoç, *J. Appl. Phys.* **2005**, *98*, 041301.
[17] D. C. Reynolds, T. C. Collins, *Phys. Rev.* **1969**, *185*, 1099 – 1103.
[18] K. Vanheusden, W. L. Warren, C. H. Seager, D. R. Tallant, J. A. Voigt, B. E. Gnade, *J. Appl. Phys.* **1996**, *79*, 7983 – 7990.

Received: June 23, 2006
Revised: August 9, 2006
Published online on November 28, 2006

Paper IV

Growth and optical properties of phosphorus-doped ZnO nanowires

D. S. Kim, J. Fallert, A. Lotnyk, R. Scholz, E. Pippel, S. Senz, H. Kalt, U. Gösele and M. Zacharias, *Solid State Communications* **143**, 570 (2007).

p-type doping of ZnO nanowires is important for functional nanodevices. Here it is demonstrated an efficient and effective growth technique for phosphorus doping in ZnO nanowires. The optical properties of doped ZnO nanowires are compared with undoped ZnO nanowires based on PL spectra.

This work was performed in collaboration with J. Fallert in the group of H. Kalt at the Universität Karlsruhe. The author of this thesis (D.S.Kim) performed all growth experiments and wrote the paper. The TEM and XRD investigations were carried out by R. Scholz and A. Lotnyk, respectively. J. Fallert measured PL spectra of doped ZnO nanowires and was involved in discussions.

Available online at www.sciencedirect.com
ScienceDirect
Solid State Communications 143 (2007) 570–573
solid state communications
www.elsevier.com/locate/ssc

Growth and optical properties of phosphorus-doped ZnO nanowires

D.S. Kim[a,*], J. Fallert[b], A. Lotnyk[a], R. Scholz[a], E. Pippel[a], S. Senz[a], H. Kalt[b], U. Gösele[a], M. Zacharias[a,c]

[a] *Max-Planck-Institute of Microstructure Physics, Weinberg 2, 06120 Halle, Germany*
[b] *Universität Karlsruhe, Institut für Angewandte Physik, Wolfgang-Gaede-Straße 1, 76131 Karlsruhe, Germany*
[c] *IMTEK, Faculty of Applied Science, Albert-Ludwigs-University Freiburg, Georges -Köhler-Allee, 79110 Freiburg, Germany*

Received 14 February 2007; received in revised form 28 May 2007; accepted 28 June 2007 by J.W.P. Hsu
Available online 17 July 2007

Abstract

Single-crystal phosphorus-doped ZnO nanowires were synthesized by using a single-source precursor-based vapor transport method. The photoluminescence spectra of phosphorus-doped ZnO nanowires and undoped nanowires are compared. While both show several shallow bound exciton complexes, the phosphorus-doped nanowires reveal an additional distinct emission feature at 3.316 eV. Additionally, the time-resolved PL measurements were conducted to characterize the recombination dynamics.

PACS: 78.66.-w; 78.66.Hf; 78.47.+p

Keywords: A. Semiconductors; A. Nanostructures; C. Scanning and transmission electron microscopy; D. Optical properties

1. Introduction

ZnO nanowires with a direct band gap of 3.44 eV and a large exciton binding energy of 60 meV, have attracted increasing interest due to its potential applications in electronics and optoelectronics. Recently, a light-emitting diode (LED) based on a ZnO homojunction film was demonstrated [1,2]. It was the result of the reliable *p*-type doping of ZnO with a high concentration of nitrogen ($\sim 10^{20} cm^{-3}$) and a low-defect density. Devices based on ZnO nanowires could provide an alternative nanoscale UV light source. The synthesis of reliable *p*-type ZnO nanowires is thus desired. Despite its importance, only few results on the doping of ZnO nanowires have been reported so far [3–5].

In this paper, we demonstrate a versatile growth technique to synthesize phosphorus-doped ZnO (ZnO:P) nanowires in a reproducible way. With this approach, we are able to prepare phosphorus-doped single-crystal ZnO nanowires. We will discuss the detailed optical properties of phosphorus-doped ZnO nanowires based on low-temperature photoluminescence (PL) and time-resolved PL (TRPL).

2. Experimental details

In the typical growth process, ZnO:P nanowires are synthesized via a vapor transport process based on a single-source precursor, Zn_3P_2. In the approach presented here, Zn_3P_2 is used as source for both Zn and P. In order to meet the conditions of the sublimation of Zn_3P_2 and the formation of the liquid droplet of Au catalyst, the temperature at the source boat and the substrate were controlled at ∼500 °C and 800 °C, respectively. The details are as follows: an alumina boat containing the Zn_3P_2 powder and a Si substrate covered with a 5 nm Au film were placed in a small quartz tube, separated typically by 7–10 cm. This small quartz tube was then placed inside a horizontal tube furnace, where the source boat was positioned upstream from the substrate and located in front of the heating zone. A constant pressure was maintained during the growth process with an Ar gas of flow rate 30 sccm. The temperature of the furnace was set to 800 °C and typically kept at the maximum temperature for 40 min.

For comparison, undoped ZnO nanowires were also produced. Here, ZnO nanocrystals, which were prepared by a chemical solution deposition (CSD), were used for nanowire nucleation instead of a metal catalyst. The 0.75 M precursor

* Corresponding author. Tel.: +49 345 5582 641; fax: +49 345 5511 223.
E-mail address: dskim@mpi-halle.de (D.S. Kim).

0038-1098/$ - see front matter © 2007 Elsevier Ltd. All rights reserved.
doi:10.1016/j.ssc.2007.06.038

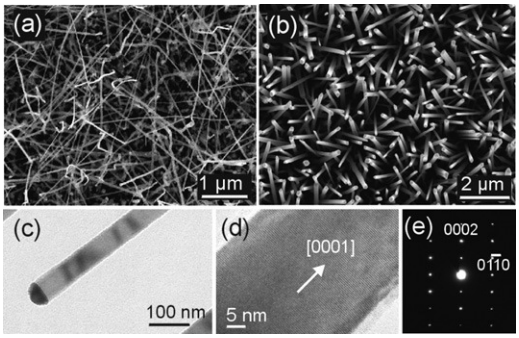

Fig. 1. SEM images of ZnO:P nanowires based on Au-assisted growth (a), and ZnO nanowires based on ZnO nanocrystals-assisted growth (b). (c) TEM image of a ZnO:P nanowire. (d) High-resolution TEM image of the ZnO:P nanowire. (e) The corresponding SAED pattern.

solution, which was prepared by stirring the components zinc acetate dihydrate and monoethanolamine in a molar ratio of 1:1 in 2-methoxyethanol for 3 h at 80 °C under Ar gas was deposited onto the Si substrate by spin coating. The as-deposited films were then preheated on a hotplate at 300 °C for 10 min. Finally the sample was annealed at 500 °C for 1 h. For nanowire growth, ZnO powder (Alfa Aesar, 99.999%) and graphite powder (Alfa Aesar, 99.9995%) were ground together (1:1 wt%) and loaded into an alumina boat. The substrate covered with the ZnO nanocrystal layer and the alumina boat were placed into a small quartz tube, separated typically by 10–11 cm. This small quartz tube was then placed inside a furnace quartz tube with the source boat positioned at the center of the heating zone and the substrate placed downstream of an Ar flow. The temperature of the furnace was set to 925 °C and typically kept at the maximum temperature for 30 min under a constant flow of Ar with 30 sccm. After the growth, the furnace was cooled to room temperature.

3. Results and discussion

The morphologies of the as-grown ZnO:P nanowires and ZnO nanowires were investigated using scanning electron microscopy (SEM). As shown in Fig. 1(a), entangled and uniform ZnO:P nanowires were grown on the Si substrate. The diameters of the nanowires range from 40–80 nm and their lengths reach a few micrometers. Fig. 1(b) shows quasi-aligned ZnO nanowires with well-defined facets on the Si substrate. The nanowires have a typical diameter of 30–100 nm and a length of a few micrometers. All wires are terminated by a flat plane. Transmission electron microscopy (TEM) analysis revealed that most of the ZnO:P nanowires are terminated by Au nanoparticles, indicating that ZnO:P nanowires were grown via a Au-assisted vapor–liquid–solid (VLS) process. Fig. 1(c) shows a representative TEM image of a ZnO:P nanowire. Fig. 1(d) shows a high-resolution TEM image of a ZnO:P nanowire with clearly resolved lattice fringes, confirming their crystallinity. Fig. 1(e) shows a selected-area electron diffraction (SAED) pattern obtained from a representative ZnO:P nanowire. It demonstrates that the nanowire is single-crystalline with a wurtzite structure and a growth direction along [0001].

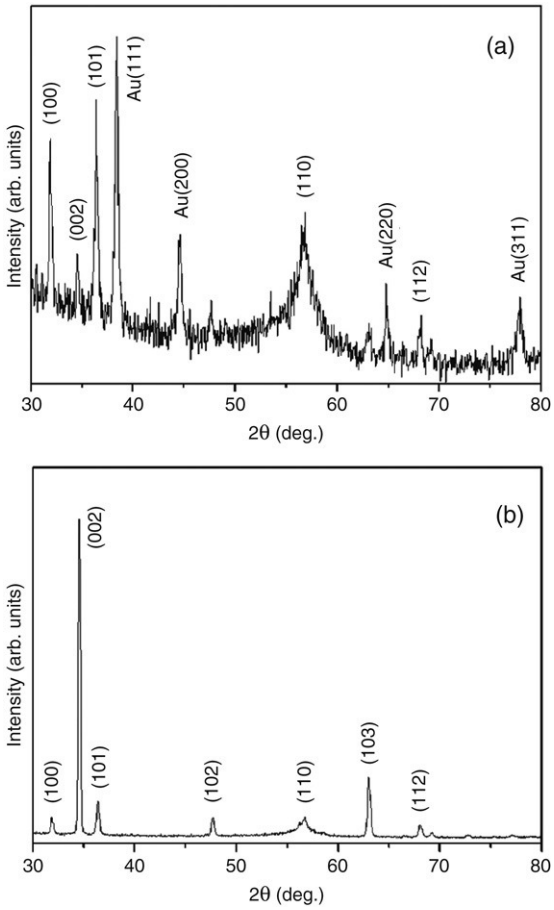

Fig. 2. XRD pattern of as-grown ZnO:P nanowires (a), and ZnO nanowires (b). The peaks of the Au used as catalyst can be seen in the sample of the doped wires.

In addition, Fig. 2(a) shows the X-ray diffraction (XRD) pattern of ZnO:P nanowires which confirms that no secondary phase exists in ZnO:P nanowires. In case of undoped ZnO nanowires, a typical XRD pattern of the hexagonal ZnO was observed as shown in Fig. 2(b).

The overall composition and the spatial distribution of phosphorus atoms in individual nanowires were investigated by energy-dispersive X-ray (EDX) spectroscopy. 4.3 at.% of phosphorus was detected at the Au-based metallic particles, located at the tip of ZnO:P nanowires. However due to the sensitivity limit of EDX (not better than approximately 1 at.%), we are not able to estimate the phosphorus content in the nanowires reliably. The EDX analysis of *p*-type GaN nanowires was also not sensitive enough to show the presence of Mg dopants [6]. Because of the difficulties in elemental analysis and electrical device fabrications for the quantitative analysis of the dopant concentration, we used low-temperature PL to prove and characterize the presence of phosphorus dopants in ZnO:P nanowires. PL spectroscopy is a very sensitive and nondestructive tool for investigating metal impurities in semiconductor nanowires [7].

PL of the samples was measured using the 325 nm line of a HeCd laser as excitation source with an intensity of $\sim$4 W/cm^2. The low-temperature PL spectra of ZnO:P and ZnO nanowires

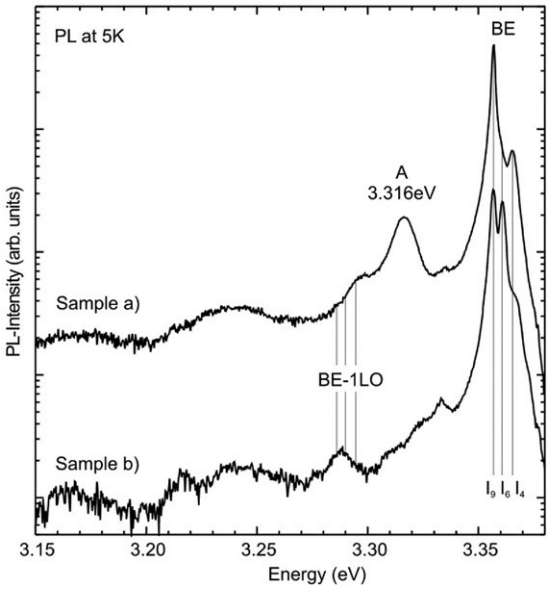

Fig. 3. Low-temperature PL spectra of as-grown ZnO:P nanowires (sample a), and ZnO nanowires (sample b), respectively.

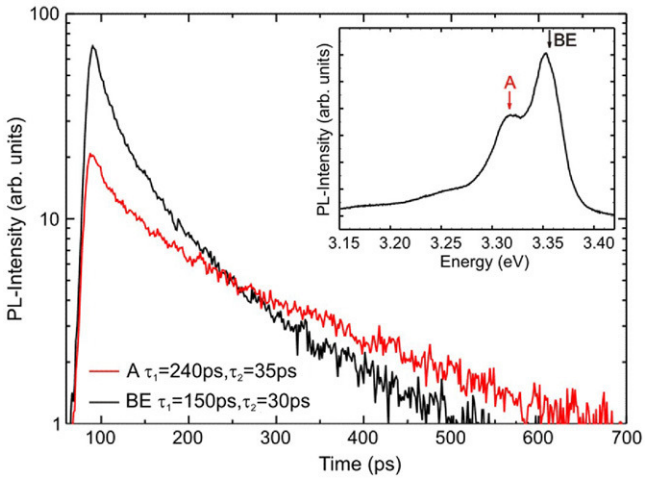

Fig. 4. Decay curves from time-resolved PL spectra of the BE and A emission peaks in ZnO:P nanowires. The inset shows the time-integrated PL spectrum.

are compared in Fig. 3. In the used liquid He-bath cryostat, a temperature of 5 K was measured in a thermal equilibrium of the copper sample holder with the attached sensor and the sample fixed on it by a heat-conducting glue. The spectrum of undoped ZnO nanowires shows typical transition features. In the present case, the strong emissions observed between 3.357 and 3.363 eV are bound exciton transitions (BE). These lines are typically labeled as I_4 (3.363 eV), I_6 (3.361 eV) and I_9 (3.357 eV) [8].

In the case of ZnO:P nanowires, the PL spectrum is again dominated by emission from shallow BE. Additionally, another emission band at 3.316 eV is observed, which is not found in the undoped ZnO nanowires. This band is in the following denoted by the letter A. Such an emission band around 3.31 eV has on one hand been reported in *p*-type nitrogen [9,10] or phosphorus [11,12] doped ZnO film. On the other hand such an emission band was also found in nominally undoped samples [11,15] and is strongly present in ZnO nanocrystals [15]. So far the physical origin of this emission is still unclear. But from our results it seems likely that this additional state is caused by the presence of phosphorus atoms in the ZnO nanowires.

Time-resolved PL (TRPL) spectroscopy was used to examine the time-dependent carrier dynamics in ZnO:P and ZnO nanowires. The signal was recorded by the use of a streak camera with a temporal resolution of 5 ps. The excitation in those measurements is accomplished by 150 fs pulses of a frequency doubled Ti:Sapphire-laser at 360 nm. In the TRPL measurement a He-flow cryostat was used and in thermal equilibrium a temperature of 13 K was measured. The decay curves of the radiative emission at the BE energy of 3.357 eV (I_9) and the A peak at 3.316 eV were monitored in Fig. 4. Both peaks show a biexponential decay, with a rapid decay component in the beginning. This is caused by the high-carrier densities shortly after the excitation pulse with several $\mu J/cm^2$. Therefore also the time-integrated PL spectrum, as shown in the upper right corner of Fig. 4, is broadened compared to the continuous wave PL measurement. The two emission bands which can be seen in the time-integrated spectrum are present at all times. While at earlier times the BE peak is dominant, the A peak contributes mainly to the emission with a monoexponential tail with a lifetime of about 240 ps at later times.

For unequivocally demonstrating that the incorporated phosphorus atoms actually lead to *p*-type doping as expected, further electrical measurements are required, and this is in progress. In general, implantation, diffusion and *in situ* doping during vapor phase or MBE growth have been adopted as methods of *p*-type doping in ZnO films. Our route to incorporate dopants in ZnO nanowires is, however, quite different from such ways of doping ZnO films. Phosphorus is incorporated into the nanowire lattice via the liquid alloy (Au–Zn) e.g., liquid-phase-assisted *in situ* doping not a vapor phase *in situ* doping. In this doping mode, the liquid–solid interface provides a low-energy site (e.g., a sink for the dopant), and facilitates the transport of dopants from the vapor to the crystal. Although all *p*-type dopants have a fairly low solubility in the ZnO lattice [13], we were able to grow phosphorus-doped ZnO nanowires. In addition, grown nanowires show no tapering. Since a few atomic layers of dopants deposited on the surface of a nanowire can dominate its overall electronic properties, dopant induced tapering is undesirable [14].

4. Conclusions

In summary, phosphorus-doped ZnO nanowires were synthesized by using a vapor transport process. Based on a single-source precursor, Zn_2P_3, single-crystal phosphorus-doped ZnO nanowires were produced in a reproducible way. Low- temperature PL spectra show that the presence of phosphorus strongly enhances a peak at 3.316 eV. We suggest that Au catalyst plays an important role for doping in ZnO nanowires.

Acknowledgements

This work was supported by the International Max Planck Research School for Science and Technology of Nanostructures (Nano-IMPRS) in Halle, the Deutsche Forschungsgemeinschaft (DFG) and the Landeskompetenznetz Baden-Wuerttemberg within the Competence Network 'Functional Nanostructures', Project A1.

References

[1] A. Tsukazaki, T. Onuma, M. Ohtani, T. Makino, M. Sumiya, K. Ohtani, S.F. Chichibu, S. Fuke, Y. Segawa, H. Ohno, H. Koinuma, M. Kawasaki, Nat. Mater. 4 (2005) 42.
[2] A. Tsukazaki, M. Kubota, A. Ohtomo, T. Onuma, K. Ohtani, H. Ohno, S.F. Chichibu, M. Kawasaki, Japan J. Appl. Phys., Part 2 44 (2005) L643.
[3] W. Lee, M.-C. Jeong, J.-M. Myoung, Acta Mater. 52 (2004) 3949.
[4] J.H. Park, I.S. Hwang, Y.J. Choi, J.G. Park, J. Cryst. Growth 276 (2005) 171.
[5] C.-L. Hsu, S.-J. Chang, Y.-R. Lin, S.-Y. Tsai, I.-C. Chen, Chem. Commun. (2005) 3571.
[6] Z. Zhong, F. Qian, D. Wang, C.M. Lieber, Nano Lett. 3 (2003) 343.
[7] J. Yoo, Y.-J. Hong, S.J. An, G.-C. Yi, B. Chon, T. Joo, J.-W. Kim, J.-S. Lee, Appl. Phys. Lett. 89 (2006) 043124.
[8] B.K. Meyer, H. Alves, D.M. Hofmann, W. Kriegseis, D. Forster, F. Bertram, J. Christen, A. Hoffmann, M. Straßburg, M. Dworzak, U. Haboeck, A.V. Rodina, Phys. Status Solidi B 241 (2004) 231.
[9] D.C. Look, D.C. Reynolds, C.W. Litton, R.L. Jones, D.B. Eason, G. Cantwell, Appl. Phys. Lett. 81 (2002) 1830.
[10] X.D. Yang, Z.Y. Xu, Z. Sun, B.Q. Sun, L. Ding, F.Z. Wang, Z.Z. Ye, J. Appl. Phys. 99 (2006) 046101.
[11] F.X. Xiu, Z. Yang, L.J. Mandalapu, J.L. Liu, W.P. Beyermann, Appl. Phys. Lett. 88 (2006) 052106.
[12] F.X. Xiu, Z. Yang, L.J. Mandalapu, J.L. Liu, Appl. Phys. Lett. 88 (2006) 152116.
[13] C.G. Van de Walle, D.B. Laks, G.F. Neumark, S.T. Pantelides, Phys. Rev. B 47 (1993) 9425.
[14] A.B. Greytak, L.J. Lauhon, M.S. Gudiksen, C.M. Lieber, Appl. Phys. Lett. 84 (2004) 4176.
[15] J. Fallert, R. Hauschild, F. Stelzl, A. Urban, M. Wissinger, H. Zhou, C. Klingshirn, H. Kalt, J. Appl. Phys. 101 (2007) 73506.

Paper V

Kirkendall effect induced evolution of coaxial ZnO/Al_2O_3 one-dimensional heterostructures: from core-shell nanowires to spinel nanotubes and mesoporous nanowires

Y. Yang, D. S. Kim, M. Knez, R. Scholz, A. Berger, E. Pippel, U. Gösele, M. Zacharias, *J. Phys. Chem. C* **112**, 4068 (2008)

Nanoscale solid state reactions between ZnO nanowires and alumina shell deposited by atomic layer deposition are closely examined. It is shown that a combination of surface diffusion and Kirkendall effect cause the formation of well defined spinel nanotubes if the reaction temperature is carefully controlled.

Y. Yang prepared the manuscript. The author of this thesis (D.S.Kim) performed the growth of ZnO nanowires and was involved in the design of the experiments and in discussions of the results.

Influence of Temperature on Evolution of Coaxial ZnO/Al_2O_3 One-Dimensional Heterostructures: From Core−Shell Nanowires to Spinel Nanotubes and Porous Nanowires

Yang Yang,*,† Dong Sik Kim,† Mato Knez,† Roland Scholz,† Andreas Berger,† Eckhard Pippel,† Dietrich Hesse,† Ulrich Gösele,† and Margit Zacharias‡

Max Planck Institute of Microstructure Physics, Weinberg 2, 06120 Halle, Germany, and IMTEK, Faculty of Applied Science, Albert-Ludwigs-University Freiburg, Georges-Köhler-Allee, 79110 Freiburg, Germany

Received: November 16, 2007; In Final Form: January 4, 2008

In this paper, we present the influence of temperature on the Kirkendall effect-related evolution of coaxial ZnO/Al_2O_3 one-dimensional heterostructures based on a solid-state reaction. Controllable fabrication of spinel $ZnAl_2O_4$-based nanotubes and porous nanowires can step-by-step be achieved from ZnO/Al_2O_3 core−shell nanowires with a change in the reaction temperature. In particular, we demonstrate that the formation of completely hollow nanotubes in this system is not strictly limited to a fixed stoichiometry of ZnO/Al_2O_3 required for the spinel-forming reaction when an annealing temperature of 800 °C is employed. Combined with atomic layer deposition, the wall thickness of the formed nanotubes can be further precisely tailored and defined. Our finding provides an effective route to fabricate spinel nanotubes as well as nanotube arrays on a large scale.

1. Introduction

Tubular nanostructures have attracted considerable attention due to their potential application in electronics, optoelectronics, catalysis, and controlled release. To be able to meet such suitable applications, nanotubes of a wide range of solids including carbon, metals, semiconductors, and/or insulators have been fabricated.[1] Until now, a variety of routes has been developed for the fabrication of nanotubes, where the most widely applied are vapor-phase synthesis using a catalyst,[2,3] template-based methods,[4,5] and thin-film rolling.[6] Recently, our group reported a new approach to produce tubular nanostructures such as spinel $ZnAl_2O_4$ nanotubes, where a thermally induced interfacial solid−solid reaction of ZnO/Al_2O_3 core−shell nanowires can directly be used to fabricate single-crystalline $ZnAl_2O_4$ nanotubes based on the Kirkendall effect.[7] Similar phenomena toward hollow nanospheres have been demonstrated by other groups. Alivisatos et al. first reported the preparation of hollow CoS nanoparticles by the sulfidation of Co nanoparticles in solution based on the Kirkendall effect.[8] The Kirkendall effect is a classical phenomenon in metallurgy. Initially, it describes a nonequilibrium mutual diffusion process through an interface of two bulk materials accompanied by the simultaneous occurrence of a vacancy diffusion to compensate for the unequal material flow. Voids can be formed at the interface as a result of condensation of excess vacancies. Since nanoscale systems involve a spatial confinement, high surface-to-volume ratios, and greater crystalline perfection relative to the bulk counterparts, void formation can be enhanced due to a more localized vacancy supersaturation. After a net material flux across the interface by a preferred outward diffusion, a single void is possible that can be supported at the center of the nanoscale materials. Such a concept of the nanoscale Kirkendall effect provides the methodology for producing hollow nanostructures composed of different compounds,[10−15] as also was outlined in a recent review article.[16]

Moreover, continuous interest in the nanoscale Kirkendall effect has initiated new experimental findings of the influence of the surface diffusion on the formation of hollow $ZnAl_2O_4$ nanostructures.[17] Derived from the available experimental results, an ideal size parameter was also proposed for the formation of completely hollow nanotubes. For instance, if a 10 nm-thick alumina shell is grown by atomic layer deposition (ALD), a critically narrow thickness range of 10−15 nm for the ZnO nanowire core is indispensable for achieving the complete transformation from core−shell structures to nanotubes at an annealing temperature of 700 °C.[7,17] However, first of all, preparing ZnO nanowires with a uniform diameter is still a challenge, and second, the reliance of the whole process on temperature is still unknown. Therefore, if one desires the fabrication of spinel nanotubes on a large scale, the careful examination of this process and its dependence on core−shell ratios as well as reaction (diffusion) temperatures is necessary.

In this study, we investigated the dynamic morphology evolution of ZnO/Al_2O_3 core−shell nanowires by controlling the synthesis temperature. On the basis of the previous findings of the Kirkendall effect and the surface diffusion effect on the production of $ZnAl_2O_4$ spinel nanotubes from a ZnO/Al_2O_3 core−shell structure, we attempted to present a clear portrait of the diffusion processes that accompanies the chemical transformations under different temperatures. In contrast to the results our group described before, it was found for the first time that the formation of a completely hollow spinel nanotube is not strictly limited to a constant stoichiometry of ZnO/Al_2O_3 core−shell structures at a higher reaction temperature of 800 °C. A further increase of the temperature to 900 °C led to the formation of porous nanowires. Besides the clarification of the related mechanism, we extend this synthetic method to epitaxially grown ZnO nanowires to produce arrays of spinel nanotubes under optimal conditions.

* Corresponding author. E-mail: yangyang@mpi-halle.de.
† Max Planck Institute of Microstructure Physics.
‡ Albert-Ludwigs-University Freiburg.

10.1021/jp710948j CCC: $40.75
Published on Web 02/22/2008

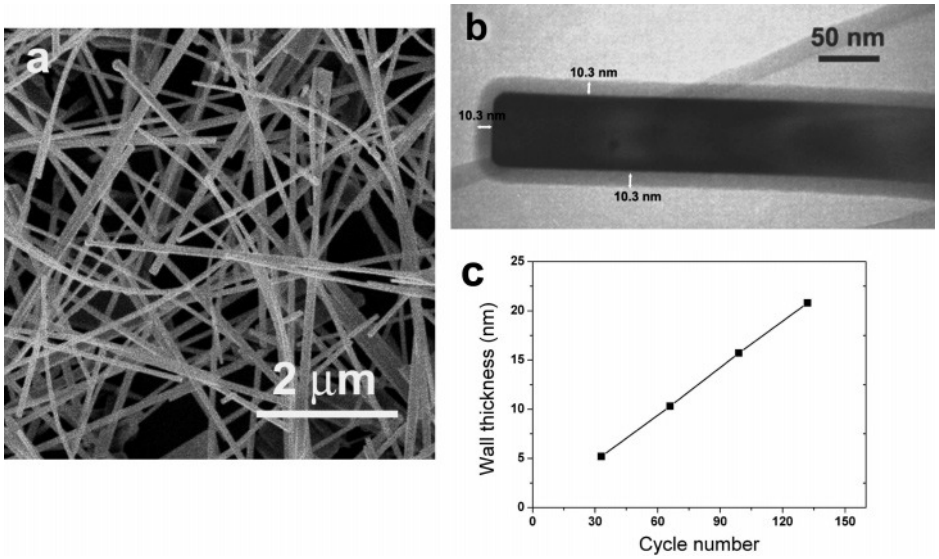

Figure 1. (a and b) SEM and TEM images of an example of the ZnO/Al_2O_3 core−shell nanowires prepared by using 66 ALD cycles. (c) Wall thickness of Al_2O_3 shell measured by TEM as a function of ALD cycle number.

2. Experimental Procedures

2.1. Methods. ZnO nanowires with various diameters were grown by a vapor transport method using Au nanoparticles as the catalyst. Detailed experimental conditions have been described previously.[18] For the epitaxial growth of ZnO nanowires, GaN/Si was used as a substrate, on which a thin Au film was deposited as the catalyst. Subsequently, the ZnO/Al_2O_3 core−shell nanowires were fabricated by depositing thin Al_2O_3 films on the as-prepared ZnO nanowires by ALD (Savannah 100, Cambridge Nanotechnology Inc.). Trimethylaluminum [$Al(CH_3)_3$, TMA] and water were selected as the aluminum precursor and oxygen reactant sources, respectively. The deposition was begun with a substrate temperature of 150 °C and a background pressure of 0.15 Torr. During each deposition cycle, TMA and water were alternately introduced into the ALD chamber in pulses of 0.3 and 1.3 s, respectively. An exposition time of 20 s and a successive purge time of 20 s under an Ar stream (10 sccm) were employed for both precursors. The thickness of the alumina shell was controlled by the number of precursor/purge cycles. Under the current deposition conditions, the average growth rate for Al_2O_3 was 1.5 Å per cycle as measured from TEM images. We used a total number of 33, 66, 99, and 132 cycles, respectively, to obtain alumina layers with adjustable thicknesses from ∼5 to ∼20 nm.

The ZnO/Al_2O_3 core−shell nanowires were then annealed in an open quartz tube furnace at 500, 600, 700, 800, and 900 °C for 5 h, respectively. For the ZnO/Al_2O_3 core−shell nanowire arrays, we performed an interfacial solid-state reaction at 800 °C for 5 h.

2.2. Instruments. The obtained nanostructures were characterized and analyzed using SEM (JEOL, JSM-6300F), TEM (JEOL, JEM-1010; Philips, CM20T), and high-resolution TEM (JEOL, JEM-4010). Scanning energy-dispersive X-ray spectra were obtained using a Philips CM20FEG scanning TEM instrument.

3. Results and Discussion

3.1. Formation of ZnO/Al_2O_3 Core−Shell Nanowires. First, we investigated the deposition of Al_2O_3 layers on ZnO nanowires. Figure 1a is a SEM image of the ZnO nanowires coated with a thin layer of Al_2O_3 by using 66 ALD cycles. The core−shell nanowires have a broad size distribution, with diameters ranging from 40 to 200 nm. TEM investigation (Figure 1b) shows an individual ZnO nanowire (dark contrast) covered by a layer of amorphous Al_2O_3 (light contrast). The Al_2O_3 layer has a very uniform thickness of 10.3 nm along the ZnO nanowire. The precise control of the shell thickness is attributed to the sequential and self-limiting ALD process, which avoids any gas-phase reaction in the system and allows the target Al_2O_3 film to grow layer-by-layer around the ZnO nanowire.[19,20] Therefore, the thickness of the Al_2O_3 shell can be accurately adjusted by the number of repeated ALD cycles. When we use a total number of 33, 66, 99, and 132 cycles, the Al_2O_3 layer deposited on the ZnO nanowire presents a conformal thickness of 5.1, 10.3, 15.5, and 20.5 nm, respectively, within the accuracy of few angstroms (see Supporting Information Figure S1). The dependence of the layer thickness on the ALD cycle number is illustrated in Figure 1c. From the linear relationship shown in the plot, the average growth rate of the Al_2O_3 layer is calculated to be 1.5 Å/cycle.

3.2. Annealing at Different Temperatures. To see how the synthesis temperature influences the nanotube formation, we used a series of ZnO nanowires coated by a 10.3 nm Al_2O_3 layer and annealed them at different temperatures but maintained the same period of 5 h. We denote the samples as samples A−E, which correspond to ZnO/Al_2O_3 core−shell nanowires annealed at 500, 600, 700, 800, and 900 °C, respectively.

3.2.1. Annealing at 500 and 600 °C. Figure 2 demonstrates the evolution of the morphology at low temperatures (500 and 600 °C). Figure 2a shows the typical TEM image of sample A. At first glance, there is no significant change in the morphology of the core−shell nanostructure after reaction. Its corresponding electron diffraction (ED) pattern in Figure 2b shows the typical set of spots for single-crystal hexagonal ZnO with a growth direction of [0001]. The diffusive halo in the center of Figure 2b might originate from the amorphous alumina since it cannot be obviously crystallized at 500 °C. Nevertheless, from the magnified image of some core−shell nanowires, a number of small voids could be detected at the interface of ZnO/Al_2O_3 (Figure 2c). The nanowire interface became intersected in sample B (Figure 2d), where irregularly shaped voids are clearer as shown in Figure 2e,f. Nucleation of voids at the ZnO core is unlikely. Previously, Maezawa et al. reported the formation of an aluminate-type phase (i.e., surface spinel) even at a synthesis

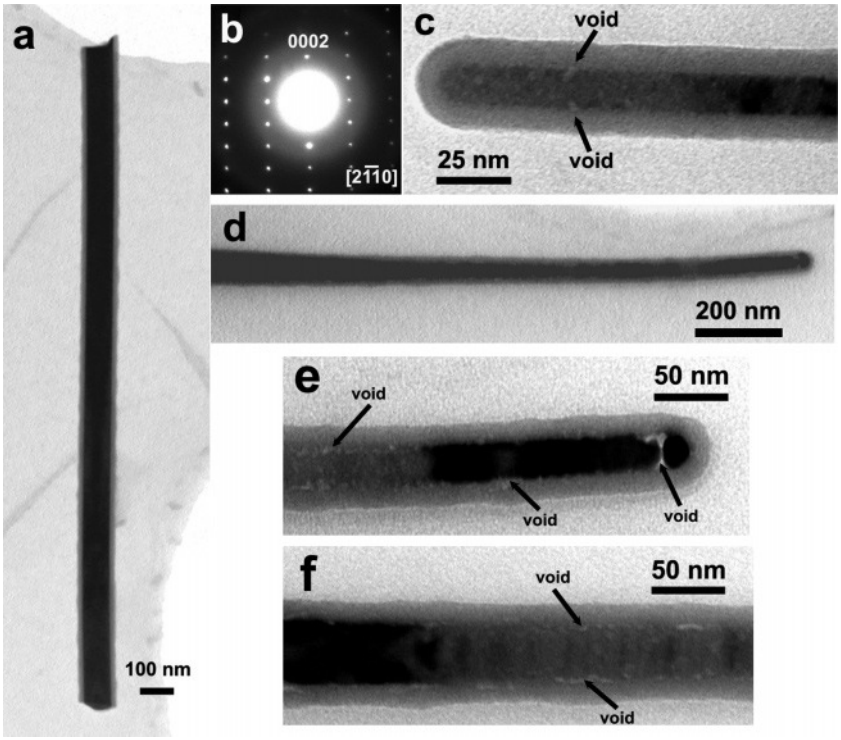

Figure 2. (a and b) Low magnification TEM image and corresponding ED pattern of a typical sample A nanowire after annealing at 500 °C. (c) TEM image of end section of a sample A nanowire. (d) TEM overview of a typical sample B nanowire after annealing at 600 °C. (e and f) Magnified images from the end and middle sections of the nanowire shown in panel d.

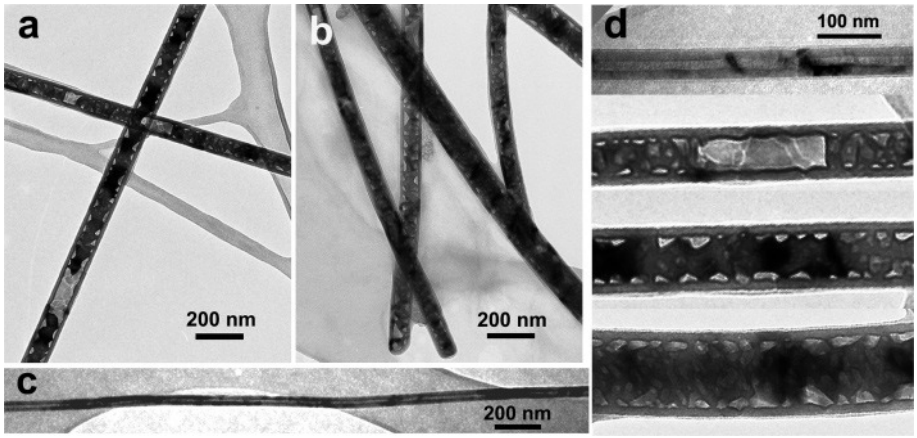

Figure 3. (a−c) TEM images of typical 1-D nanostructures of sample C after annealing at 700 °C. (d) Outline of differently sized 1-D nanostructures of sample C.

temperature of 400 °C.[21] This interaction involves the diffusion of Zn ions into tetrahedral sites in a surface lattice of Al_2O_3 to form spinel-like structures. The scattered small voids along the interface of sample A can be understood as a consequence of the redistribution of zinc ions from the core into the alumina followed by coalescing vacancies to voids. This implies that the reaction begins at temperatures as low as 500 °C. The gradually developed voids at 600 °C in sample B indicate a greater diffusion of ZnO into the alumina subsurface. However, the diffusion is limited at this temperature. Indeed, no more change upon morphology took place even after the annealing of sample B for 20 h. Note that the tip of the core−shell nanowires is the preferential site for void evolution (Figure 2e), which may be related to a high interface energy near the boundary due to its highest curvature.

3.2.2. Annealing at 700 °C. Figure 3 presents the typical TEM images of sample C annealed at 700 °C. The main structural feature for the most part of the annealed nanowires was the encapsulation of the ZnO core in the spinel nanotubes (Figure 3a,b), which have been confirmed by structural analysis (data not shown). Large voids distributed along the interface clearly show the existence of bridge-like linkages between the residual ZnO core and the spinel shell. Completely hollow spinel nanotubes already could be found in this case, as shown in Figure 3c. As compared to the other 1-D structures (Figure 3a,b), these nanotubes have a very narrow outer diameter of 30−40 nm, consistent with the results reported before.[7,17] Figure 3d sums up all the typical 1-D nanostructures of sample C, where the wall thickness of the differently sized nanostructures similarly falls into the range of 15−20 nm.

The Kirkendall effect-induced voids are initially formed from the bulk diffusion, which is driven by a 1-D steady-state bulk flux related to the concentration gradient. Since ZnO has been identified to be the dominant diffusing species in the ZnO/Al_2O_3 couple,[7] the diffusion-controlled process will generate a series of voids at the interface with the spinel $ZnAl_2O_4$ formed.

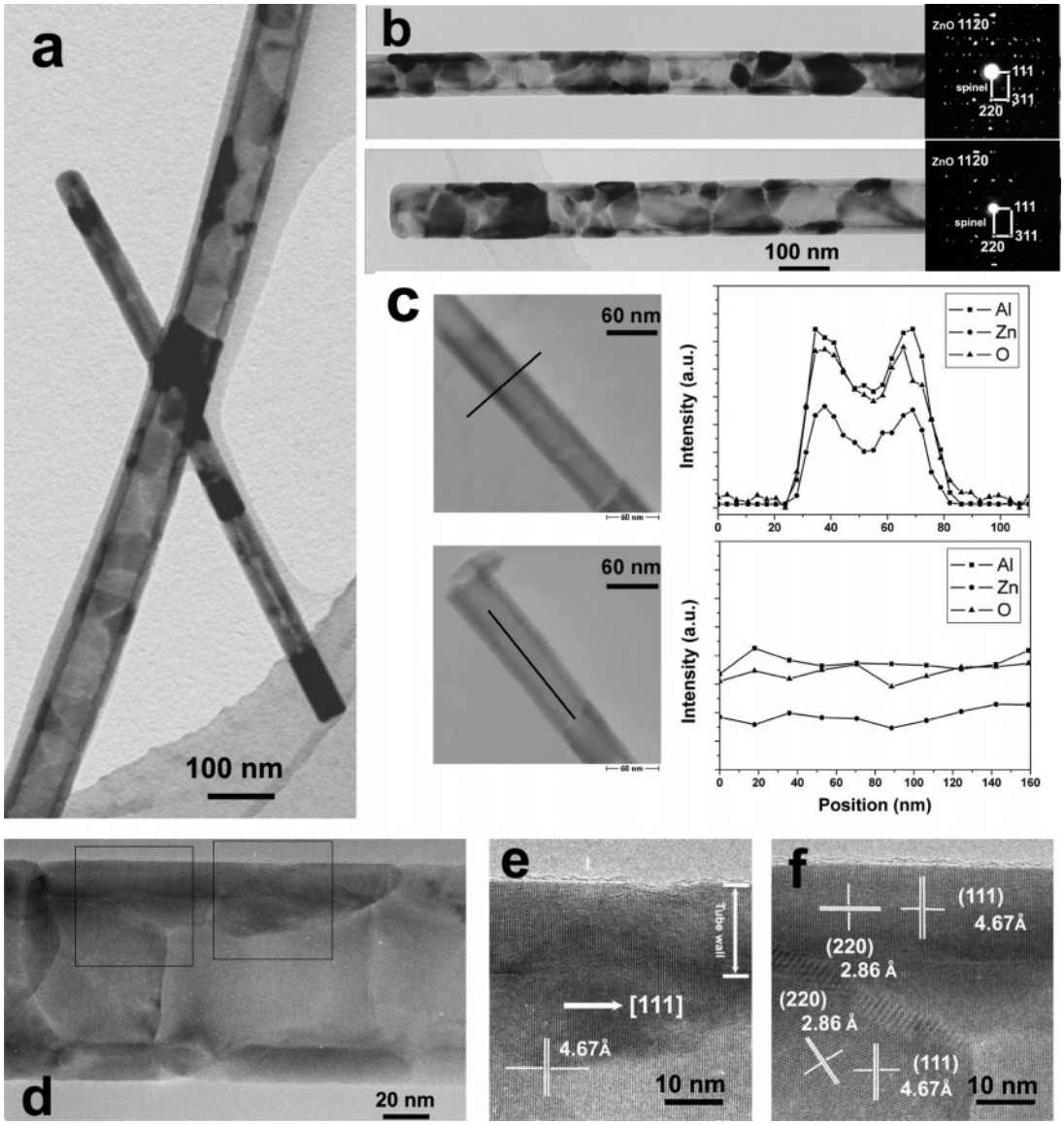

Figure 4. (a) Low magnification TEM image of spinel nanotubes with different diameters after annealing at 800 °C (sample D). (b) Two isolated spinel nanotubes and their corresponding ED pattern. (c) Intensity profile of Zn, Al, and O across and along one tube diameter. (d) Atomic-resolution TEM image of a spinel nanotube. (e and f) Images magnified from the selected area in panel d.

Considering that the activation energy of the ZnO surface diffusion (158 kJ/mol)[22] is much lower than that of bulk diffusion (347−405 kJ/mol),[23] it is reasonable that the adatoms of the remaining ZnO will dominantly diffuse along the pore surface to the reaction front. With the gradual formation of $ZnAl_2O_4$ through the one-way diffusion of ZnO, vacancies are continuously generated and flow inward. Once the ZnO core exceeds the amount required for a complete transformation of the Al_2O_3 shell, unconsumed ZnO would still exist in the interior. As a result, interrupted tubes with segmented voids or mesoporous nanowires containing unequally sized voids would be formed. From an experimental point of view, reaction in a vapor or solution phase looks more favorable than a solid−solid reaction for achieving the complete transformation of the core since the supply of the shell material is sufficient under the former conditions. Thus, it seems that on this condition (700 °C), only for samples having a narrow diameter distribution, such a solid−solid reaction of core−shell nanowires will be suitable for a large-scale synthesis of nanotubes or for transferring a whole array of nanowires into spinel nanotubes.

3.2.3. Annealing at 800 °C. In the case of sample D involving 800 °C annealing, we find that all the core−shell nanowires were transformed into completely hollow nanotubes irrespective of their dimension ratio (Figure 4a). Hollow tubular structures were even formed for tapered nanowires (see Supporting Information Figure S2). Figure 4b shows the TEM image of two isolated nanotubes with a rather large diameter in the range of 100−110 nm. In both cases, the entire tube wall is composed of multiple crystal domains. However, the corresponding ED pattern clearly reveals that the tubular structure grows preferentially with the (111) planes of cubic $ZnAl_2O_4$ perpendicular to the tube axis. The local composition of the nanotube was investigated with EDX spectra by line scanning across and along a nanotube axis (Figure 4c). The intensity profile of elements Al, Zn, and O across the nanotube presents a valley-like shape characteristic of completely hollow nanotubes. However, the nanotubes seem not to be composed of a pure spinel phase since we detected weak diffraction spots of hexagonal ZnO in the ED patterns (Figure 4b). This conclusion was further confirmed by EDX analysis. For a formed nanotube with a diameter of 70 nm (Figure S3a), the atomic ratio of elements Zn/Al is about 1.4:1, deviating from the theoretical value of 0.5:1 calculated from the chemical formula of $ZnAl_2O_4$. Thus, some Zn or ZnO is possibly mixed with the spinel.

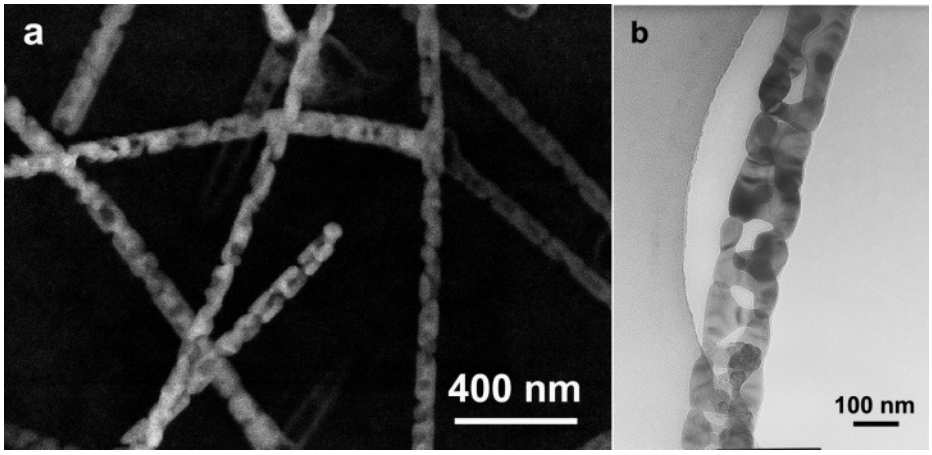

Figure 5. (a and b) SEM and TEM images of porous nanowires of sample E after annealing at 900 °C.

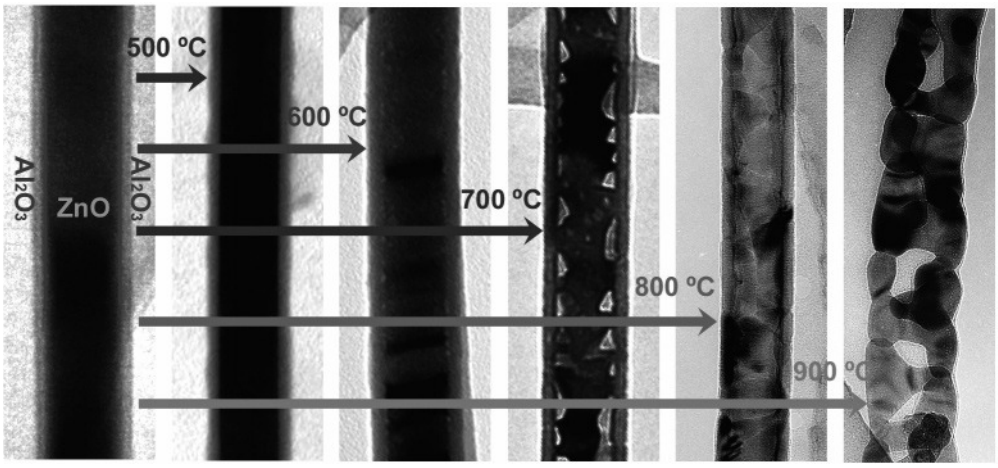

Figure 6. Outline of ZnO/Al_2O_3 core−shell nanowires with an excess core for the solid-state reaction annealed at different temperatures.

Nevertheless, the EDX line scanning parallel to the tube axis (Figure 4c) as well as the elemental mapping (Figure S3b) exhibits a quite uniform distribution of Zn, Al, and O in the whole region of the nanotube, and no enriched areas of Zn were found. Figure 4d illustrates an atomic resolution TEM image of a 110 nm-thick polycrystalline nanotube. From the magnified images near the tube-edge region (Figure 4e,f), the lattice image of a discrete crystalline wall with a thickness of around 15 nm can be observed. Although domains or grain boundaries with different crystal orientations exist, the (111) $ZnAl_2O_4$ spinel plane with an interplanar spacing of 4.67 Å in the long single-crystalline sections is always vertical to the tube axis, consistent with the results of the ED pattern, pointing to a (111) texture. Note that we did not find any ZnO nanocrystals during our TEM investigations.

Evidently, a temperature of 700 °C assured a complete transformation of Al_2O_3 and the corresponding ZnO involved in this solid−solid reaction. However, the excess ZnO core in the spinel nanotube was hardly affected at this temperature even after a longer annealing time. When the reaction temperature was increased to 800 °C, the diffusion of the remaining ZnO once frozen at 700 °C seems to be triggered. Krost et al. observed that epitaxial ZnO layers could be flattened at a high annealing temperature (900 °C).[24] Its mechanism was ascribed to a redistribution of ZnO clusters on the surface based on the Gibbs−Thomson effect. This means that the residual ZnO core with a very rough surface (see, i.e., Figure 3) might be unstable at a higher temperature such as 800 °C in our nanoscale system. The excess ZnO is likely to diffuse along the void surface toward the spinel wall and reach its outer surface, where most of it is desorbed or evaporated from the tube.[25−27] Some residual Zn and O ions are probably homogeneously dissolved in the spinel matrix similar to what is known for the $MgAl_2O_4$ spinel system.[28] In this case, the formed tubular structures can be regarded as Zn-rich spinel nanotubes. Alternatively, ZnO might form a thin layer attached to the inner surface of the tube wall.

Similar as to what was observed for the formation of nanospheres based on the Kirkendall effect, the spinel shell tends to crystallize in larger grains at a high reaction temperature of 800 °C.[10,15] The appearance of such a textured graining structure can be ascribed to the simultaneous nucleation of spinel at multiple contact points along the longitudinal axis of each nanowire induced by surface diffusion. Moreover, the lattice rearrangement from a wurtzite ZnO to a cubic $ZnAl_2O_4$ during the migration of ZnO is another important reason. However, the formed $ZnAl_2O_4$ nanotubes exhibit preferential ordering of the (111) planes perpendicular to the tube axis. For an fcc structure such as spinel $ZnAl_2O_4$, the surface energy of different facets follows {111} < {100} < {110}. Therefore, {111} is the dominant facet that encloses the crystal.[29] On the other hand, in addition to the textured graining structure, cation antiphase boundaries, a general phenomenon for a spinel system may be present.[30] The grain nucleated at different positions only generates cation stacking faults. The oxygen sublattice can remain identical on each side of the spinel grain, which also favors the orientation of the formed spinel nanotube.

3.2.4. Annealing at 900 °C. When the reaction proceeded at 900 °C, dramatic changes upon the morphology were observed

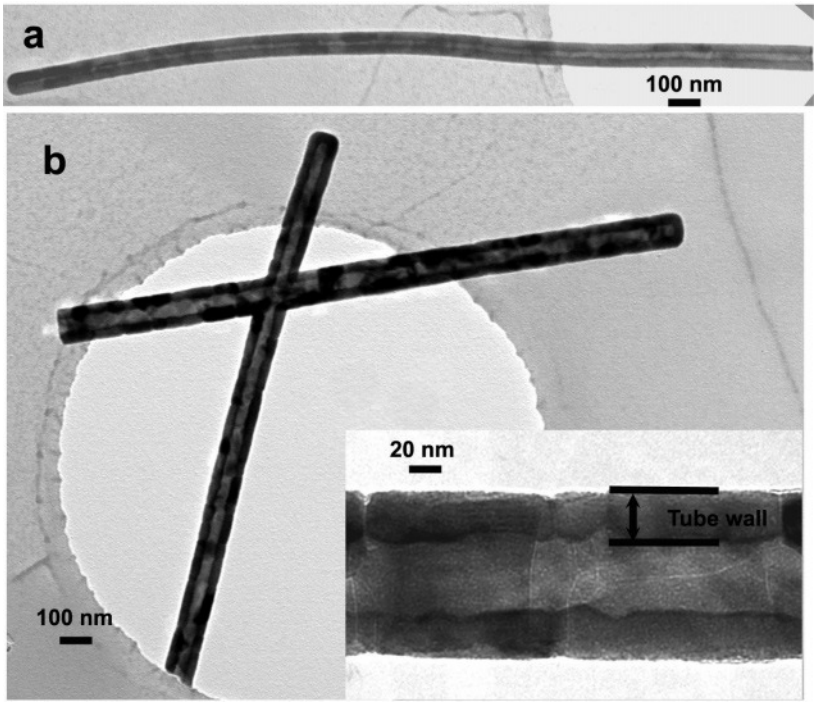

Figure 7. (a and b) TEM images of ZnO nanowires coated by 20.5 nm alumina layer after reaction at 800 °C for 5 h. Inset in panel b is an enlarged view of a nanotube structure.

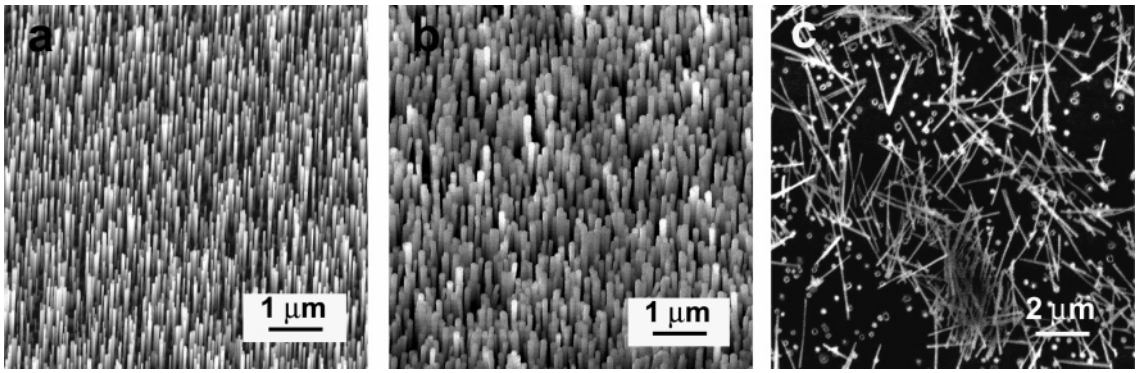

Figure 8. (a) SEM image of ZnO nanowire arrays grown on a GaN/Si substrate. (b) SEM image of ZnO nanowire arrays coated with a 20.5 nm alumina layer after reaction at 800 °C for 5 h. (c) Fractured interface between the spinel nanotubes and the substrate.

(sample E). Figure 5a shows a typical SEM image, where porous nanowires with different diameters were observed. The TEM image in Figure 5b further demonstrates that the 1-D porous structure consists of crystalline domains with a string of voids included in the interior. In a theroretical study by Tu and Gösele, the thermal stability of the hollow nanostructures, especially those formed on the basis of the Kirkendall effect, was discussed.[31] It was pointed out that a nanotube with thick walls should thermodynamically be rather unstable. To decrease the surface energy, atoms are inclined to diffuse from the nanotube outer surface to the inner region. Partial voids are finally eliminated, leading to the formation of a string of voids instead of a hollow cylinder for reducing its surface area. For the hollow spinel nanostructures generated at 900 °C, the high temperature would significantly increase the inner concentration of thermal vacancies under a negative pressure. These vacancies gradually went to the sink on the outer surface of the nanotube. Some parts of the wall, especially where the grain boundaries exist, will collapse. Eventually, discontinuous voids will be formed in the core.

3.2.5. Outline of 1-D Nanostructures Obtained at Different Annealing Temperatures. On the basis of the previous investigations, the influence of temperature on the conversion of single-crystalline ZnO nanowires covered by a 10.3 nm-thick Al_2O_3 layer is concluded in Figure 6. Importantly, it is revealed that a higher reaction temperature such as 800 °C can lead to the formation of completely hollow spinel nanotubes regardless of the initial core−shell diameter ratio. Besides, all the resulting nanotubes are characterized by an approximately identical wall thickness, which is determined by the deposited alumina layer.

3.3. Fabrication of Spinel Nanotubes with Thicker Tube Walls at 800 °C. Since the thickness of the alumina shell can be precisely tuned by ALD, a large-scale fabrication of $ZnAl_2O_4$-related nanotubes with an adjustable wall thickness is expected. To prove the concept further, ZnO nanowires were coated by a 20.5 nm Al_2O_3 layer. As shown in Figure 7a,b, all the core−shell nanowires could be transformed into completely hollow nanotubes after annealing at 800 °C for 5 h. From the inset of Figure 7b, the wall thickness was found to be 30 nm, as expected.

3.4. Large-Scale Fabrication of Vertically Arranged Spinel Nanotube Arrays at 800 °C. In a last experiment, we applied this method to vertically aligned ZnO nanowires for demonstrating vertically arranged spinel nanotube arrays. Figure 8a shows the SEM image of the as-prepared ZnO nanowire array grown on a GaN/Si substrate. After the ALD deposition of a 20.5 nm-

thick alumina layer and annealing at 800 °C for 5 h, the array structure is well-conserved (Figure 8b). TEM observations confirm that all the aligned 1-D nanostructures are textured grainy nanotubes independent of their diameter (Figure S4). Figure 8c shows an SEM image where open ends on the substrate are visible together with the corresponding nanotubes.

4. Conclusion

In summary, the evolution of coaxial ZnO/Al_2O_3 core−shell nanowires at different temperatures was studied in detail. The results reveal that the initial voids formed at the core−shell interface originate from the migration of ZnO based on the Kirkendall effect. The dynamics is accelerated at 700 °C, favored by the surface diffusion of ZnO along the present void surface. Completely hollow spinel nanotubes can be formed at this temperature provided that the ZnO core is totally consumed by the solid−solid reaction. At a higher temperature of 800 °C, the unconsumed ZnO core can be further removed via diffusion, desorption, and redistribution processes. Therefore, all the starting core−shell nanowires with various diameters are transformed into completely hollow nanotubes. The wall thickness is approximately determined by the initial thickness of the deposited alumina layer. Reactions at 900 °C lead to the formation of porous nanowires, which are derived from the collapsing of the spinel nanotubes due to their thermal instability. As the most important point, our results demonstrate that at a suitable reaction temperature, either freestanding or vertically aligned spinel nanotubes with a controllable wall thickness can be fabricated on a large scale via the Kirkendall effect-induced approach.

Acknowledgment. This work was supported by the Deutsche Forschungsgemeinschaft and the German Federal Ministry of Education and Research (BMBF).

Supporting Information Available: TEM images of ZnO/Al_2O_3 core−shell nanowires prepared by different ALD cycles, hollow tubular structures formed from tapered nanowires and spinel nanotubes formed on the GaN/Si substrate, and EDX spectrum and elemental mapping of spinel nanotubes. This material is available free of charge via the Internet at http://pubs.acs.org.

References and Notes

(1) Xia, Y.; Yang, P.; Sun, Y.; Wu, Y.; Mayers, B.; Gates, B.; Yin, Y.; Kim, F.; Yan, H. *Adv. Mater.* **2003**, *15*, 353.
(2) Dekker, C. *Phys. Today* **1999**, *52*, 22.
(3) Iijima, S. *Nature (London, U.K.)* **1991**, *354*, 56.
(4) Goldberger, J.; He, R.; Zhang, Y.; Lee, S.; Yan, H.; Choi, H. J.; Yang, P. *Nature (London, U.K.)* **2003**, *422*, 599.
(5) Wang, Y.; Wu, K. *J. Am. Chem. Soc.* **2005**, *127*, 9686.
(6) Schmidt, O. G.; Eberl, K. *Nature (London, U.K.)* **2001**, *410*, 168.
(7) Fan, H. J.; Knez, M.; Scholz, R.; Nielsch, K.; Pippel, E.; Hesse, D.; Zacharias, M.; Gösele, U. *Nat. Mater.* **2006**, *5*, 627.
(8) Yin, Y.; Rioux, R. M.; Erdonmez, C. K.; Hughes, S.; Somorjai, G. A.; Alivisatos, A. P. *Science (Washington, DC, U.S.)* **2004**, *304*, 711.
(9) Smigelskas, A. D.; Kirkendall, E. O. *Trans. AIME* **1947**, *171*, 130.
(10) Yin, Y.; Erdonmez, C. K.; Cabot, A.; Hughes, S.; Alivisatos, A. P. *Adv. Funct. Mater.* **2006**, *16*, 1389.
(11) Li, Q.; Penner, R. M. *Nano Lett.* **2005**, *5*, 1720.
(12) Wang, Y.; Cai, L.; Xia, Y. *Adv. Mater.* **2005**, *17*, 473.
(13) Zeng, H. C. *J. Mater. Chem.* **2006**, *16*, 649.
(14) Chiang, R. K.; Chiang, R. T. *Inorg. Chem.* **2007**, *46*, 369.
(15) Peng, S.; Sun, S. *Angew. Chem., Int. Ed.* **2007**, *46*, 4155.
(16) Fan, H. J.; Gösele, U.; Zacharias, M. *Small* **2007**, *3*, 1660.
(17) Fan, H. J.; Knez, M.; Scholz, R.; Hesse, D.; Nielsch, K.; Zacharias, M.; Gösele, U. *Nano Lett.* **2007**, *7*, 993.
(18) Kim, D. S.; Ji, R.; Fan, H. J.; Bertram, F.; Scholz, R.; Dadgar, R.; Nielsch, K.; Krost, A.; Christen, J.; Gösele, U.; Zacharias, M. *Small* **2007**, *3*, 76.
(19) Leskelä, M.; Ritala, M. *Angew. Chem., Int. Ed.* **2003**, *42*, 5548.
(20) Peng, Q.; Sun, X. Y.; Spagnola, J. C.; Hyde, G. K.; Spontak, R. J.; Parsons, G. N. *Nano. Lett.* **2007**, *7*, 719.
(21) Maezawa, A.; Okamoto, Y.; Imanaka, T. *J. Chem. Soc., Faraday Trans. 1* **1987**, *83*, 665.
(22) Birnboim, A.; Olorunyolemi, T.; Carmel, Y. *J. Am. Ceram. Soc.* **2001**, *84*, 131.
(23) Tomlins, G. W.; Routbort, J. L.; Mason, T. O. *J. Am. Ceram. Soc.* **1998**, *81*, 869.
(24) Krost, A.; Christen, J.; Oleynik, N.; Dadgar, A.; Deiter, S.; Bläsing, J.; Krtschil, A.; Forster, D.; Bertram, F.; Diez, A. *Appl. Phys. Lett.* **2004**, *85*, 1496.
(25) Fan, H. J.; Scholz, R.; Kolb, F. M.; Zacharias, M.; Gösele, U. *Solid State Commun.* **2004**, *130*, 517.
(26) Wang, X.; Summers, C. J.; Wang, Z. L. *Adv. Mater.* **2004**, *16*, 1215.
(27) Zhou, J.; Liu, J.; Wang, X.; Song, J.; Tummala, R.; Xu, N. S.; Wang, Z. L. *Small* **2007**, *3*, 622.
(28) Alper, A. M.; McNally, R. N.; Ribbe, P. G.; Doman, R. C. *J. Am. Ceram. Soc.* **1962**, *45*, 264.
(29) Wang, Z. L.; Mohamed, M. B.; Link, S.; El-Sayed, M. A. *Surf. Sci.* **1999**, *440*, 809.
(30) Hesse, D.; Bethge, H. *J. Cryst. Growth* **1981**, *52*, 875.
(31) Tu, K. N.; Gösele, U. *Appl. Phys. Lett.* **2005**, *86*, 93111.

Paper VI

Surface reaction of ZnO nanowires with electron-beam generated alumina vapor

H.J. Fan, A. Lotnyk, R. Scholz, Y. Yang, D. S. Kim, E. Pippel, D. Hesse, M. Zacharias, *J. Phys. Chem. C* **112**, 6770 (2008).

The reaction of ZnO nanowires with vapor phase alumina shells is studied. Phase boundary reactions dominate at the surface and result in rugged nanowires composed of ZnO nanowires and spinel particles.

H. J. Fan prepared the manuscript and designed the experiments. The author of this thesis (D.S.Kim) performed growth experiments of ZnO nanowires and was involved in discussions.

Surface Reaction of ZnO Nanowires with Electron-Beam Generated Alumina Vapor

Hong Jin Fan,*,†,‡ Andriy Lotnyk,† Roland Scholz,† Yang Yang,† Dong Sik Kim,† Eckhard Pippel,† Stephan Senz,† Dietrich Hesse,† and Margit Zacharias†,#

Max Planck Institute of Microstructure Physics, Weinberg 2, 06120 Halle, Germany, Department of Earth Sciences, University of Cambridge, Cambridge CB2 3EQ, United Kingdom, Faculty of Applied Science (IMTEK), Albert-Ludwigs-University Freiburg, Georges-Köhler-Allee, 79110 Freiburg, Germany

Received: December 28, 2007; In Final Form: February 22, 2008

Single-crystal ZnO nanowires are reacted at 800−900 °C in vacuum with alumina vapor generated by electron beam evaporation. The morphology changes after the solid−vapor reactions are studied in detail using electron microscopy and compared to other similar spinel nanostructures. Unlike other solid−vapor reactions like $MgO-Al_2O_3$ and $ZnO-Ga_2O_3$ where a continuous spinel layer is formed, the reaction of ZnO nanowires with alumina vapor is unique. The initially smooth surfaces of ZnO nanowires become rugged due to surface decomposition without the growth of spinel layers. A formation mechanism is proposed that the surface reaction of ZnO with alumina vapor might constitute a process of a unilateral transport of ZnO and the associated surface diffusion.

Introduction

The controlled fabrication and assembly has been the mainstream of the nanowire research driven by their application potential as building blocks for semiconductor electronic and optoelectronic circuits.[1,2] On the other hand, nanowires are also widely used as chemical (reactive) or physical (nonreactive) templates for nanotubes and core−shell nanowires.[3−5] The ZnO nanostructure is one of most studied systems, but the main attention is put to their structural, optical, and optoelectronic properties. ZnO is also a reactive material. A number of spinel-type ternary compound nanostructures, for example, $ZnAl_2O_4$,[6,7] Zn_2SiO_4,[8] Zn_2TiO_4,[9] Zn_2SnO_4,[10] $ZnGa_2O_4$,[11] $ZnFe_2O_4$,[12] $ZnSb_2O_4$,[13] have been synthesized either through solid-state reactions of the ZnO nanowire precursor with other corresponding oxides or in situ alloying.

Spinel oxides have potential applications in sorbents, battery materials, catalysts, humidity sensors, phosphors, and magnetic data storage. Some recent reports[14] on 1D spinel nanomaterials indicate an increasing attention to the nanoscale fabrication and characterization of spinel materials.

Solid-state reactions of type $AO + B_2O_3 \rightarrow AB_2O_4$ are a common way for the fabrication of spinel oxides. Traditional studies on spinel-formation reactions are usually conducted at planar interfaces or in form of powder mixture by bringing two solid binary oxides, or a solid oxide and a vapor or liquid phase, into contact at high temperatures (>1000 °C).[15] The growth process of classical spinel oxides (e.g., $ZnFe_2O_4$ and $MgAl_2O_4$) involves Wagner's cation counterdiffusion mechanism, namely, cations migrating through the reaction interface in opposite directions and the oxygen sublattice remaining essentially fixed.[16,17] The reaction of ZnO (wurzite structure, $a = 3.250$ Å, $c = 5.207$ Å) with Al_2O_3 into $ZnAl_2O_4$ spinel (cubic structure, $a = 8.088$ Å) is special: the growth mechanism involves the diffusion of both Zn and O and an effective unilateral transfer of ZnO into the spinel (see Figure S1 in Supporting Information). This was first pointed out by Bengtson and Jagitsch,[18] and later readdressed by Navias,[19] Branson,[20] and Keller et al.[21] This means that an inert marker plane placed at the initial interface will be found at the ZnO/spinel interface for the $ZnO-Al_2O_3$ reaction, whereas in the case of the $MgO-Al_2O_3$ reaction, the marker plane is within the spinel layer. In our recent experiment of solid−solid interface reactions of core−shell nanowires, hollow spinel nanotubes were developed directly from $ZnO-Al_2O_3$, whereas spinel shells were based on $MgO-Al_2O_3$.[22] This is consistent with the diffusion mechanism and a consequence of the spatial confinement given by the cylindrical symmetry of the reaction.

Depending on whether it is a solid−solid or solid−vapor reaction, the ZnO-based spinel nanostructures mentioned above[6−13] show different morphologies. For the particular interesting $ZnO-Al_2O_3$ system, no report has been made so far for the reactions of solid ZnO with alumina vapor. In this study, ZnO nanowires were reacted in vacuum with alumina vapor generated by e-beam evaporation. E-beam evaporation in vacuum is a standard method used widely for solid−vapor reactions on bulk substrates,[23,24,25] due to its merits of easy control of the deposition rate and the substrate temperature. Interestingly, after reaction, the ZnO nanowire surface becomes rugged due to decomposition, and some of the wires are coated by small spinel nanoparticles, a structure dramatically different from that after a solid−solid reaction. This provides a route toward single-crystalline chainlike ZnO nanowires, which are difficult to grow by other methods. Such rough ZnO nanowires might be more advantageous for photocatalytic and/or gas sensing behavior because of a higher surface area compared to that of smooth wires.

Experimental Section

Vertically aligned ZnO nanowires on GaN/Si substrates were synthesized inside a horizontal double-tube resistance furnace via a vapor transport and deposition method.[26] The nanowire samples were then subjected to aluminum oxide vapor. The latter

* Corresponding author. E-mail: hfan05@esc.cam.ac.uk.
† Max Plank Institute of Microstructure Physics.
‡ University of Cambridge.
# Albert-Ludwigs-University Freiburg.

10.1021/jp712135p CCC: $40.75
Published on Web 04/10/2008

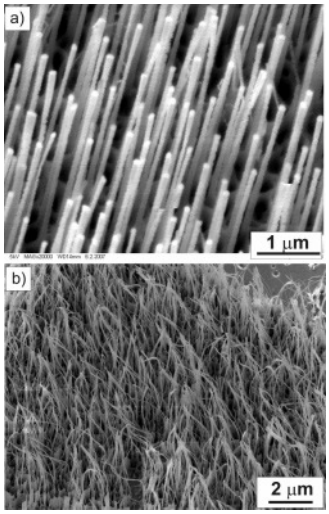

Figure 1. SEM images of the ZnO nanowires after reacting with Al_xO_y vapor. Thick wires (~100 nm) retain their vertical alignment (a) and those thin ones (<50 nm) become curved (b).

was generated in a high-vacuum chamber by electron-beam evaporation of pressed Al_2O_3 powder tablets. The samples were hanging over the electron-beam evaporator with the nanowires facing the alumina source. The distance between evaporator and the substrates is ≈20 cm, which is quite large. This minimizes the heat load on the sample and thus prevents a rise in sample temperature during deposition. The sample was heated to 800−900 °C in a tube furnace directly by thermal irradiation, before it was subjected to the vapor beam. The base pressure of the system was $<2 \times 10^{-5}$ mbar. During deposition pure oxygen was introduced to establish a pressure of 1×10^{-4} mbar. The reaction time was in the range of 10−160 min. For comparison, one ZnO nanowire sample was annealed under similar conditions except that no alumina vapor was generated. After deposition, the samples were kept in the vacuum chamber and allowed to cool to room temperature.

Results

The ZnO nanowires stand vertically to the GaN surface before being subjected to the alumina vapor at 800 or 900 °C. After reaction, thick nanowires retain the vertical alignment (Figure 1a) whereas those thin ones generally lose their alignment and become randomly oriented (see Figure 1b). Detailed transmission electron microscopy (TEM) investigation reveals that the initially smooth nanowires transform into a rugged morphology with necks on the surface. The degree of decomposition depends mainly on the temperature. Elongated reactions at 900 °C result in more-rugged surface than reaction at 800 °C. In addition, the nanowires after reaction at 900 °C have tiny particles attached at the necklike thinner parts of their surface. In contrast, the nanowires after the 800 °C reaction regardless of their thickness have no attachment of such nanoparticles and the whole wires become chainlike. We will examine the structures after reaction at the two temperatures separately.

Figure 2 shows the representative chainlike morphology of those thin (<50 nm) nanowires after being subjected to alumina vapor at 800 °C. TEM analysis and the selected area electron diffraction (SEAD) pattern in Figure 3 revealed that the wires are not spinel $ZnAl_2O_4$, as anticipated from solid−solid reaction,[6] or the reaction of vapor Zn with a solid alumina matrix.[7] Instead, they contain mainly ZnO lattice without obvious growth of a spinel layer. The scanning EDX spectrum along the length of such chainlike wire (Figure 3c) shows a small amount of Al

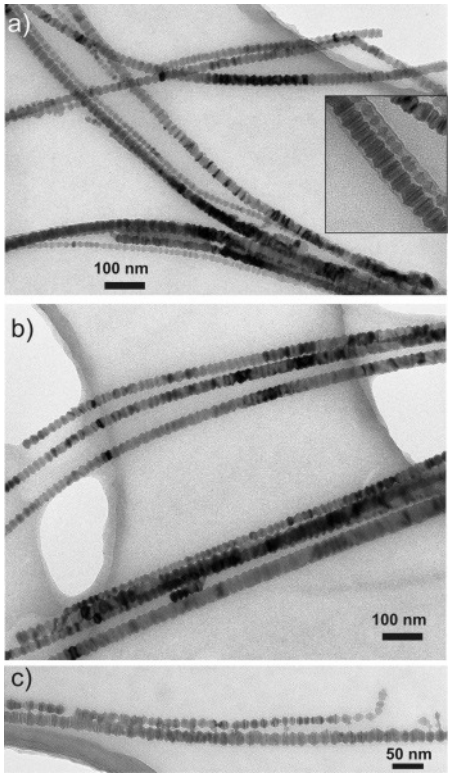

Figure 2. TEM images showing the general structure after the initially smooth ZnO nanowires were subjected to alumina vapor at 800 °C for 80 min. Inset in (a) is a close-up view.

far below the stoichiometric percentrage of Zn spinel, which might come from a thin alumina layer on the surface. Furthermore, the reacted wires also contain a large amount of defects visible as lines across the diameter. Figure 3a gives an example of such defects in a thin nanowire. The nature of these defects is unknown at present stage, but is most likely due to consumption of the near-surface Zn and O atoms by the reaction with alumina vapor.

Experiments were also conducted at 800 °C for various periods of time ranging from 10 to 160 min (see Figure S2 in Supporting Information). The nanowire surface was slightly rugged at early reactions and the surface roughness appeared unchanged for reactions until 160 min. Again no outer layer of spinel was observed.

When the reaction temperature was raised to 900 °C, spinel formed by the solid−vapor reaction on the nanowire surface. Figure 4a−c gives an overview of the reacted wires after reaction at 900 °C for 160 min (some unreacted wires are also present as will be discussed later). A SEAD pattern recorded from one of the rugged wires is shown in Figure 4d. In addition to the dominating wurtzite ZnO spots in $[1\bar{2}10]$ transmission direction, weak spots fitting to $ZnAl_2O_4$ spinel can be identified. The maximum depth of the necks is ≈42 nm. Again, the ZnO crystal lattice body was preserved from the initial nanowire. Spinel nanoparticles were attached to the wire surface, mainly in the necks (Figure 5a). The measured lattice plane distance perpendicular to the wire axis corresponds to $d_{(0002)} = 0.26$ nm of wurtzite ZnO. High-resolution TEM examination of the particles on the wire surface verified the phase of the wire body and the surface particles to be wurzite ZnO and cubic $ZnAl_2O_4$, respectively. The lattice images of two representative particles are shown in Figure 5b,c from which the lattice spacings are measured: 4.04 and 4.67 Å, fitting to the *d*-spacings of (002) and (111) $ZnAl_2O_4$ planes, respectively.[27] Figure 5d−f displays

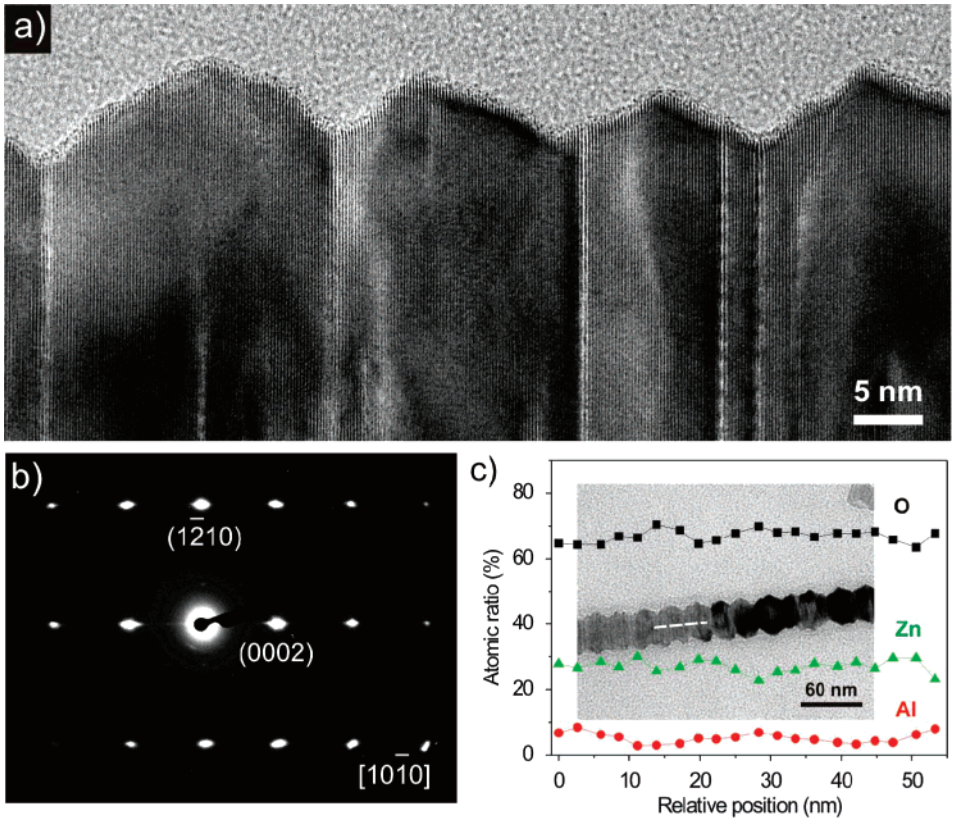

Figure 3. (a) HRTEM image of the wire surface (Figure 2) showing the necks and corresponding defect lines. (b) Electron diffraction pattern of a rugged wire verifying the absence of lattice spots from Zn spinel. (c) Typical spectra of atomic percentages of Zn, Al, and O along the dashed line in the inset image determined by EDX. The atomic ratio of oxygen is not real because of the characteristics of the instrument.

the fast Fourier transformation (FFT) patterns from two surface particles, as well as that from the wire body. Both particles are in [−110] transmission, and the $ZnAl_2O_4$ (111), (002), and (220) spots can be easily indexed.

Discussion

The change in surface structure is not caused by thermal evaporation of the ZnO nanowires[8] due to vacuum annealing. This is because, as shown above (Figure 4a), some smooth wires were also found in the sample subjected to vacuum reaction. These smooth wires were intact due to blockage from the alumina vapor by the sample holder during the reaction. If vacuum annealing were the cause, all the wires should be transformed. Furthermore, we annealed one ZnO nanowire sample under the same conditions without introducing alumina vapor. The surfaces of these nanowires remained intact (see Supporting Information, Figure S3). The equilibrium total vapor pressure of ZnO near 900 °C is about 4.0×10^{-5} mbar,[28] which is close to the background pressure in the chamber. Therefore, evaporation of the solid ZnO nanowires is insignificant and cannot explain the formation of the necks.

Let us now make a comparison to other spinel 1D nanostructures. First, our previously reported $ZnAl_2O_4$ spinel nanotubes were obtained via a solid−solid interface reaction of ZnO−Al_2O_3 core−shell nanowires.[6] In this case, the unilateral (outward) transport of ZnO into spinel resulted in hollow tubular nanowires, as a result of spatial confinement given by the cylindrical symmetry of the reaction. Moreover, control experiments were conducted in which the ZnO nanowires were coated with a 3 nm thick ALD alumina shell (to compare the results of solid−vapor and solid−solid reactions with a comparable spinel particle size). The resulting structure is internally porous composite wires with an outer smooth spinel shell of about 3 nm.[29] Therefore, a continuous and uniform covering of alumina is the key to the formation of a smooth spinel layer.

Second, for comparison we also conducted the solid−gas reaction to MgO nanowires (thickness ∼50−100 nm) under identical conditions as the ones described above. Generally, a continuous spinel-type compound layer was formed surrounding the remaining MgO core. An example of such structure and its corresponding composition analysis is shown in Supporting Information, Figure S4. The result is qualitatively the same as that through a solid−solid interface reaction of MgO−Al_2O_3 core−shell nanowires that we reported previsouly.[22] It is also in consistence with the result of solid−vapor reactions on single-crystal MgO substrates[23] and with solid−solid reactions between sapphire substrates and MgO thin films.[30]

Finally, in the experiment by Li et al.[11b] ZnO nanowires were in situ reacted with Ga−O vapor at 500 °C for 30−60 min, forming an outer shell of $ZnGa_2O_4$ spinel. No hollow interior or rippled surface was observed. Similarly, our preliminary results show that an interfacial solid−solid reaction of ZnO core nanowire with a 20 nm thick Fe_2O_3 shell resulted in ZnO−$ZnFe_2O_4$ core−shell nanowires. This indicates that a diffusion process different from the ZnO−Al_2O_3 system had occurred in the ZnO−Ga_2O_3 and ZnO−Fe_2O_3 reactions.

The above comparison leads to the suggestion that the formation of the necks might be correlated to the unilateral transfer of ZnO into the forming spinel particles during the surface reaction between ZnO and the impinged alumina. On the basis of this, a model is proposed as follows.

The alumina vapor species (Al_xO_y) impinge the ZnO nanowire surface and locally react with ZnO due to the substrate temperature (900 °C). Because of a slow evaporation process,

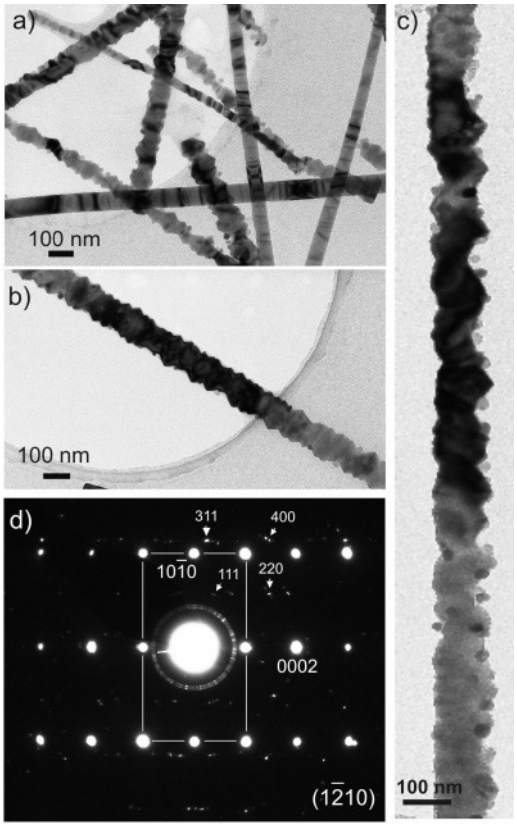

Figure 4. (a−c) TEM images of general morphology of the rugged wires after reaction with Al_xO_y vapor at 900 °C for 160 min, showing the etching-like surface necks and attachment of particles. Note also some smooth nanowires collected from the same sample but not reacted with Al_xO_y vapor. (d) Selected area diffraction pattern recorded from one reacted wire. The 4-digital indexes are spots from ZnO, while 3-digital ones fit $ZnAl_2O_4$ spinel.

discontinuous $ZnAl_xO_y$ islands are formed, similar to the early stage of the solid−vapor reaction on a planar substrate.[23] At the reaction interface, nanogaps analogous to the Kirkendall-type voids are generated as a result of the outward diffusion of ZnO into the spinel particles.[6] At this stage, diffusion of ZnO along the surface of the necks to the reaction interface (namely, bottom of the clusters) might become the major material delivery mode, compared to the volume diffusion.[31] The subsequent Al_xO_y atoms, which do not diffuse into the volume of the nanowires, stay preferably at the surface necks or around the ZnO/spinel cluster interfaces, which are low-energy sites compared to the smooth surfaces. With the enlargement of the gaps by losing surface ZnO atoms, deeper necks as seen in Figure 3 are developed. It is noteworthy that this process is similar to the reaction of TiO_2 substrate with e-beam generated BaO vapor, as reported by some of the authors.[31d] In the latter case, voids were observed on top of the substrate as a result of surface diffusion of TiO_2 during the solid−vapor reaction, roughening the original smooth TiO_2 surface.

In the experiments conducted by Wang et al.[7b] where anodic alumina membranes reacted with Zn vapor, a thin (<4 nm) layer of $Zn_4Al_{22}O_{37}$ phase was detected after reaction at 650 °C for <600 min, whereas a ~15 nm thick $ZnAl_2O_4$ spinel layer was obtained at higher temperatures for longer reaction time (800 min). The $Zn_4Al_{22}O_{37}$, with an hcp crystal structure, is a transition phase of the final spinel phase. In our experiments, the small nanoparticles were determined to be Zn spinel based on HRTEM images and the diffraction patterns (Figure 5b−f). The possibility of the formation of a similar thin transitional

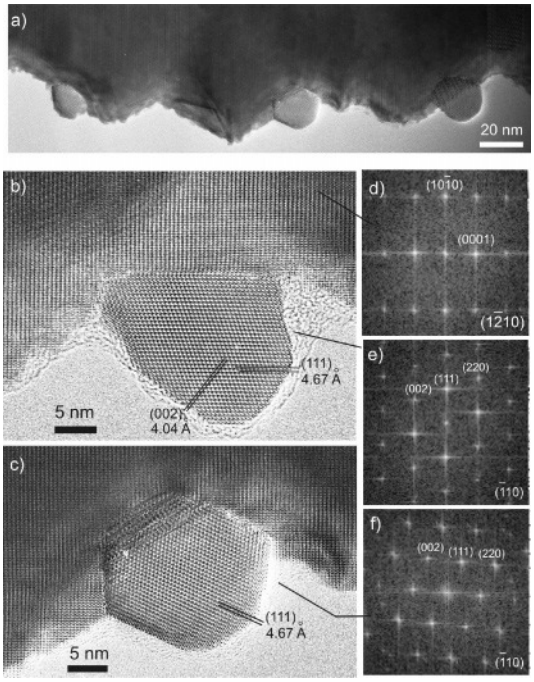

Figure 5. (a) Surface structure of the initially smooth ZnO nanowires after reacting with alumina vapor at 900 °C for 160 min. (b,c) HRTEM pictures of two particles, showing the wire body is ZnO and particles are $ZnAl_2O_4$ spinel. (d−f) FFT patterns taken from the wire body particle in panels b and c, respectively (The indexes sit above the spots).

layer of $Zn_4Al_{22}O_{37}$ in our experiment is small because of the following reasons: first, our higher growth temperature of 900 °C should enhance the growth of Zn spinel and bypass the transition phase. Second, our growth was limited by amount of alumina, in contrast to Wang's case where the growth was limited by the volume diffusion of Zn into the solid alumina. Therefore, the reaction in our experiments did not favor the occurrence of the Zn-deficient phase $(ZnO)_4-(Al_2O_3)_{11}$.

In the case of other systems like MgO−Al_2O_3 and ZnO−Ga_2O_3, the cations counterdiffuse during the solid−vapor reaction so that a layer of spinel shell, or polycrystalline islands, is grown around the remaining core. No pits on the nanowires are formed. Therefore, the deposition of Al_xO_y atoms on the surfaces of the MgO nanowires is relatively continuous. Volume diffusion is the sole material exchange mechanism for the reaction because a continuous solid interface is maintained.[32]

Conclusion

In summary, a solid−vapor reaction of ZnO nanowires at 900 °C in vacuum with alumina vapor does not result in the anticipated $ZnAl_2O_4$ spinel nanowires, but rather in rippled wires of a preserved ZnO phase. By comparing to the result of a similar experiment on MgO nanowires, as well as other spinel oxide 1D nanostructures like $ZnGa_2O_4$, the morphology change is correlated to the unilateral transport of ZnO into alumina during the $ZnAl_2O_4$-forming surface reaction and the associated development of gaps at the interface. Moreover, we propose that surface diffusion of ZnO is the dominating mass transport process enhancing the formation of necks and thus of the rippled morphology of the wires.

As a general conclusion, it appears that both the details of a spinel forming reaction on nanowires (used as substrate and one reactant) and the morphology of the growing spinel phase critically depend on the kind of diffusion mechanism (unilateral or counterdiffusion) and on the state of aggregation (vapor or solid) of the second reactant.

Acknowledgment. We thank Dr. A. Dadgar for providing the GaN/Si substrates and Dr. A. Berger for performing preliminary EDX analysis of the $MgAl_2O_4$ sample.

Supporting Information Available: Experimental details for growth of MgO nanowires, schematics of the accepted diffusion mechanisms for spinel formation, SEM images of ZnO nanowires after reaction with alumina vapor at 800 °C for 10, 40, 80, and 160 min, and SEM images of the ZnO nanowires after being subjected to vacuum annealing. This information is available free of charge via the Internet at http://pubs.acs.org.

References and Notes

(1) Lieber, C. M.; Wang, Z. L. *MRS Bulletin* **2007**, *32*, 99.
(2) Fan, H. J.; Werner, P.; Zacharias, M. *Small* **2006**, *2*, 700.
(3) Xiong, Y.; Mayers, B. T.; Xia, Y. *Chem. Commun*. **2005**, 5013.
(4) Goldberger, J.; Fan, R.; Yang, P. *Acc. Chem. Res*. **2006**, *39*, 239.
(5) (a) Shen, G. Z.; Bando, Y.; Ye, C. H.; Yuan, X. L.; Sekiguchi, T.; Golberg, D. *Angew. Chem. Int. Ed*. **2006**, *45*, 7568. (b) Hu, J. Q.; Bando, Y.; Liu, Z. W.; Zhan, J. H.; Golberg, D. *Angew. Chem. Int. Ed.* **2004**, *43*, 63. (c) Liu, Z.; Zhang, D.; Han, S.; Li, C.; Lei, B.; Lu, W.; Fang, J.; Zhou, C. *J. Am. Chem. Soc.* **2005**, *127*, 6. (d) Han, S.; Li, C.; Liu, Z.; Lei, B.; Zhang, D.; Jin, W.; Lei, X.; Tang, T.; Zhou, C. *Nano Lett.* **2004**, *4*, 1241.
(6) Fan, H. J.; Knez, M.; Scholz, R.; Nielsch, K.; Pippel, E.; Hesse, D.; Zacharias, M.; Gösele, U. *Nat. Mater*. **2006**, *5*, 627.
(7) (a) Wang, Y.; Wu, K. *J. Am. Chem. Soc.* **2005**, *127*, 9686. (b) Wang, Y.; Liao, Q.; Lei, H.; Zhang, X. P.; Ai, X. C.; Zhang, J. P.; Wu, K. *Adv. Mater.* **2006**, *18*, 943.
(8) Zhou, J.; Liu, J.; Wang, X.; Song, J.; Tummala, R.; Xu, N. S.; Wang, Z. L. *Small* **2007**, *3*, 622.
(9) (a) Manik, S. K.; Bose, P.; Pradhan, S. K. *Mater. Chem. Phys.* **2003**, *82*, 837. (b) Yang, Y.; Sun, X. W.; Tay, B. K.; Wang, J. X.; Dong, Z. L.; Fan, H. M. *Adv. Mater.* **2007**, *19*, 1839.
(10) (a) Wang, J. X.; Xie, S. S.; Yuan, H. J.; Yan, X. Q.; Liu, D. F.; Gao, Y.; Zhou, Z. P.; Song, L.; Liu, L. F.; Zhao, X. W.; Dou, X. Y.; Zhou, W. Y.; Wang, G. *Solid State Commun.* **2004**, *131*, 435. (b) Jie, J. S.; Wang, G. Z.; Han, X. H.; Fang, J. P.; Yu, Q. X.; Liao, Y.; Xu, B.; Wang, Q. T.; Hou, J. G. *J. Phys. Chem. B* **2004**, *108*, 8249. (c) Chen, H. Y.; Wang, J. X.; Yu, H. C.; Yang, H. X.; Xie, S. S.; Li, J. Q. *J. Phys. Chem. B* **2005**, *109*, 2573.
(11) (a) Chang, K. W.; Wu, J. J. *J. Phys. Chem. B* **2005**, *109*, 13572. (b) Li, Y. J.; Lu, M. Y.; Wang, C. W.; Li, K. M.; Chen, L. J. *Appl. Phys. Lett*. **2006**, *88*, 143102.
(12) Zacharias, M.; Kim, D. S. Max Planck Institute of Microstructure Physics and Albert-Ludwigs-University Freiburg, unpublished, 2008.
(13) Zeng, D. W.; Xie, C. S.; Dong, M.; Jiang, R.; Chen, X.; Wang, A. H.; Wang, J. B.; Shi, J. *Appl. Phys. A* **2004**, *79*, 1865.
(14) (a) Wu, X. C.; Tao, Y. R.; Han, Z. J.; Zhang, B. D. *J. Mater. Chem.* **2003**, *13*, 2649. (b) Bae, S. Y.; Seo, H. W.; Na, C. W.; Park, J. H. *Chem. Commun.* **2004**, *16*, 1834. (c) Zhang, Z. T.; Rondinone, A. J.; Ma, J. X.; Shen, J.; Dai, S. *Adv. Mater.* **2005**, *17*, 1415. (d) Bae, S. Y.; Lee, J.; Jung, H.; Park, J.; Ahn, J. P. *J. Am. Chem. Soc*. **2005**, *127*, 10802.
(15) Schmalzried, H. *Solid State Reactions*; Verlag Chemie: Weinheim, 1974.
(16) Carter, R. E. *J. Am. Ceram. Soc.* **1961**, *44*, 116.
(17) Rigby, E. B.; Cutler, I. B. *J. Am. Ceram. Soc.* **1965**, *48*, 95.
(18) Bengtson, B.; Jagitsch, R. *Arkiv Kemi, Mineral. Geol.* **1947**, *24A*, 1.
(19) Navias, L. *J. Am. Ceram. Soc.* **1961**, *44*, 434.
(20) Branson, D. L. *J. Am. Ceram. Soc.* **1965**, *48*, 591.
(21) Keller, J. T.; Agrawal, D. K.; McKinstry, A. *Adv. Ceram. Mater.* **1988**, *3*, 420.
(22) Fan, H. J.; Knez, M.; Scholz, R.; Nielsch, K.; Pippel, E.; Hesse, D.; Gösele, U.; Zacharias, M. *Nanotechnology* **2006**, *17*, 5157.
(23) Sieber, H.; Hesse, D.; Pan, X.; Senz, S.; Heydenreich, J. *Z. Anorg. Allg. Chem*. **1996**, *622*, 1658.
(24) Sieber, H.; Hesse, D.; Werner, P. *Philos. Mag. A* **1997**, *75*, 889.
(25) (a) Lotnyk, A.; Senz, S.; Hesse, D. *Solid State Ionics* **2006**, *177*, 429. (b) Lotnyk, A.; Senz, S.; Hesse, D. *Acta Mater.* **2007**, *55*, 2671. (c) Lotnyk, A.; Senz, S.; Hesse, D. *J. Phys. Chem. C* **2007**, *111*, 6372.
(26) (a) Fan, H. J.; Lee, W.; Scholz, R.; Dadgar, A.; Krost, A.; Nielsch, K.; Zacharias, M. *Nanotechnology* **2005**, *16*, 913. (b) Fan, H. J.; Fuhrmann, B.; Scholz, R.; Himcinschi, C.; Berger, A.; Leipner, H.; Dadgar, A.; Krost, A.; Christiansen, S.; Gösele, U.; Zacharias, M. *Nanotechnology* **2006**, *17*, S231.
(27) JCPDS number: 82−1539. The spots in the FFT patterns fit better to $ZnAl_2O_4$ (lattice parameter: 8.0875 Å) than to $\gamma-Al_2O_3$ which has a fcc structure with a lattice parameter of 7.924Å.
(28) *Landolt-Börnstein: Numerical Data and Functional Relationships in Science and Technology*; Springer-Verlag: Berlin, 1982; Vol. 17, p 358.
(29) Yang, Y. Max Plank Institute of Microstructure Physics. Private communication. See also Yang, Y., et al. *J. Phys. Chem. C* **2008**, *112*, 4068.
(30) Hesse, D.; Senz, S.; Scholz, R.; Werner, P.; Heydenreich, J. *Interface Sci.* **1994**, *2*, 221.
(31) (a) Burton, W. K.; Cabrera, N.; Frank, F. C. *Philos. Trans. R. Soc. London, Ser. A* **1951**, *243*, 299. (b) Louchev, O. A. *Appl. Phys. Lett*. **1997**, *71*, 3522.. (c) Fan, H. J.; Knez, M.; Scholz, R.; Hesse, D.; Nielsch, K.; Zacharias, M.; Gösele, U. *Nano Lett.*. **2007**, *7*, 993. (d) Lotnyk, A.; Senz, S.; Hesse, D. *Microsc. Microanal.* **2007**, *13*, 380.
(32) Gorla, C. R.; Mayo, W. E.; Liang, S.; Lu, Y. *J. Appl. Phys.* **2000**, *87*, 3736.

Paper VII

Synthesis and optical properties of ZnO and carbon nanotube based coaxial heterostructures

D.S. Kim, S.-M. Lee, R. Scholz, M. Knez, U. Gösele, J. Fallert, H. Kalt, M. Zacharias, *Appl. Phys. Lett.*, **93**, 103108/1-3 (2008).

The characteristics of ZnO nanostructures synthesized by atomic layer deposition (ALD) on carbon nanotubes is studied. Depending on the surface chemical properties of the template the resulting nanoshells of ZnO show unique optical properties.

The author of this thesis (D.S.Kim) wrote the paper and interpreted the results. R. Scholz and S.-M. Lee did TEM investigations and ALD depositions, respectively. J. Fallert from the group of H. Kalt at the Universität Karlsruhe performed PL measurements and was involved in discussions.

Synthesis and optical properties of ZnO and carbon nanotube based coaxial heterostructures

D. S. Kim,[1,a] S.-M. Lee,[1] R. Scholz,[1] M. Knez,[1] U. Gösele,[1] J. Fallert,[2] H. Kalt,[2] and M. Zacharias[3]
[1]*Max Planck Institute of Microstructure Physics, Weinberg 2, 06120 Halle, Germany*
[2]*Institut für Angewandte Physik, Universität Karlsruhe, Wolfgang-Gaede-Straße 1, 76131 Karlsruhe, Germany*
[3]*IMTEK, Faculty of Applied Science, Albert-Ludwigs-University Freiburg, Georges-Köhler-Allee 103, 79110 Freiburg, Germany*

(Received 22 January 2008; accepted 9 June 2008; published online 10 September 2008)

Carbon nanotubes and ZnO based functional coaxial heterostructured nanotubes have been fabricated by using atomic layer deposition. An irregular structured shell composed of ZnO nanocrystals was deposited on pristine nanotubes, while a highly defined ZnO shell was deposited on the tubes after its functionalization with Al_2O_3. Photoluminescence measurements of the ZnO shell on Al_2O_3/nanotube show a broad green band emission, whereas the shell grown on the bare nanotube shows a band shifted to the orange spectral range. © *2008 American Institute of Physics*. [DOI: 10.1063/1.2952487]

Carbon nanotube (CNT) based composite materials are of particular interest because of their potential application in advanced electronics and optoelectronics. Modifications of CNTs with metal[1,2] and semiconductor nanocrystals[3,4] for the enhancement of optical and electrical properties of the composites have already been demonstrated. For instance, superconducting tin nanowires filled in CNTs showed a critical magnetic field more than 30 times higher than that of bulk metallic tin.[5] CNT films when employed as conducting scaffolds in a TiO_2 based photoelectrochemical cell showed an enhancement of the photoconversion efficiency by a factor of 2.[6]

Due to the fact that ZnO is a *n*-type semiconductor with a direct wide band gap and a large exciton binding energy of 60 meV, CNTs coupled with ZnO are promising composite materials for applications in optoelectronic devices. For example, coaxial heterostructured nanotubes with a *p*-channel CNT (Ref. 7.) combined with a *n*-channel ZnO shell may be able to be integrated into logical inverters.

Various synthetic strategies based on physical and chemical processes for getting composites have been established so far.[8] The approaches of such modifications have been reviewed in a recent review article.[9]

With the recent advance in the design of CNT composites, it is possible to coat CNTs with oxide materials by atomic layer deposition (ALD). ALD is a chemical thin film deposition method that can be used to deposit a variety of materials including oxides and metals at rather low temperatures.[10] Nanotubes were coated coaxially with continuous and radially isotropic amorphous Al_2O_3 layers.[11] However, ZnO nanoparticles or morphologically not well-defined ZnO layers were grown on nanotubes for field-emission applications.[12,13] For the development of promising nanoscale composite materials based on ZnO and CNTs a better understanding of the growth behavior involved in their formation is required. In this work, we fabricate coaxial nanotubes with highly defined morphologies of ZnO by employing an intermediate Al_2O_3 coating on the nanotubes using ALD. Detailed structure characterizations of the ZnO shells, which were determined by the surface properties of the templates, are presented and optical properties of the ZnO shells will be discussed as well.

CNTs [purity >60%] were obtained from Nanothinx. Al_2O_3 and ZnO shells were deposited on the nanotubes by ALD (Savannah 100, Cambridge Nanotechnology Inc.). For the synthesis of coaxially heterostructured nanotubes, a powder of CNTs was fixed by an adhesive tape on a glass substrate. Trimethylaluminum $[Al(CH_3)_3]$, diethylzinc $[Zn(C_2H_5)_2$, DEZ], and H_2O were selected as the aluminum precursor, zinc precursor, and oxygen reactant sources, respectively. To optimize the growth conditions, the deposition temperature was varied from 40 to 120 °C. Shorter precursor exposure and longer purging time were attempted to achieve uniform ZnO layers, composed of small and uniform nanocrystals. Here, ZnO depositions were carried out within specific deposition temperatures, precursor exposure, and purging times. The deposition was started with a substrate temperature of 70 °C and a background pressure of 0.15 Torr. For ZnO deposition, DEZ and H_2O were alternately introduced into the ALD chamber with pulses of 0.4 and 1.5 s, respectively. An exposition time of 30 s followed by a purge time of 30 s in a 10 SCCM (SCCM denotes cubic centimeter per minute at STP) Ar flow were employed for both precursors. The shell thickness was controlled by the number of precursor/purge cycles. 50 cycles were used for the deposition of 10 nm of Al_2O_3 and 70 cycles for the deposition of 25 nm of ZnO. In the following we denote the CNT/ZnO and CNT/Al_2O_3/ZnO tube samples as type A and type B tubes for simplicity. The preparation process of type B tubes is illustrated schematically in Fig. 1.

Figure 2(a) shows a transmission electron microscopy (TEM) image of the typical morphology of CNTs prior to deposition. Most of the nanotubes are multiwall tubes. Figure 2(b) shows the typical morphology of a ZnO CNT. The deposited ZnO, composed of ZnO nanocrystals, was observed to be not uniform and discontinuous along the tube.

[a]Electronic mail: dskim@mpi-halle.de.

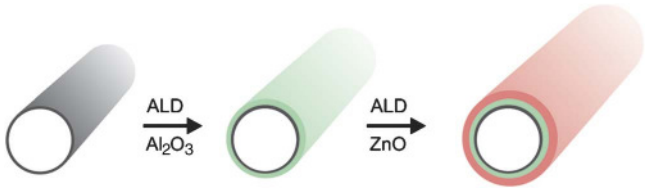

FIG. 1. (Color online) Schematic view of the fabrication process of CNTs covered by a thin Al_2O_3 layer and subsequently by a layer of ZnO (type B tube). The thickness of the ZnO and the Al_2O_3 shell is controlled by the number of ALD cycles.

Due to the chemical properties of the carbon nanotubes and the unique self-assembly characteristics of ZnO, the morphology of the ZnO shell is highly irregular. A CNT is a micromolecular form of carbon, which can be regarded as graphitic layers (sp^2-hybridized carbon atoms) rolled up into a cylindrical form. A perfect CNT is chemically inert. However, curvature-induced pyramidalization and misalignment of the π-obitals of the carbon atoms induce a local strain, which makes the nanotube more reactive than a flat graphene sheet.[14] ZnO has a tetrahedral fundamental unit cell where the Zn ions are surrounded by O ions and vice versa, caused by the sp^3-hybridized orbit. Since the normal direction to each plane of the tetrahedron is parallel to the *c*-axis, ZnO nanocrystals have a preferential orientation toward the *c*-axis. The existence of uncompensated polarity in ultrathin ZnO films was predicted based on first principles simulations.[15] We suggest that the polarity of ZnO clusters is involved in the formation of ZnO nanocrystals. In contrast to ZnO deposition, the Al_2O_3 shells formed a uniform coat on the nanotubes. Figure 2(c) shows Al_2O_3/CNT heterotube structures with a 10 nm amorphous Al_2O_3 shell. Even though, conformal coating of either ZnO or Al_2O_3 on CNTs was not expected since precursor molecules are unlikely to interact with the chemically inert surface of the carbon nanotube. Recently, it was suggested and demonstrated that chemical fuctionalization is required for uniform Al_2O_3 coating on carbon nanotubes.[10] It was also predicted that DEZ molecules should become physically adsorbed on the wall of nanotubes based on first principles electronic structure calculation.[11] Nucleation of ZnO might be initiated at defect sites or impurities along the nanotube. However, we were able to coat the nanotubes with an Al_2O_3 shell reproducibly without any intentional pretreatment of the carbon nanotube surfaces. The necessary functionalization of the carbon nanotubes may be coming from the gas phase during sample handling. For functionalization of nanotubes certain molecules

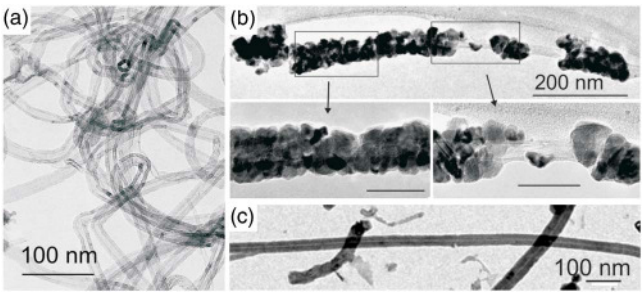

FIG. 2. (Color online) (a) TEM image of a pristine CNT. (b) TEM image of a ZnO/CNT tube. Scale bars in the enlarged images are 100 and 50 nm, respectively. (c) TEM image of a Al_2O_3/CNT tube. Uniform coating with Al_2O_3 is visible.

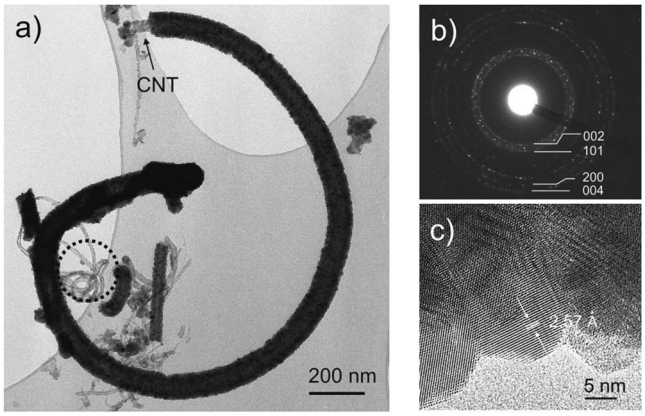

FIG. 3. (a) TEM image of a type B tube. The thin layer of Al_2O_3 is not clearly visible. Some bare CNTs, e.g., one indicated by the doted circle, are from the core side of the powder where precursor molecules were not able to react with the CNTs. (b) SAED pattern of type B tubes. (c) HRTEM image of nanocrystalline ZnO shell of type B tube.

such as NO_2 can be used as shown by the Gordon group.[10] Presumably such molecules or other chemicals which perform a similar functionalization adsorb physically from laboratory air, thus initiating an Al_2O_3 growth by ALD. However, one cannot exclude a possible chemical reaction of the precursor molecules with the nanotube wall.

Taking advantage of the homogeneous Al_2O_3 coating, we were able to deposit a well defined ZnO shell on the Al_2O_3/CNT tubes as shown in Fig. 3(a). The thickness of the ZnO shell is ~25 nm. The selected area electron diffraction (SAED) pattern of the coated ZnO shell in Fig. 3(b) reveals that the structure corresponds to polycrystalline ZnO. Figure 3(c) shows a high-resolution TEM (HRTEM) image of one of these nanocrystals, in which the atomic distances confirm the hexagonal lattice.

In addition, note that the growth rates of 2 Å/cycle for Al_2O_3 and 3.5 Å/cycle for ZnO, respectively, are somewhat larger than expected for a regular ALD process. Considering the comparatively low purging time at those temperatures, it can be expected that after the water half-cycle there is still remaining water adsorbed on the CNTs, thus contributing to an additional CVD component to the ALD deposition. The water molecules, however, might contribute to the functionalization of the CNTs for the deposition process.

Figure 4 shows typical photoluminescence (PL) spectra of type A and type B tubes. The PL of the samples was measured using the 325 nm line of a HeCd laser as excitation source. Upon optical excitation above the bandgap, typically electrons and holes form quickly excitons. At room temperature the near band edge emission at ~3.2 eV is due to the radiative decay of free excitons and their phonon replicas. It is found in both kinds of samples that the dominant part of the emission originates from excitons which have relaxed to deeper defect states. The type A tubes showed a broad deep center luminescence peaked at ~2.1 eV and the type B tubes at ~2.5 eV. The deep level emission (DLE) may have several possible causes. Emission in the green spectral range is commonly reported in bulk ZnO and ZnO nanowires. Extrinsic impurities (Cu and Li)[16] as well as intrinsic defects (oxygen vacancies)[17] are discussed as responsible defects for green luminescence band. The emission in the orange spectral range is most often associated with oxygen interstitials.[18]

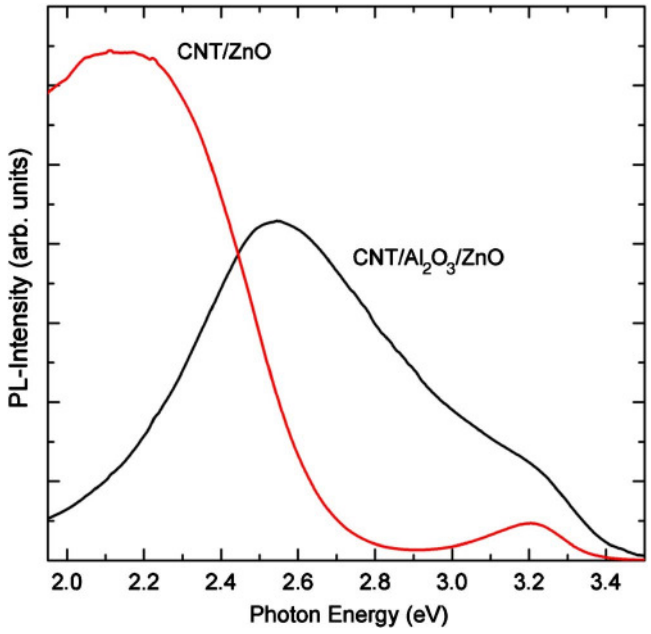

FIG. 4. (Color online) Room temperature PL spectra of CNT/ZnO (type A tubes) and CNT/Al_2O_3/ZnO tube (type B tubes).

Since the growth was performed with the identical setup without any intentional doping, the difference in the DLE between type A and B tubes is very likely caused by a different stoichiometry induced during deposition on the templates.

It is known that charge and energy transfer between a conjugated species and carbon nanotubes can occur in a photoexcited state.[19] It was found that the intensity ratio of UV/visible emission of type A tubes is four times lower than that of type B tubes. This quenching could originate from a charge transfer of photoexcited electrons from ZnO to the empty electronic states of the nanotube. In type B tubes this quenching would then be suppressed by a thin layer of Al_2O_3. However, alternative reasons cannot be excluded, such as a lower quality of the ZnO shell of type A tubes.

In summary, CNTs functionalized by ZnO or Al_2O_3 shells realizing coaxial nanotubes were prepared by ALD. It was found that the morphology of the ZnO shell on nanotubes was not well defined due to the inert surface properties of the CNT template and to the unique self-assembly characteristics of ZnO. However, if an amorphous Al_2O_3 shell was used as intermediate layer covering the nanotube, the final morphology of the ZnO shell became smooth and controllable. The comparison of the PL properties showed that the position of the DLE band of ZnO shells depends on the absence or presence of the intermediated Al_2O_3 shell.

This work was supported by the International Max Planck Research School for Science and Technology of Nanostructures (Nano-IMPRS) at Halle. S.-M.L. and M.K. greatly acknowledge the financial support by the German Federal Ministry for Education and Research (BMBF) under Contract No. 03X5507. M. Z. acknowledges the financial support by the German Research Foundation /DFG) under Contract No. Za 191/18-2.

[1]B. R. Azamian, K. S. Coleman, J. J. Davis, N. Hanson, and M. L. H. Green, Chem. Commun. (Cambridge) **2002**, 366.
[2]D. S. Kim, T. Lee, and K. E. Geckeler, Angew. Chem., Int. Ed. **45**, 104 (2006).
[3]J. M. Haremza, M. A. Hahn, and T. D. Krauss, Nano Lett. **2**, 1253 (2002).
[4]V. Švrček, C. Pham-Huu, M.-J. Ledoux, F. Le Normand, O. Ersen, and S. Joulie, Appl. Phys. Lett. **88**, 033112 (2006).
[5]L. Jankovic, D. Gournis, P. N. Trikalitis, I. Arfaoui, T. Cren, P. Rudolf, M.-H. Sage, T. T. M. Palstra, B. Kooi, J. De Hosson, M. A. Karakassides, K. Dimos, A. Moukarika, and T. Bakas, Nano Lett. **6**, 1131 (2006).
[6]A. Kongkanand, R. Martínez Domínguez, and P. V. Kamat, Nano Lett. **7**, 676 (2007).
[7]R. Martel, T. Schmidt, H. R. Shea, T. Hertel, and Ph. Avouris, Appl. Phys. Lett. **73**, 2447 (1998).
[8]M. A. Correa-Duarte, N. Sobal, L. M. Liz-Marzan, and M. Giersig, Adv. Mater. (Weinheim, Ger.) **16**, 2179 (2004).
[9]D. Tasis, N. Tagmatarchis, A. Bianco, and M. Prato, Chem. Rev. (Washington, D.C.) **106**, 1105 (2006).
[10]M. Knez, K. Nielsch, and L. Niinistö, Adv. Mater. (Weinheim, Ger.) **19**, 3425 (2007).
[11]D. B. Farmer and R. G. Gordon, Nano Lett. **6**, 699 (2006).
[12]Y.-S. Min, E. J. Bae, J. B. Park, U. J. Kim, W. Park, J. Song, C. S. Hwang, and N. Park, Appl. Phys. Lett. **90**, 263104 (2007).
[13]J. M. Green, L. Dong, T. Gutu, J. Jiao, J. F. Conley, Jr., and Y. Ono, J. Appl. Phys. **99**, 094308 (2006).
[14]S. Niyogi, M. A. Hamon, J. Hu, B. Zhao, P. Bhowmik, R. Sen, M. E. Itkis, and R. C. Haddon, Acc. Chem. Res. **35**, 1105 (2002).
[15]J. Goniakowski, C. Noguera, and L. Giordano, Phys. Rev. Lett. **98**, 205701 (2007).
[16]R. Dingle, Phys. Rev. Lett. **23**, 579 (1969).
[17]F. H. Leiter, H. R. Alves, A. Hofstaetter, D. M. Hofmann, and B. K. Meyer, Phys. Status Solidi B **226**, R4 (2001).
[18]S. A. Studenikin, N. Golego, and M. Cocivera, J. Appl. Phys. **84**, 2287 (1998).
[19]H. Ago, M. S. P. Shaffer, D. S. Ginger, A. H. Windle, and R. H. Friend, Phys. Rev. B **61**, 2286 (2000).